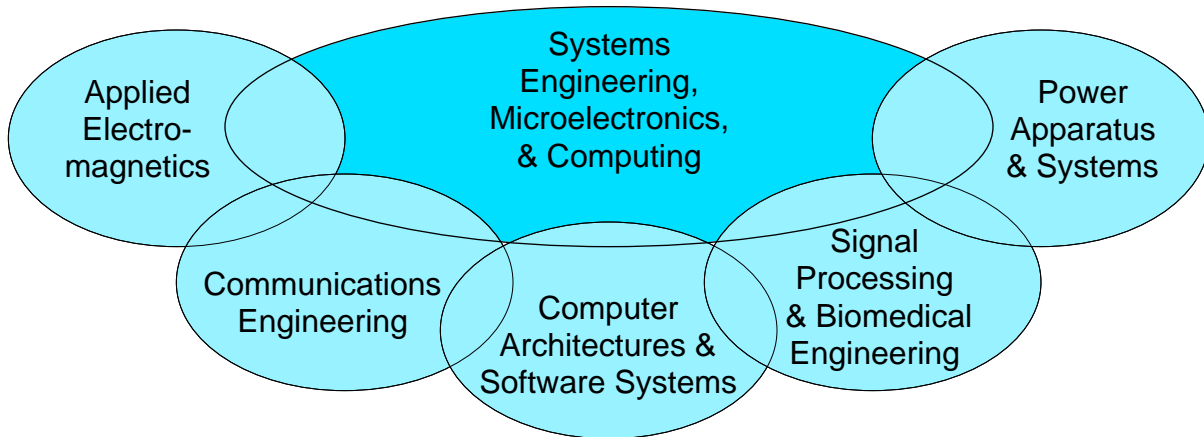


# GRADCON 98

GRADUATE STUDENT  
CONFERENCE

**May 15, 1998**  
**St. John's College**  
**University of Manitoba**  
**Winnipeg, Manitoba, Canada**



Presented by:

**Department of Electrical and Computer Engineering**

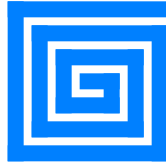


With sponsorship from:

**Faculty of Graduate Studies;**  
**Internet Innovation Centre; Industry Liaison Office;**  
**Association of Professional Engineers of the Province of Manitoba (APEM);**  
**TRLabs (Telecommunications Research Laboratories);**  
**Manitoba Hydro;**  
**IEEE Winnipeg Section;**  
**IEEE Chapters: Communications, Computer, Biomedical,**  
**Power Engineering, and Waves**

<http://www.ee.umanitoba.ca/~gradcon/>

This page is left  
intentionally blank



**GRADUATE STUDENT CONFERENCE**

# **GRADCON'98**

**May 15, 1998**

*St. John's College  
University of Manitoba  
92 Dysart Road  
Winnipeg, MB Canada*

*Edited by W. Kinsner*



**Department of Electrical and Computer Engineering  
University of Manitoba  
15 Gillson Street  
Winnipeg, Manitoba R3T 5V6, Canada  
Winnipeg, Manitoba, Canada**

*Version 1.41; 79 pp.*

**<http://www.ee.umanitoba.ca/~gradcon/>**

## SUMMARY

### Preamble

Experience in presenting research results is of increasing importance to our postgraduate students. Sharing the results within the university and with industry is also critically important.

Consequently, in January 1997 before the Flood (BF), I proposed the concept of a Ph.D. Student Conference to the deans of the Faculty of Graduate Studies (with approximately 77 programs in postgraduate studies, including 42 Ph.D. programs) and the Faculty of Engineering (with approximately 100 to 120 Ph.D. students) who approved the concept in principle.

On February 6, 1997, the idea was approved by the Graduate Studies Committee of the Faculty of Engineering, and later by the Department of Electrical & Computer Engineering. This first Graduate Student Conference, GRADCON'98, involved Ph.D. students only, and had following objectives:

### Objectives

1. To provide a forum for senior Ph.D. students to share their research results with others;
2. To strengthen links between the various engineering departments, and also between the university, industry and general public;
3. To provide a convenient means of evaluating students for the Annual Review Form;
4. To provide a record of current research in the form of Proceedings;

### Conference Format

The conference format included the following three parts:

- (i) Oral presentation (15 minutes),
- (ii) Poster presentation (105 minutes); and
- (iii) An extended summary (up to four pages) for the Proceedings which appears in an electronic form on the Web, and in a printed form.

Gradcon'98 had 32 papers submitted, and 30 presented (as two students were out of town).

A printed version of the Gradcon'98 Proceedings can be obtained from the Department of Electrical & Computer Engineering. An electronic version of Gradcon'98 Proceedings is located at

<http://www.ee.umanitoba.ca/~gradcon/>

W. Kinsner <kinsner@ee.umanitoba.ca>  
Conference Chair & Editor  
May 15, 1998

## Acknowledgments

### Individuals

My thanks go to **Mrs. Mary Morrison**, Administrative Assistant, Department of Electrical & Computer Engineering for finalizing many arrangements required by this conference.

I would also like thank **Dr. Rob Menzies**, Head of our Department, and **Dr. Ani Gole** for their continuous support during the preparation of the conference.

### Organizations

I would like to acknowledge assistance from other units, organizations and companies, including:

- University of Manitoba:
  - Faculty of Graduate Studies
  - Internet Innovation Centre
  - Industry Liaison Office
  - St. John's College
- Telecommunications Research Laboratories (TRLabs)
- MTS Advanced
- IEEE (the Institute of Electrical and Electronics Engineers) Winnipeg Section
  - IEEE Communications Chapter
  - IEEE Computer Chapter
  - IEEE Engineering in Medicine & Biology Chapter
  - IEEE Power Engineering Chapter
  - IEEE Waves Chapter
- Association of Professional Engineers of the Province of Manitoba (APEM)

## Invited Lunch Speakers

### **Dr. Rob MENZIES**

Head, Department of Electrical & Computer Engineering

### **Dr. Ed KUFFEL**

Former Dean, Faculty of Engineering

### **Dr. Wendy DAHLGREN**

Acting Dean, Faculty of Graduate Studies

### **Dr. Joanne KESELMAN**

Vice President, Research & External Programs

### **Mr. Len DACOMBE**

Director, TRLabs (Telecommunications Research Laboratories), Winnipeg

## **COPYRIGHT & DISCLAIMERS**

### **COPYRIGHT**

Copyright of each abstract presented in these proceedings is retained by the corresponding author and his/her collaborator(s).

### **DISCLAIMER NOTE 1**

This document is provided **as is**, without any warranty or guarantee of any kind, either express or implied, concerning the content or accuracy of the information provided. This document may include technical inaccuracies or typographical errors.

### **DISCLAIMER NOTE 2**

The name "University of Manitoba" and/or the University of Manitoba logo may NOT be used in any advertising or publicity pertaining to distribution of the information contained in this document without specific, written prior permission from the University of Manitoba.

## TABLE OF CONTENTS

	PAGE
Summary . . . . .	ii
Acknowledgment . . . . .	iii
Invited Lunch Speakers . . . . .	iii
Copyright and Disclaimers . . . . .	vi

### BOOK OF EXTENDED SUMMARIES

#### SESSION A

A1	Sima Noghian "Gain Control of Annular Slot Array Antenna" Advisor: L. Shafai . . . . .	1
A2	Kin Yip Sze "Substrate Thickness in a Microstrip Reflectarray" Advisor: L. Shafai . . . . .	4
A3	Qiubo Ye "Development of Algorithms for Solving Electromagnetic Interactions with Large Structures" Advisor: L. Shafai . . . . .	8
A4	Ling Yun Lee "Electromagnetic Analysis of Interconnect Circuits Using Asymptotic Waveform Evaluation" Advisor: I.R. Ciric	
A5	Wujun Quan "Multilevel Iterative Method for the Solution of Electro- magnetic Integral Equations based on the Multi-p Hierarchical Bases" Advisor: I.R. Ciric	
A6	David R. Swatek "Progress in Single Integral Equations for Wave Scattering Analysis" Advisor: I.R. Ciric	
A7	Alex Tugulea "Losses in Microstrip Lines Using Two-Dimensional Equations for Planar Circuits" Advisor: I.R. Ciric	
A8	Ming Zhang "Computing Electromagnetic Fields in Inhomogeneous Media Using Lattice Gas Automata" Advisor: G. Bridges	

A9	Inas El-Babli "Reconstruction of Three-Dimensional Inhomogeneous Bodies Using Unrelated Illumination" Advisor: A. Sebak . . . . .	12
A10	Ashraf Badawi "Efficient Numerical Analysis for Aperture-Coupled Microstrip Antenna" Advisor: A. Sebak . . . . .	16
A11	D.P. Gray "Two Methods for Efficiency Increase of Triplate Array" Advisor: L. Shafai . . . . .	20
A12	B. Ghosh, N. Simons, L. Shafai, A. Ittipiboon, A. Petosa, and M. Cuhaci "Extraction of Scattering Matrix Coefficients of NRD and Waveguide Discontinuities by the TLM Method" Advisor: L. Shafai . . . . .	22

## **SESSION B**

B1	Saleh Mneina "Linear Phase Data Transmission Filters" Advisor: Advisor: G.O. Martens	
B2	Sihong Lei "Review of TCP over Wireless Networks" Advisor: D. Blight . . . . .	26
B3	Ha Hoang Nguyen "Turbo Processing Techniques for Digital Communications over Wireless Mobile Fading Channels" Advisor: E. Shwedyk . . . . .	28
B4	Reza Fazel-Rezai "Upper Limb Dynamic Analysis" Advisor: E. Shwedyk . . . . .	31
B5	Rajen M. Murugan "An Improved Electrical Impedance Tomography (EIT) Algorithm for the detection of Early Stages of Breast Cancer" Advisors: A. Wexler and R. Gordon	
B6	Hongwei Li "An Adaptive Impedance Relay for the Transmission Line" Advisor: P.G. McLaren	
B7	Mojtaba Mohaddes "Control of Optimal PWM Voltage Source Inverter using Sigmoid and Piecewise Linear Artificial Neural Networks" Advisor: P.G. McLaren . . . . .	35

B8	Dharshana Muthumuni "Internal Faults in Synchronous Machines and Transformers" Advisor: P.G. McLaren	
B9	David A.N. Jacobson "Stability Domain Calculations of Period-1 Ferroresonance in a Nonlinear Resonant Circuit" Advisor: R.W. Menzies	
B10	Wieslaw T. Kwasnicki "High Speed Transient Stability - A Multiprocessing Solution" Advisor: A. Gole . . . . .	39

## SESSION C

C1	Dean McNeill "Issues in the Embedded Neural Control of Autonomous Robots" Advisor: Advisor: H.C. Card	
C2	Imran Khan "Adaptive Algorithms for personal Agents" Advisor: H.C. Card . . . . .	43
C3	Peter Czezowski "Computational Intelligence in ATM Call Admission Control" Advisor: W. Pedrycz . . . . .	47
C4	Douglas Holmes "Modelling Emergent Behaviours for Construction Tasks" Advisor: W. Pedrycz . . . . .	51
C5	Sinisa Iliskovic "The Data Mining in Databases with Decision Trees" Advisor: W. Pedrycz	
C6	Sajid Hussain "Personal Proxy Cache" Advisor: R.D. McLeod . . . . .	55
C7	Richard Dansereau "Progressive Image Transmission Using Wavelet and Other Fractal Techniques" Advisor: W. Kinsner . . . . .	58
C8	Pradeepa Yahampath "Segmentation and Compact Representation of Moving Objects in Facial Image Sequences" Advisor: W. Kinsner . . . . .	62
C9	Fan Mo "Power System Transients Characterization and Classification using Wavelets and Neural Networks" Advisor: W. Kinsner . . . . .	66

**INDEX OF AUTHORS** . . . . . 70-71

# GAIN CONTROL OF ANNULAR SLOT ARRAY ANTENNA

*Sima Noghianian*

Department of Electrical and Computer Engineering,  
The University of Manitoba, Winnipeg, MB R3T 5V6, Canada

*sima@ee.umanitoba.ca*

Advisor: Professor Lot. Shafai, *Shafai@ee.umanitoba.ca*

**Abstract**—Two methods of gain improvement have been studied and compared. The effect of these methods on the bandwidth of antenna are studied.

## I. INTRODUCTION

Wireless and satellite communication are becoming important for business and private use. A wireless system requires efficient and high gain antenna at low cost. Printed antenna such as micro-strip antennas are attractive in wireless communication because of light weight, low profile and compatibility with MMIC circuits. However one of their major disadvantages is low gain. Annular slot array antennas enjoy all the advantages of planar structure, while they have high gain.

In this paper annular slot array antenna working in  $TM_{11}$  mode is studied and some methods of gain improvement are suggested.

## II. ANTENNA CONFIGURATION

The configuration of annular slot array antenna is shown in Fig. 1. The basic element is a slotted radial waveguide. Slots are co-centred and continues. Radiation is in broadside. The radial waveguide can be filled by a dielectric, but in this study it is filled with air. The slots are located at multiples of  $\lambda_0$  from the centre. Slot width is  $0.1\lambda_0$  and waveguide height is  $0.4\lambda_0$ . Thickness of waveguide walls is  $0.02\lambda_0$ .

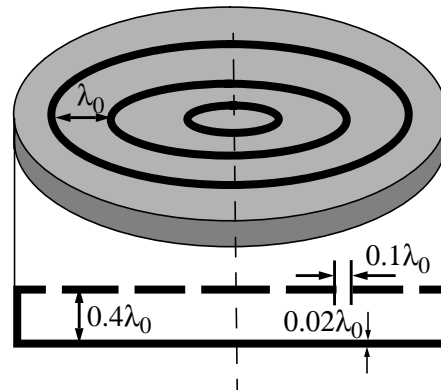


Fig. 1. Annular slot array antenna configuration

## III. ANALYSIS METHOD

All the simulations have been done by the “Multi-Body Electromagnetic Scattering” (MBES) package developed by the University of Manitoba. This software uses the method of moment for bodies of revolution. The antenna fields are expanded in terms of Fourier series of the azimuthal angle and three dimensional problem is broken into several two dimensional ones. The excitation is simulated by dipoles. To cancel higher order modes two dipoles with  $180^\circ$  phase difference are used. The location of feeds are:  $x = \pm 0.2\lambda_0$ ,  $z = 0.1\lambda_0$ .

#### IV. RESULTS AND DISCUSSION

Two methods for gain improvement are suggested. First one is by adding a radome made of dielectric material with dielectric constant  $\epsilon_r$ . The effects of dielectric constant and dielectric thickness are studied. The simulations have been done for two and three slot antennas. Fig. 2 shows the gain for different dielectric constants and different thicknesses. The improvement of up to 2dB for two-slot antenna and 5dB for three slot antenna can be observed.

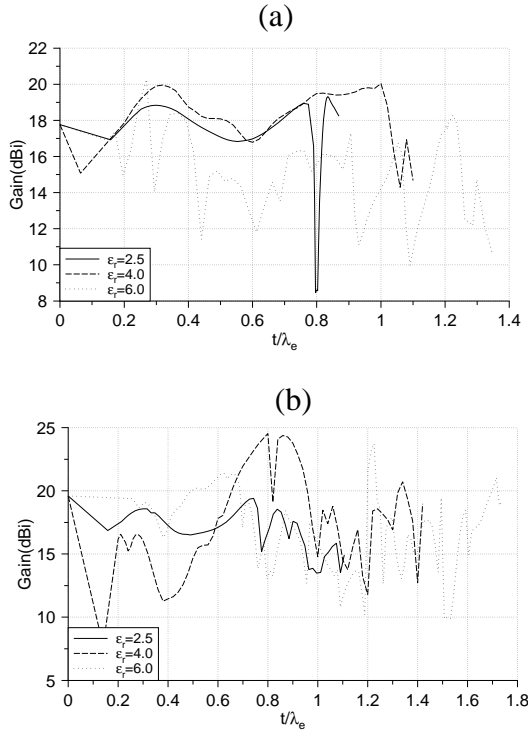


Fig. 2. Gain variation vs. dielectric thickness (a) two-slot antenna (b) three-slot antenna

The first method is expensive and makes the antenna heavy and bulky. The other method which is low cost, is adding conducting strips at a distance of quarter free-space wavelength, as shown in Fig. 3.

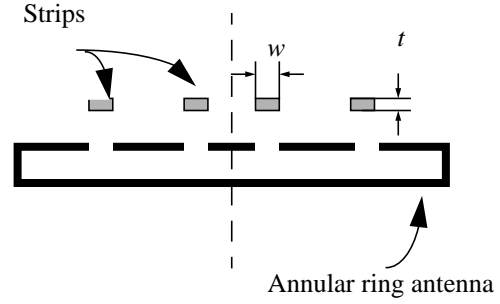


Fig. 3. Antenna configuration with conducting strips

Table (1) shows the results for different combinations of strip width ( $w$ ) and strip thickness ( $t$ ). It can be observed that for  $t = 0.2\lambda_0$ , for all strip widths gain is maximum. The best results for both two and three slot antenna are given by  $w = 0.4\lambda_0$  and  $t = 0.2\lambda_0$ , which is about 2.4 dB improvement for 2-slot antenna and 3.3 dB for three slot antenna.

$w$	$t/\lambda_0$	2-slots Gain(dBi)	3-slots Gain(dBi)
without strips		15.971	17.837
$0.3\lambda_0$	0.1	16.693	19.255
	0.2	17.550	20.160
	0.3	17.162	19.044
$0.4\lambda_0$	0.1	17.122	20.508
	0.2	18.367	21.111
	0.3	17.126	18.592
$0.5\lambda_0$	0.1	16.961	20.952
	0.2	17.719	20.982
	0.3	16.276	18.503

Table (1) Gain(dBi) for different combinations of strip sizes

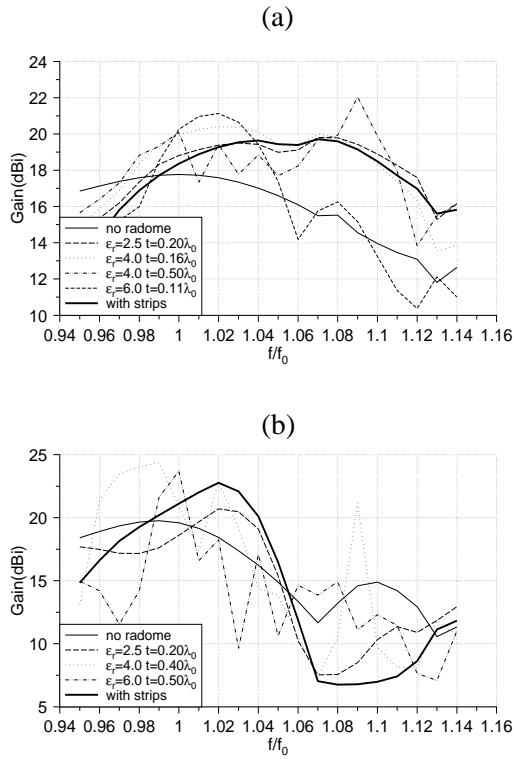


Fig. 4. Gain variation vs. frequency change  
 (a) two-slot antenna (b) three-slot antenna

For some selected cases the effect of frequency change is studied. Fig. 4 shows the results. It can be seen that both adding a radome and strips slightly shift the centre frequency and decreases the bandwidth, but adding strips have less effects on bandwidth than dielectric radome.

## V. CONCLUSION

Two methods of gain improvement for annular slot array antenna are discussed. Results for two and three slot antennas are given. Effects of these methods on the bandwidth are studied. In general both methods show good improvement in gain, but they cause frequency shift and decrease bandwidth. Adding conducting strips has advantage of less cost and weight and effect on the bandwidth.

**Acknowledgement**—The financial support provided by the University of Manitoba through Graduate Fellowship is highly appreciated.

# SUBSTRATE THICKNESS IN A MICROSTRIP REFLECTARRAY

K. Y. Sze  
(Advisor: L. Shafai)

Department of Electrical and Computer Engineering  
University of Manitoba, Winnipeg, Manitoba, Canada R3T 5V6

**Abstract:** The effects of substrate thickness on the performance of a microstrip reflectarray are investigated. These effects are analyzed in terms of specular reflection coefficients due to incident plane waves. Numerous plots for different substrate thicknesses are generated for discussion in this article.

## I. INTRODUCTION

Substrate thickness is indeed an important consideration in the design of a microstrip reflectarray. A thick dielectric sheet as substrate provides an improved bandwidth performance, but it is much heavier. As such, honeycomb substrates, which have relative permittivities of approximately equal to that of free space ( $\epsilon_r = 1.0$ ), are very widely used because of its light-weight considerations. It is also more durable than other substrate materials in spaceborne environment.

However, a thick substrate has a large unattainable phase range [1][2]. In fact, more investigation is required to further understand the effects of thick substrate on the performance of a microstrip reflectarray. This is thus the objective of this article. To approximate the honeycomb substrate here,  $\epsilon_r = 1.0$  is utilized.

## II. THEORY

Fig. 1 illustrates the cross-section schematic of a reflectarray. The feed is positioned at  $z = z_f$  along the  $z$ -axis, with the wave from the feed incident on the  $n$ -th patch through a path length  $L_n$ . The approach of the analysis employed here is similar to that discussed in [2].

It is generally known that an electrically thick microstrip substrate can sustain a considerable amount of surface wave energy. As a result, significant effects of substrate surface coupling appear, and thus, is especially strong for a substrate thickness of greater than  $0.1\lambda_0$ , where  $\lambda_0$  is the free space wavelength [3].

The required electrical thickness for a grounded infinite dielectric sheet corresponding to a certain surface wave cut-off frequency is derived from [4] as

$$\frac{h}{\lambda_c} = \frac{n}{4\sqrt{\epsilon_r - 1}} \quad ; \quad n = 0, 1, 2, \dots \quad (1)$$

where  $h/\lambda_c$  is the substrate electrical thickness in terms of the cut-off wavelength and  $\epsilon_r$  is the relative permittivity of the substrate. This formulation will be used to compare with the results produced from the reflectarray modeling.

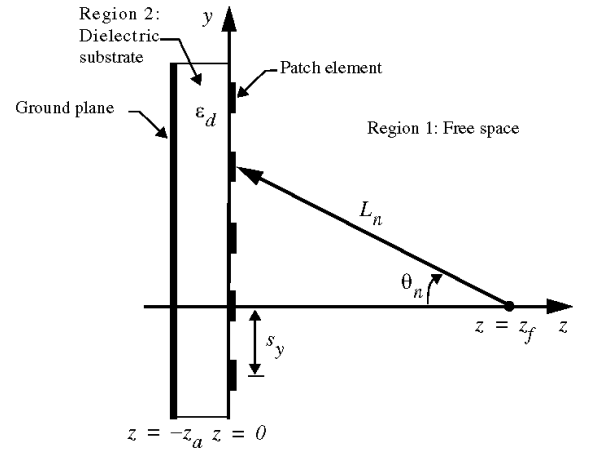


Fig. 1: Schematic of microstrip reflectarray (cross-section).

## III. NUMERICAL RESULTS

A TE-to- $z$  incident plane wave at  $\phi = 89.9^\circ$  is assumed in the analysis. For this,  $\vec{E}$  is  $x$ -directed and the frequency utilized is  $f_0$ . The conductive patch dimensions  $a$  and  $b$  are fixed as  $a = b = 0.75\text{cm}$ . The element spac-

ings for the x- and y- directions are  $s_x = s_y = 1.25\text{cm}$ , respectively. Also in this article, the specular reflection coefficient magnitude is denoted as  $A_R$ , and its phase as  $\psi_R$ , respectively.

From Fig. 2, it is observed that the patch resonances are unattainable at lower frequencies for normal incident plane waves, given the above mentioned physical parameters. However, as the frequency is increased, the phase minima extend downwards with very slight shifts to the left. Such changes are most sensitive in the first minima. Fig. 3 compares the difference in sensitivities between the first and second minima. A marked difference in reflection phase  $\psi_R$  is observed for higher frequencies.

An increase in relative permittivity  $\epsilon_r$  lowers the reflection phase curve, as can be seen from Fig. 4. This is especially significant for a very thick substrate. Plots for higher  $\epsilon_r$  will be addressed in the presentation. A correlation is found between the locations of minima and maxima of Fig. 4 and the required electrical thicknesses  $h/\lambda_c$  of a grounded infinite dielectric sheet given in Table 1. That is, the  $h/\lambda_c$  values coincide closely with the locations of minima and maxima in the figure. Of course, the array of thin conducting patches does contribute to the small shifts of values from those given in the table.

The critical angle  $\theta_{ic}$  at the onset of higher-order mode propagations is independent of substrate thickness, as illustrated in Fig. 5 through Fig. 8. In fact, all these cases satisfy the well-known phased array grating lobe criterion  $|\sin\theta_m| \leq \lambda_o/s - 1$ , where  $\theta_m$  is the phase maximum scan angle,  $s$  is the element spacing and  $\lambda_o$  is the free space wavelength [5]. For instance, in Fig. 5 and Fig. 6,  $\theta_{ic} \approx 22.63^\circ$ , and this matches well with  $\theta_m = 22.69^\circ$ . (It should be noted from Fig. 5 that, for the case of  $z_a = 0.0798\text{cm}$  (i.e.  $z_a/\lambda_o = 0.0461$ ), a resonance is attained for  $\theta_i = 0^\circ$  at  $f_o = 17.320\text{GHz}$ .) It is verified here that, for the case of  $z_a = 0.0798\text{cm}$  and within the range of  $\theta_{ic} < \theta_i < 75^\circ$ , both the specular(00-th) and the 01-th Floquet modes propagate, thus contributing to a very significant decrease (more than 50%) in specular reflection magnitude, as is shown in Fig. 6.

As for the thick substrate case of  $z_a = 0.3175\text{cm}$  (i.e.  $z_a/\lambda_o = 0.1833$ ), this problem is further complicated by the possibility of strong substrate surface wave. Nevertheless, full specular reflections occur for all the substrate thicknesses considered when  $\theta_i < \theta_{ic}$ . For reflectarray applications as such, the subtended (half) angle of the reflectarray must be much less than  $\theta_{ic}$ .

Except for the shift in critical angle  $\theta_{ic}$  due to the phased array grating lobe effects, the reflection phase curve computed for resonance at  $\theta_i = 0^\circ$  generally remains unaffected as the substrate thickness  $z_a/\lambda_o$  increases. However, for a thick enough substrate in which higher-order surface wave modes propagate, interference phenomena between surface wave coupling and direct radiation coupling [3] tends to vertically shift the reflection phase curve. These behaviors are as illustrated in Fig. 7.

Referring to Fig. 8, the critical frequency  $f_{oc}$  at the onset of higher-order mode propagations due to grating lobe effects is found to be approximately 23.97GHz for all the substrate thicknesses considered, for which  $\epsilon_r = 2.5$ . Again, full specular reflections are observed from the figure prior to  $f_{oc}$ . As observed in Fig. 9, the first resonant frequencies for these cases fall between the range of 8GHz and 12GHz. In fact, the resonant frequency decreases as the substrate thickness increases. In doing so, the frequency bandwidth around the resonant frequency increases as well and this supports the bandwidth widening claims in [1].

#### IV. CONCLUSION

The effects of substrate thickness in a microstrip reflectarray are analyzed in terms of specular reflection coefficient due to an incident plane wave.

The resonance cannot always be achieved by just changing  $z_a$  alone. However, it can be attained by increasing the frequency or relative permittivity and varying  $z_a$  such that the phase minimum crosses over the zero-phase line. Except for the shifting effect on the reflection phase, the change in substrate thickness has negligible effect on the reflection magnitude before the onset of grating lobes. In other words, the substrate surface wave influences only the reflection phase before the onset. It is also confirmed that a

thick substrate increases the frequency bandwidth around the resonant frequency.

## V. ACKNOWLEDGMENTS

The research work for this article was fully supported by the National Science and Engineering Research Council of Canada. The author would also like to thank Dr. L. Shafai for his kind assistance and support throughout this research.

## REFERENCES

- [1] David M. Pozar, Stephen D. Targonski, H. D. Syrigos; "Design of millimeter wave microstrip reflectarrays"; *IEEE Trans. on Antennas and Propag.*, vol. 45, no. 2; February 1997; pp. 287-296.
- [2] K. Y. Sze, L. Shafai; "Analysis of phase variation due to varying patch length in a microstrip reflectarray", Accepted for publication in the *1998 IEEE Antennas and Propag. Society International Symp.*.
- [3] L. D. Bamford, J. R. James, A. F. Fray; "Minimising mutual coupling in thick substrate microstrip antenna arrays", *Electronics Lett.*, vol. 33, no. 8; April 1997; pp. 648-650.
- [4] Roger F. Harrington; *Time-harmonic Electromagnetic Fields*; McGraw-Hill Book Company, New York; 1961.
- [5] Robert J. Mailloux; *Phased Array Antenna Handbook*; Artech House, Norwood, MA; 1994.

Table 1: The required electrical thicknesses for a grounded infinite dielectric sheet corresponding to a surface wave cut-off frequency of 11.761GHz.

Surface wave mode	Substrate thickness $h/\lambda_c$		
	$\epsilon_r = 2.50$	$\epsilon_r = 3.27$	$\epsilon_r = 4.50$
0	0.0000	0.0000	0.0000
1	0.2041	0.1659	0.1336
2	0.4082	0.3319	0.2673
3	0.6124	0.4978	0.4009
4	0.8165	0.6637	0.5345
5	1.0206	0.8297	0.6682

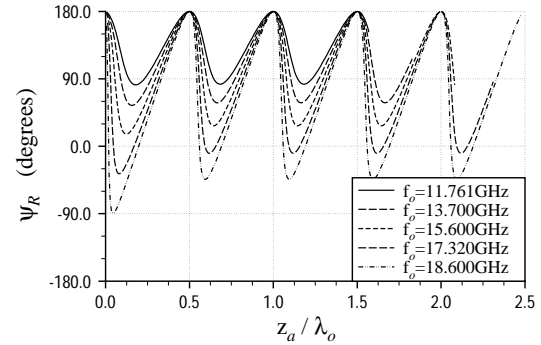


Fig. 2: Effects of increasing substrate thickness ( $\epsilon_r = 1.0$ ) for varying frequencies.

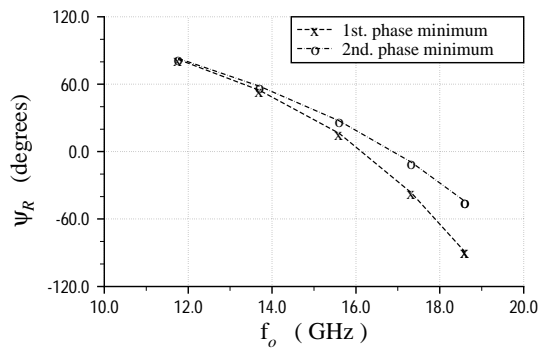


Fig. 3: Comparing frequency sensitivities of the first and second minima of Fig. 2.

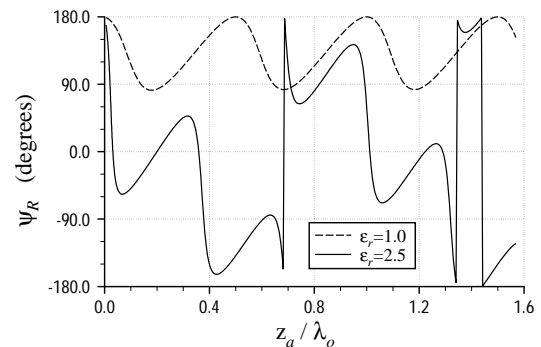


Fig. 4: Effects of increasing substrate thickness for different relative permittivities, with  $f_o = 11.761\text{GHz}$ .

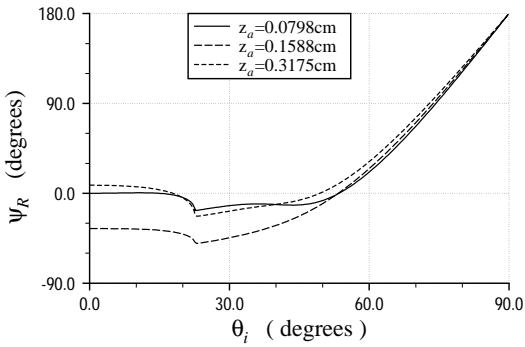


Fig. 5: Reflection phase sensitivities with respect to increasing incident angle at  $f_0 = 17.320\text{GHz}$  for various substrate thicknesses ( $\epsilon_r = 1.0$ ).

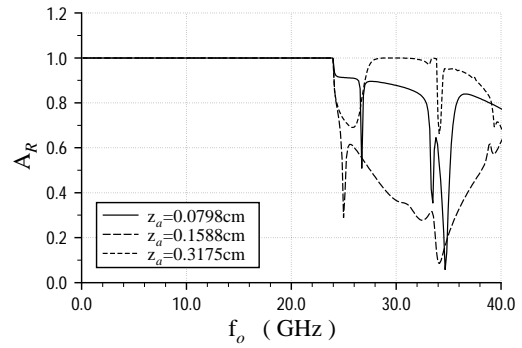


Fig. 8: Variations of reflection magnitude with respect to increasing frequency for different substrate thicknesses ( $\epsilon_r = 2.5$ ), with  $\theta_i = 0^\circ$ .

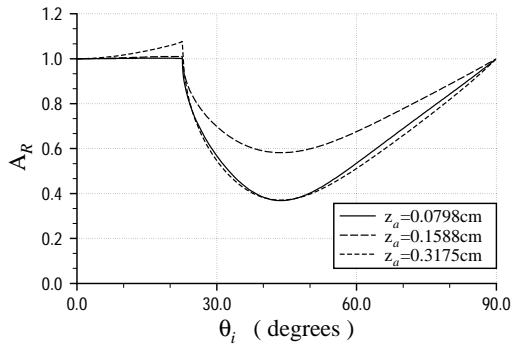


Fig. 6: Reflection magnitude sensitivities with respect to increasing incident angle at  $f_0 = 17.320\text{GHz}$  for various substrate thicknesses ( $\epsilon_r = 1.0$ ).

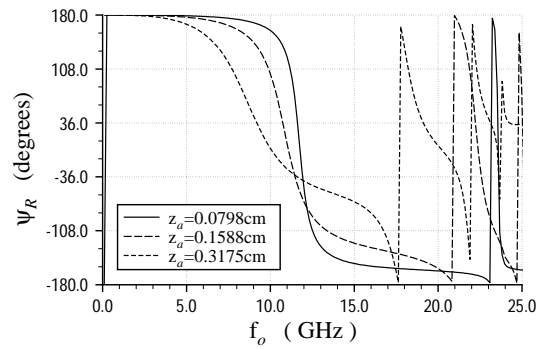


Fig. 9: Variations of reflection phase with respect to increasing frequency for different substrate thicknesses ( $\epsilon_r = 2.5$ ), with  $\theta_i = 0^\circ$ .

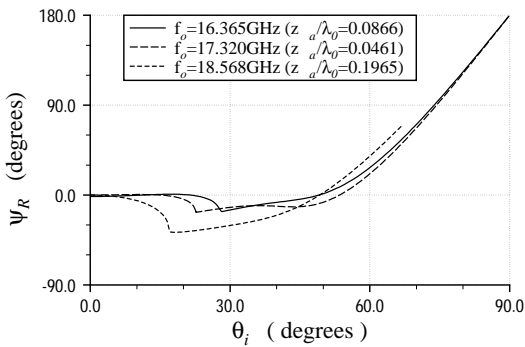


Fig. 7: Shifting of critical angle  $\theta_{ic}$  due to increasing resonance frequency.

# DEVELOPMENT OF ALGORITHMS FOR SOLVING ELECTROMAGNETIC INTERACTIONS WITH LARGE STRUCTURES

Qiubo Ye

Computational Electromagnetics Lab., E-mails: qiuboye@ee.umanitoba.ca

Advisor: L.Shafai, E-mail:shafai@ee.umanitoba.ca

**Abstract** - Techniques for solving electromagnetic scattering from electrically large and perfectly conducting structures are studied. Two methods are applied to study the 2-dimensional problems and can depress the internal resonances. One method is applied to 3-dimensional cases. The guideline for the use of these methods to obtain the accurate solutions are provided.

## I. INTRODUCTION

The method of moment (MoM) is a common numerical technique for solving integral equations. A limitation of this method, when used to analyse scattering problems, is that the electrical dimensions of the scattering body cannot be larger than a few wavelengths since large bodies result in large matrices which dictate excessive computer storage and execution time. In addition, the accumulation of errors while inverting large matrices greatly impairs the accuracy of the solution.

Among the various approaches which are proposed to circumvent the computational difficulties, the progressive numerical method (PNM) [Shaf77] and the spatial decomposition technique (SDT) [Umas92] reduce the matrix size and retain all the physics of the scattering and interaction. The basic idea is dividing a large object into small regions and calculating the small regions one by one, but still considering the coupling effect among all the regions. We find that the SDT should be modified to get the convergent results and then becomes a special case of the PNM. We will show that the PNM can efficiently depress the internal resonances.

In 3-dimensional case, it was observed that a straightforward application of PNM to large scatterers does not yield an accurate solution. A Projection Iterative Method (PIM) [Bo92] is a convergent guaranteed method which is not widely introduced and applied in electromagnetics. In this method, the solution is improved by means of an orthographic projection procedure. The decomposition technique is that the unknowns are not decomposed in space. A series of sub-equations defined on subdomains are solved in each iterative step. The computer memory is much less than that of the direct method for the original equation when the sub-equation size is small. The iteration can be accelerated by the use of the relaxation factor.

## II. NUMERICAL METHODS FOR 2-D OBJECTS

### A. Algorithms of PNM and modified SDT

It is known that the solutions of the electric or magnetic field integral equations, using the MoM, can be

reduced to a matrix equation of the form,

$$[G] [I] = [E] \quad (1)$$

where  $[E]$  is the excitation matrix,  $[I]$  is the unknown current distribution, and  $[G]$  is an  $N \times N$  square matrix representing the coefficients obtained from expanding the unknown function. Expanding the matrix in its component forms, equation (1) can be written as

$$\begin{bmatrix} [G_{11}] & [G_{12}] & \bullet & \bullet & \bullet & [G_{1n}] \\ [G_{21}] & [G_{22}] & \bullet & \bullet & \bullet & [G_{2n}] \\ \bullet & \bullet & \bullet & \bullet & \bullet & \bullet \\ \bullet & \bullet & \bullet & \bullet & \bullet & \bullet \\ \bullet & \bullet & \bullet & \bullet & \bullet & \bullet \\ [G_{n1}] & [G_{n2}] & \bullet & \bullet & \bullet & [G_{nn}] \end{bmatrix} \begin{bmatrix} [I_1] \\ [I_2] \\ \bullet \\ \bullet \\ \bullet \\ [I_n] \end{bmatrix} = \begin{bmatrix} [E_1] \\ [E_2] \\ \bullet \\ \bullet \\ \bullet \\ [E_n] \end{bmatrix} \quad (2)$$

where  $[G_{11}]$ ,  $[G_{22}]$ , ...,  $[G_{nn}]$  are  $M \times M$  square matrices with  $M \ll N$ . Geometrically, this is equivalent to subdividing an object into several small sub-regions. Using PNM, field relation in the first region, while neglecting the interactions from the remaining sections of the object, can be simplified to

$$[G_{11}] [I_1] = [E_1] \quad (3)$$

and the solution of which gives approximately the required current distribution  $[I_1]$ . Similarly, assuming the current distribution in the second region can be determined mainly by the contribution of the first region and the excitation, the unknown field relation can be expressed as

$$[G_{22}] [I_2] = [E_2] - [G_{21}] [I_1] \quad (4)$$

The solution of this equation then gives the required current  $[I_2]$ . This process can be applied successively until the required current distribution for the last region is found. In general, for the  $l^{\text{th}}$  region, the field relation is

$$[G_{ll}] [I_l] = [E_l] - \sum_{i=1}^{l-1} [G_{li}] [I_i] \quad (5)$$

Note that the solution of the field problem by using the above method gives increasingly larger errors towards the outer edge of each region because of the coupling effect from the adjoining region. In order to have a reasonable solution an overlapping region may be used to improve the accuracy of the solution. Considering region  $R_1$ , one may discard  $P$  inaccurate solutions at the edge from its all  $M$  solutions and retain the rest. The second region  $R_2$  begins from where the inaccurate solutions are discarded. This procedure continues until the entire object has been covered.

The procedures to calculate scattering problem using the SDT are suggested in [Umas92]. While using the SDT to calculate scattering problem, we found that the concept of the virtual interface currents was not realizable and it made the results divergent. It was also found that the given initial current distribution had no obvious effect on the computing time and results. Also when applying the SDT to TE cases, the iterative procedure could not make the results more accurate, except for the infinite strip case. We hence modified the SDT by:

- 1) eliminating the virtual interface current.
- 2) setting the initial currents to zero. This procedure saved the time and effort needed to compute these currents.
- 3) eliminating the iteration step for the TE case, as it could not result in convergence of the solution.

After these modifications the SDT became, actually, a special case of the PNM in which there are no overlapping regions.

### B. Computed Results

Consider two dimensional scattering problems by assuming that the perfect conducting rectangular cylinder is infinitely long. The incident field is taken as a plane wave. The cross section of a cylinder, the sub-regions  $R_1, R_2, \dots$ , and the overlapping regions are shown in Fig. 1.

In order to show the effectiveness of the PNM, the current distribution and bistatic RCS of a TM plane wave incident on an infinite rectangular scatterer using MoM and PNM are plotted in Fig. 2(a) and (b) respectively. The results by MoM and PNM agree well.

As mentioned before, the modified SDT is the PNM without the discarded current pulse samples. In the TM case iteration procedure works well with modified SDT. The modified SDT solutions could be very close to the full matrix MoM's by increasing the iteration number.

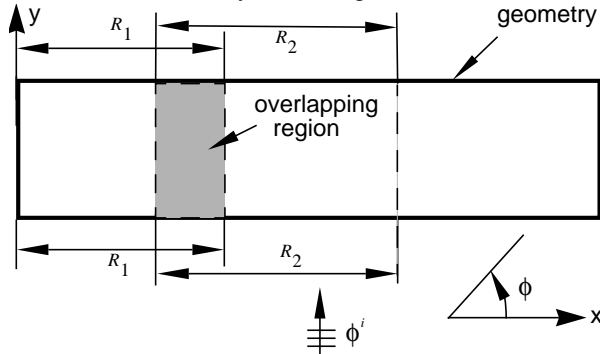


Fig.1 The cross section of a conducting cylinder, the sub-regions  $R_1, R_2, \dots$ , and the overlapping regions.

It should be mentioned that in PNM larger overlapping region sizes can result in more accurate results. Usually the overlapping region size equal to  $1/4 - 1/5$  of the sub-region size is good enough to reach the full

MoM solution. The PNM, when incorporated with iterative procedure [Ye96], needs much less iteration number to achieve the same accuracy as that of modified SDT.

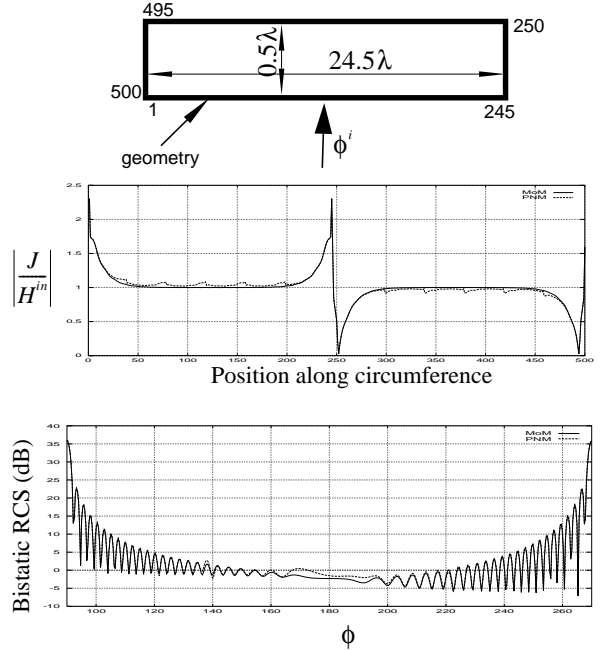


Fig.2 (a)Current distribution and (b)bistatic RCS of Infinite rectangular cylinder using PNM, compared with MoM (TM case),  $M = 100$ ,  $P = 20$ , total number of current pulses  $N = 500$ .

The procedures similar to the TM case discussed earlier are carried out for TE case. The performance of the PNM is examined here for an infinite circular cylinder. The results are provided in Fig. 3(a) and (b). It should be mentioned that the sub-region distribution should begin from the illuminating side and spread out to non-illuminating side. Otherwise insignificant results would come out.

A large amount of computational work has been done for infinite cylinders. We tried to use different sub-region sizes and different discarded pulse samples. It appeared that the results were basically not dependent on both of them. From our work we found that for small objects the PNM's current distribution does not agree well with the MoM's, but the main lobes of the bistatic RCS agree excellently.

It was found that, the iteration case in the SDT does not work, and the results remain relatively the same. This is contrary to the TM case, where iteration continues to improve the solution accuracy.

### C. Depressing the Internal Resonances

It is well known that using MoM in conjunction with either the EFIE or MFIE produces spurious surface currents on conducting bodies at the internal resonance frequencies which correspond to waveguide modes at

cutoff in the interior of the cylinder, since the determinant of  $[G]$  becomes zero. Many methods have been proposed to overcome this problem, but have their own deficiencies. By handling each sub-region separately, PNM avoids to calculate the whole ill-conditioned MoM matrix equation and therefore depresses the internal resonances.

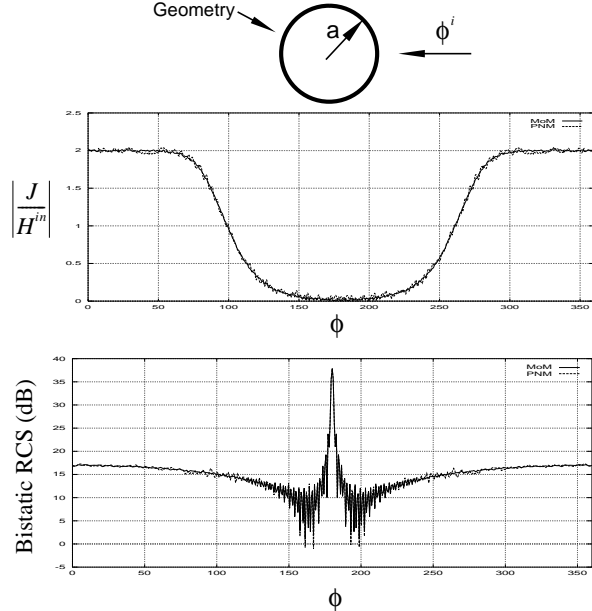


Fig.3 Infinite circular cylinder's (a)current distribution and (b)bistatic RCS using PNM, compared with MoM (TE case),  $ka=100, N = 2000, M = 100, P = 20$ .

To illustrate this an example of the TE plane wave normally incident on an infinite circular cylinder is shown, in which the internal resonance takes place if  $ka=13.324$ . The results are provided in Fig. 4(a) and (b). As we can observe, the PNM results depress the internal resonance and reasonable agreement with the analytic solutions is achieved

### 3. NUMERICAL METHOD FOR 3-D OBJECTS: PROJECTION ITERATIVE METHOD (PIM)

This section includes the formulation of PIM, the application of PIM to sphere and finite cylinder, the analysis of its convergence and accuracy, and the use of the relaxation factor to accelerate the iteration.

#### A. PIM Formulation

Based on the conventional 3-D (MoM) with triangular surface patches [Rao82], a matrix equation calculating the surface currents can be obtained for a perfect conducting scatterer by an incident plane wave,

$$[Z] [I] = [V] \quad (6)$$

where  $[Z]$  is an impedance matrix,  $[V]$  is a column vector due to incident field, and  $[I]$  is the unknown current. When the scatterer is electrically large,  $[Z]$  is also large

and equation (6) can not be solved by simple numerical method on the ordinary computers. The formulation of using PIM to solve it is given below..

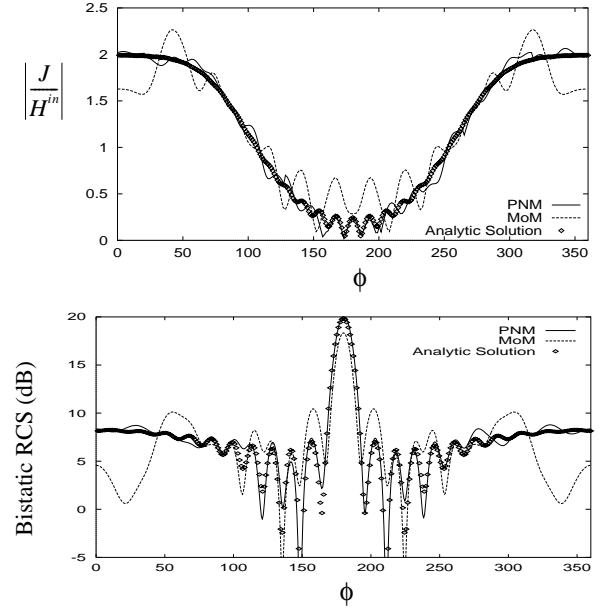


Fig.4 Infinite circular cylinder's (a)current distribution and (b)bistatic RCS using PNM, compared with analytic solution and MoM at internal resonance (TE case),  $ka=13.324, N=266, M=53, p=8$ .

By dividing the coefficient matrix into  $N$  sub-matrices which is equal to dividing the scatterer into  $N$  subregions, (6) can be rewritten into the following component matrix equations,

$$[Z_i] [I] = [V_i], \quad i=1,2, \dots, N \quad (7)$$

where  $[V_i]$  is the excitation on the  $i^{th}$  subregion of the scatterer.  $[Z_i]$  is the corresponding sub-matrix which is not square.

Let  $D_i$  be the set of solutions satisfying equation (7) and  $[I_0^{(0)}]$  be arbitrary initial solution. Denote  $[I_0^{(1)}]$  the orthographic projection of  $[I_0^{(0)}]$  on  $D_1$ . Then

$$\begin{cases} [Z_1] [I_0^{(1)}] = [V_1] \\ \|[I_0^{(1)}] - [I_0^{(0)}]\| = \min \end{cases} \quad (8)$$

Based on equation (8), the current can be calculated by the iterative formula,

$$[I_0^{(1)}] = [I_0^{(0)}] + [Z_1]^\dagger \left( [Z_1] [Z_1]^\dagger \right)^{-1} \left( [V_1] - [Z_1] [I_0^{(0)}] \right) \quad (9)$$

where  $[Z_1]^\dagger$  is the adjoint operator of  $[Z_1]$ . Once  $[I_0^{(1)}]$  is obtained,  $[I_0^{(2)}]$  can be calculated based on the second component matrix equation, ..., and  $[I_0^{(N)}]$  can be calculated based on the  $N^{th}$  component matrix equation. Then the newly updated current is used as the initial value for the second iteration. This process continues and the number of the iteration depends on the desired accuracy.

The iteration can be accelerated by relaxation factor such as that in Gauss-Seidel iterative method.

### B. Numerical Results and Analysis

The current distributions on the sphere illuminated by a plane wave axially are presented on the Fig.5 by accelerated PIM. The corresponding relative errors are also provided on the same graphs. It is obvious that the currents are gradually convergent to their MoM solutions and very close to them after 40 iterations. The relative errors are calculated using PIM and analytical solutions and after 40 iterations they actually become the errors between the analytical and MoM solutions. These errors can be improved using more triangular surface patches while segmenting the sphere.

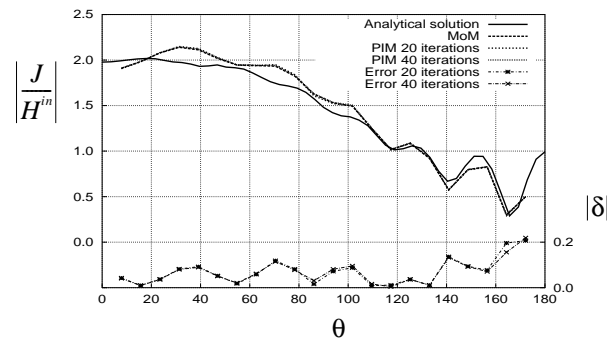


Fig.5 The current on the sphere illuminated by a plane wave axially by PIM with  $\omega = 1.8$  and 2 subregions for 20 and 40 iterations, compared with the analytical and MoM solutions. The relative errors are also provided.

PIM is also applied to a finite cylinder with top and bottom diameter  $2a = 0.55\lambda$  and height  $h = 0.1\lambda$ . Fig.6 is  $J$  by accelerated PIM.  $J$  represents the current from  $s=0$  to 1 along the contour on the E plane.

### 4. CONCLUDING REMARKS

The PNM divides the object into smaller parts and uses the concept of overlapping regions. It reduces the matrix size. Therefore the computer storage and the program running time are saved. Accurate solutions can be obtained for the TM case and good agreement with the full matrix MoM can be achieved for the TE case.

The SDT should be modified by not taking the virtual interface currents into account. The iteration procedure converges for the TM case, but not for the TE case except for an infinitely thin strip. Actually, the modified SDT is a special case of PNM in which the discarded pulse samples are zero.

The PNM is a simple and effective algorithm to eliminate the internal resonances without facing the ill-conditioned situation in which erroneous results would be obtained.

PIM's iterative procedure can make MoM equation solution convergent. It's decomposition technique can

save the computer storage, but more subregions will result in slow convergence rate.

The convergence rate can be accelerated by introducing the relaxation factor  $\omega$  to the PIM formulation. The optimum value of  $\omega$  is  $1.5 \leq \omega \leq 1.8$ .

In PIM with optimum  $\omega$ , normally, less than 30 iterations are needed to obtain convergent results regardless of the matrix size.

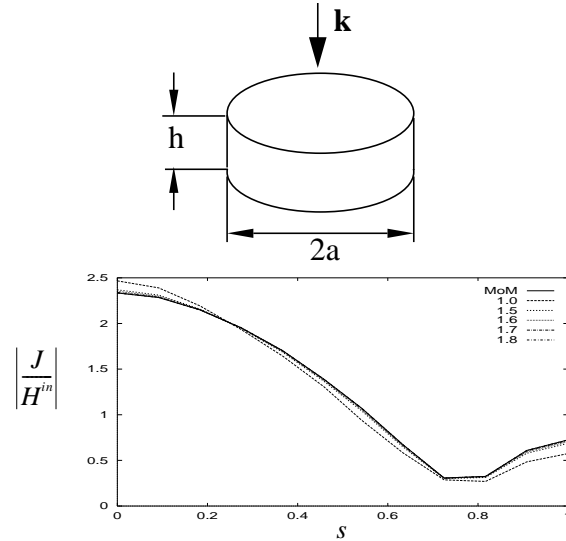


Fig.6  $J$  by PIM with 2 subregions, 50 iterations, and different  $\omega$ , compared with MoM solution.

### Acknowledgement

This work is supported by NSERC of Canada and IMT Corp., WPG, MB.

### References

- [Shaf77] L. Shafai, "A progressive numerical method and its application to large field problems in antennas and electromagnetic scattering," *Can. Elec. Eng. J.* 1977, 2, (4), pp. 17-23
- [Umas92] K. R. Umashankar, S. Nimmagadda, and A. Taflov, "Numerical analysis of electromagnetic scattering by electrically large objects using spatial decomposition technique," *IEEE Trans.*, 1992, AP-40, (8), pp. 867-877.
- [Bo92] Y. M. Bo and W. X. Zhang, "A Convergent Projective Iteration Method Combined with Spatial Decomposition for Solving EM Problems," *IEEE AP-S International Symposium, 1992 Digest Volume 1*, pp. 208-211.
- [Rao82] S. M. Rao, D. R. Wilton and A. W. Glisson, "Electromagnetic scattering by surface of arbitrary shape", *IEEE AP-30*, No. 3, May 1982, pp.409-418.
- [Ye96] Qiubo Ye, L. Shafai and S. Kashyap, "Large electromagnetic scattering computation using iterative Progressive Numerical Method," *Proc. of IEEE AP-S International Symposium, Baltimore, U.S.*, Jul. 1996.

# Reconstruction of Three Dimensional Inhomogeneous Bodies Using Unrelated Illumination

*Inas El-Babli*

Department of Electrical and Computer Engineering  
University of Manitoba, Winnipeg, Manitoba, Canada R3T 5V6  
<elbabli@ee.umanitoba.ca>

Advisor: *Abdel Razik Sebak*, <sebak@ee.umanitoba.ca>

*Abstract*--The unrelated illumination method is used to estimate the complex permittivities of three-dimensional inhomogeneous dielectric bodies. Starting from the integral representation of the electric field and using the method of moments, the object under investigation is illuminated by a group of unrelated incident fields. Computer simulations show that the method can be used to overcome the severe ill-posedness of the three-dimensional problem even in the presence of noise and with the use of only one detector to measure the external scattered field.

## 1 INTRODUCTION

In the last decade several numerical techniques have been developed for solving the inverse electromagnetic scattering problems and microwave imaging of inhomogeneous dielectric bodies. In particular two approaches have been utilized. The first is the microwave diffraction tomography [1]. It is a generalization of the classical x-ray computed tomography by taking into consideration the diffraction effects. This method can only handle low contrast, lossless bodies.

The second approach aims to solve the exact equation of the electromagnetic inverse scattering problem by numerical methods such as the method of moments (MoM) [2]. In which the problem solution is reduced to the solution of linear system of algebraic equations. Unfortunately the scattering matrix which governs the external scattered field induced by an internal equivalent current is highly ill-conditioned. Thus any attempt to compute its inverse makes the system ill-posed especially in the presence of noise. Several regularization techniques have been used [3], [4] aiming to reduce the effect of ill-conditioning. These employ priori information either to select a suitable regularization parameter or to enforce convergence in iterative techniques. Moreover, most of these techniques require the presence of a few number of scatterers and employ multiview illumination and some are only applicable to two-dimensional problems.

In this paper, the unrelated illumination method which has been tested before with two-dimensional bodies [5], is extended to handle three-dimensional inhomogeneous dielectric bodies. The method utilizes the method of moments (MoM) to discretize the nonlinear integral equation which relates the scattered field data and the complex permittivity. Yet, it differs from the other previous techniques in that the way of acquiring information helps overcoming the ill-posedness nature of the problem. This is maintained by the proper arrangement of the polarization and the direction of the incident electric fields aiming to illuminate the body with a group of unrelated incident fields. Numerical simulations are carried out to assess the method and to test its robustness in the presence of measured data uncertainties.

## 2 MATHEMATICAL FORMULATION

Consider an inhomogeneous dielectric body of arbitrary shape that is characterized by a dielectric constant  $\epsilon_r(r)$  and an electric conductivity  $\sigma(r)$ , both generally variable from point to point. The body is illuminated in free space by an incident wave with electric field  $E^i$ . The total electric field  $E$  at an arbitrary point  $r$  can be expressed as:

$$E(r) = E^i(r) + E^s(r) \quad (1)$$

where  $E^s(r)$  is the scattered field. Using the equivalent current modelling, the external scattered field  $E^s(r)$  can be written as:

$$E^s(r) = \int_v J_{eq}(r') \cdot \bar{\bar{G}}(r, r') dv' \quad (2)$$

where  $\bar{\bar{G}}$  denotes the free space dyadic Green's function and  $J_{eq}(r)$  is the equivalent current density given by:

$$\begin{aligned} \mathbf{J}_{eq}(r) &= k_o^2 \left( \epsilon_r(r) - 1 + \frac{\sigma(r)}{-j\omega\epsilon_o} \right) \mathbf{E}(r) \\ &= \tau(r) \mathbf{E}(r) \end{aligned} \quad (3)$$

Where  $\tau(r)$  is usually referred to as the contrast or the object function. Using equations (1) and (2), the total electric field  $\mathbf{E}(r)$  can thus be expressed as:

$$\mathbf{E}(r) = \int_v \mathbf{J}_{eq}(r') \cdot \bar{\bar{\mathbf{G}}}(r, r') dv' + \mathbf{E}^i(r') \quad (4)$$

Dividing the body into  $N$  cells and using the MoM [2] with pulse basis function and point matching procedure, equation (4) is transformed into:

$$\mathbf{E} = [\mathbf{G}_1] \mathbf{J}_{eq} + \mathbf{E}^i \quad (5)$$

Substituting for the equivalent current density, this can be rewritten as:

$$([\mathbf{G}_1] [\tau] - [\mathbf{I}]) \mathbf{E} = -\mathbf{E}^i \quad (6)$$

where  $\tau$  is a  $3N \times 3N$  diagonal matrix whose elements are the complex permittivities of each cell in the body:

$$\tau_{nn} = k_o^2 \left( (\epsilon_r(n) - 1) + j \frac{\sigma(n)}{\omega\epsilon_o} \right) \quad (7)$$

Similarly, the scattered field can be expressed in matrix form as:

$$[\mathbf{G}_2] [\tau] \mathbf{E} = \mathbf{E}^s \quad (8)$$

The matrix  $\mathbf{G}_1$  which is a  $3N \times 3N$  matrix, depends on the operating frequency and geometry of the cells. The matrix  $(\mathbf{G}_1 \tau - \mathbf{I})$  is always well posed. The matrix  $\mathbf{G}_2$  is  $3M \times 3N$ , where  $M$  is the number of measuring points, depends on the operating frequency, geometry of the cells and the relative positions of the cells and the measuring points.  $\mathbf{G}_2$  is highly ill-conditioned especially when a large dielectric body is involved. Thus trying to solve the system by computing its inverse renders the system ill-posed and forces the use of regularization techniques.

Usually  $\mathbf{E}^i$  is a  $3N \times 1$  vector but by using a  $3N$  unrelated incident fields (unrelated illumination method),  $\mathbf{E}^i$  is a  $3N \times 3N$  matrix which can be inverted. To obtain these  $3N$  unrelated incident fields a planar phased array is used and by adjusting the polarization of its elements we can obtain a diagonally dominant incident matrix.

Writing equation (6) in the form:

$$[\mathbf{E}] = -([\mathbf{G}_1] [\tau] - [\mathbf{I}])^{-1} [\mathbf{E}^i] \quad (9)$$

and substituting (9) into (8):

$$[\mathbf{G}_2] [\tau] ([\mathbf{G}_1] [\tau] - [\mathbf{I}])^{-1} [\mathbf{E}^i] = -[\mathbf{E}^s] \quad (10)$$

Making use of the fact that the incident matrix is well conditioned and thus invertible, (10) can be further written in the form:

$$\begin{aligned} & \left( [\mathbf{E}^s] [\mathbf{E}^i]^{-1} [\mathbf{G}_1] + [\mathbf{G}_2] \right) [\tau] \\ &= [\mathbf{E}^s] [\mathbf{E}^i]^{-1} \end{aligned} \quad (11)$$

where the only unknown is  $\tau$ . Denoting

$$[\Psi] = [\mathbf{E}^s] [\mathbf{E}^i]^{-1} [\mathbf{G}_1] + [\mathbf{G}_2] \quad (12)$$

and

$$[\Phi] = [\mathbf{E}^s] [\mathbf{E}^i]^{-1} \quad (13)$$

Equation (9) can be written in a simplified form as:

$$[\Psi] [\tau] = [\Phi] \quad (14)$$

and the elements of the diagonal matrix  $\tau$  are obtained by comparing the corresponding elements at any row of  $[\Phi]$  and  $[\Psi]$ . The complex permittivity of the  $n^{\text{th}}$  cell is given by:

$$\tau_{nn} = \Phi_{mn} / \Psi_{mn} \quad (15)$$

### 3 NUMERICAL SIMULATIONS AND RESULTS

In this section we report and discuss numerical results of computer simulations that have been performed to assess the capabilities of this technique. The numerical simulations are carried out using only one detector. Because of the three-dimensional nature of the problem, there are three measured values. A phased planner array is used to illuminate the body with a group of unrelated incident field. The values of the scattered electric field at the detector is obtained via a numerical program that can determine the direct scattering from three-dimensional inhomogeneous dielectric bodies.

In the absence of noise and irrespective of the permittivity distribution within the body under investigation, the relative mean square error of the reconstructed permittivity  $\delta\epsilon_r$  and conductivity  $\delta\sigma_r$  is found to be negligible.

$$\delta\epsilon_r = \frac{\left[ \sum_{n=1}^N (\epsilon_{rn} - \epsilon'_{rn}) \right]^{1/2}}{\left[ \sum_{n=1}^N \epsilon_{rn}^2 \right]^{1/2}} \quad (16)$$

Where  $\epsilon_{rn}$  and  $\epsilon'_{rn}$  stand for the values of the original relative dielectric permittivity and of the reconstructed relative dielectric permittivity in the  $n^{\text{th}}$  cell respectively. Similarly,

$$\delta\sigma_r = \frac{\left[ \sum_{n=1}^N (\sigma_{rn} - \sigma'_{rn}) \right]^{1/2}}{\left[ \sum_{n=1}^N \sigma_{rn}^2 \right]^{1/2}} \quad (17)$$

Where  $\sigma_{rn}$  and  $\sigma'_{rn}$  stand for the values of the original conductivity and of the reconstructed conductivity in the  $n^{\text{th}}$  cell respectively.

In order to study the effect of the measured data uncertainties on the reconstruction process, we added to the scattered field at the detector a random noise complex array. The real and imaginary parts of this array are constituted by two independent sequences of random variables with zero mean and a variance that can be varied to obtain different signal to noise (S/N) ratios.

Numerical simulations were carried out to test the method sensitivity to cell size, number of scatterers within the body and the strength of these scatterers [6]. The obtained results has proven the method to be reliable in reconstructing the permittivity distribution of lossless bodies even in the presence of noisy scattered field data.

In the following numerical simulations, the method is applied to lossy and geometrically complex inhomogeneous dielectric bodies.

We start with a rough model of the human head. The head is divided into five layers and 209 cells each is  $2 \times 2 \times 2 \text{ cm}$ . Fig. 1 shows the consecutive layers constituting the head and the different kinds of tissue involved. The values of the conductivity and the permittivity of different tissues are given in Table 1. Numerical simulation is carried out.

TABLE 1. Dielectric constants & conductivities and for human tissue at 300 MHz.

Tissue	Permittivity	conductivity
Bone	5.7	0.072
Skin	17.6	0.44
Muscle/Brain	53.0	1.33
Eye	80.0	1.9

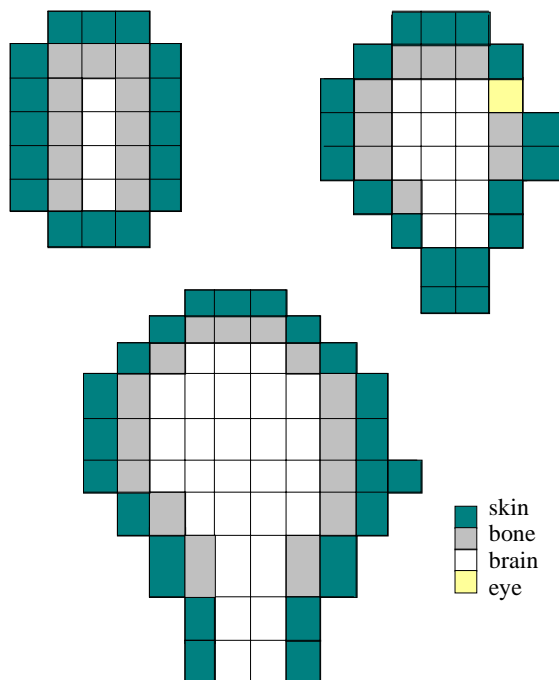


Fig 1 Five different layers forming the human head

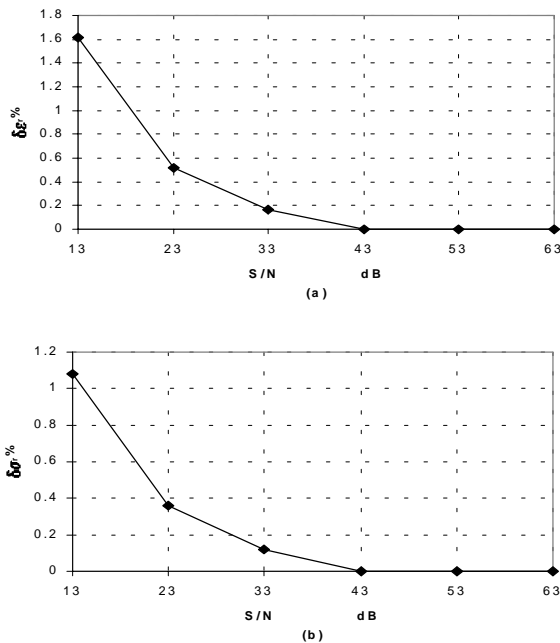
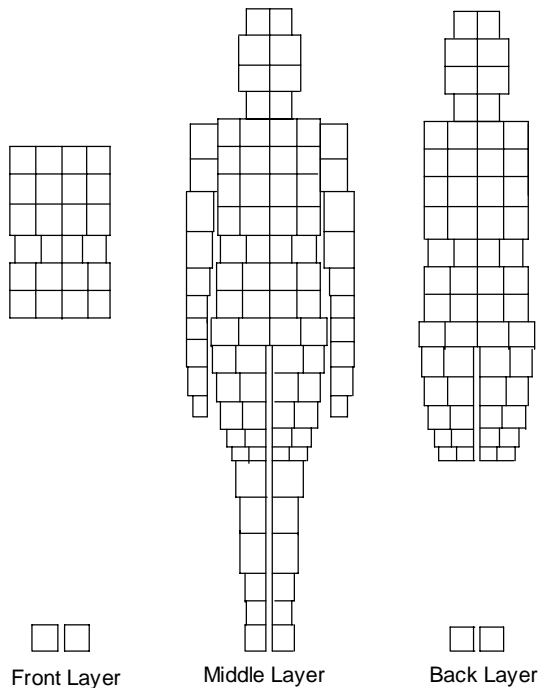


Fig.2 Percentage error in the permittivity (a), and conductivity (b) versus S/N.

Fig. 2(a) shows the percentage error for the reconstructed permittivity versus the signal to noise ratio and Fig. 2(b) shows the percentage error for the reconstructed conductivity. As shown the error is very

low even for small S/N ratios thus allowing accurate reconstruction of both.

The following simulation involves the use of a 180 cell model of human body (Fig. 3). This model is characterized by a variable cell size together with the fact that the average values for the conductivity and permittivity for the different tissues have been substituted in certain cells. Fig. 4(a) shows the percentage error in the permittivity versus the signal to noise ratio, and Fig. 4(b) shows the percentage error in the conductivity versus the signal to noise ratio. As shown by the plots, good reconstruction in the presence of very noisy data for both the conductivity and the permittivity were obtained.



**Fig3** Three layers constituting the 180-cell human body model.

#### 4 CONCLUSION

The unrelated illumination method is used for solving three-dimensional electromagnetic nonlinear inverse scattering problems. The method requires that the body under investigation is illuminated by a group of unrelated incident fields, thus forcing the incident matrix to be nonsingular. The method although similar to the multi-view illumination methods has the advantage of providing accurate reconstruction for geometrically complex lossy bodies using only one measuring point or detector and without any iterations.

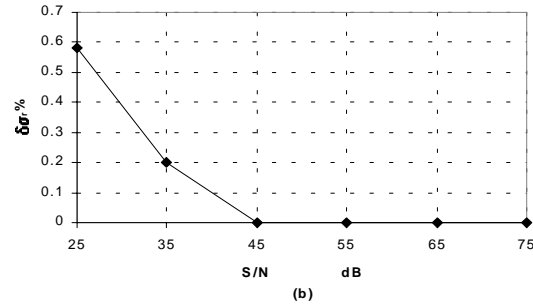
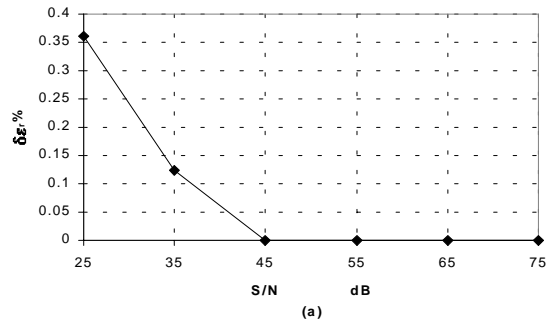


**Fig4.** Percentage error in the permittivity (a), and conductivity (b) versus S/N.

#### REFERENCES

- [1] E. Wolf, "Three-dimensional structure determination of semi-transparent objects from holographic data," *Opt. Commun.*, vol. 1, pp. 153-156, 1969
- [2] D. K. Ghodgaonkar, O. P. Gandhi, and M. J. Hagmann, "Estimation of complex permittivities of three-dimensional inhomogeneous biological bodies," *IEEE Trans. Microwave Theory Technol.* MTT-31, pp. 442-446, 1983.
- [3] S. Coarsi, S. Ciaramella, and L. Gragnani, "On the use of regularization techniques in numerical inverse-scattering solutions for microwave imaging applications," *IEEE Trans. Microwave Theory Technol.* vol. MTT-43, pp. 632-640, 1995.
- [4] Y. Qin and I. R. Ciric, "High resolution electromagnetic imaging of lossy objects in the presence of noise," *IEEE Trans. Magnetic*, vol. MI-31, pp. 1936-1939, 1995
- [5] W. Weiyan and Z. Shourong, "Unrelated illumination method for electromagnetic inverse scattering of inhomogeneous lossy dielectric bodies," *IEEE Trans. Antennas Propagat.* vol. 40, pp. 1292-1296, 1992.
- [6] El-Babli, I and A. Sebak, "Estimation of complex bodies using unrelated illumination," *Proc. 1997 IEEE AP-S conf. rencapp.* 1718-1721, 1997.

# EFFICIENT NUMERICAL ANALYSIS FOR APERTURE-COUPLED MICROSTRIP ANTENNA

*Ashraf Badawi*

Electrical and Computer Engineering Dept., University of Manitoba

<badawi@ee.umanitoba.ca>

Advisor: **Abdel Razik Sebak**, <sebak@ee.umanitoba.ca>

**Abstract--This article provides an accurate and computationally efficient method for the analysis of aperture coupling from microstrip line to microstrip patch, which is of significant interest in applications involving multilayered media. The accuracy of this method is ensured by satisfying all the boundary conditions through a mixed electric-magnetic current integral equation formulation, combined with the moment method. Computational efficiency is achieved by limiting the discretization to only the strips and apertures and by using the accurate and rapidly convergent complex images. Close agreement has been obtained between our results for the input impedance, published results, and experiment, over a wide frequency range.**

## I. INTRODUCTION

In the fields of microwave integrated circuits and antennas, there is a growing trend toward fabricating circuits made of more than one dielectric layer. These multilayered circuits have smaller size and less parasitic coupling between the active and passive elements which are separated by a ground plane. To achieve optimum design of the multilayered structures, it is important that an accurate and computationally efficient method be developed which can be easily interfaced with available optimization design software. Several methods have been presented in the literature to analyze the fundamental transition between a microstrip line and a microstrip patch through an aperture, as shown in Fig. 1. Some of these methods, like the TLM [1], require the discretization of the entire volume of the circuit. They are, therefore, very slowly convergent and require excessive memory. Also, the application of the integral equation technique of electric current only EFIE [2], requires segmenting the entire conducting surface of the transition, including the infinite microstrip ground plane. Therefore, the EFIE is numerically inefficient for solving the aperture coupling problem.

A more efficient form of the integral equation

technique was applied in [3] for the analysis of the aperture coupled microstrip antennas. Unlike the EFIE, which uses only electric currents, this technique uses both electric and magnetic currents which flow on the strips and apertures, respectively. This limits the discretization to only the strips and apertures, and therefore saves a lot of memory and computation time. However, [3] evaluates the time-consuming numerical integration of Sommerfeld integrals to obtain the spatial Green's functions of the structure. Therefore, there is still need for a technique that is faster and hence more suitable for use with current CAD programs.

In this article, we use a mixed electric-magnetic current integral equation formulation as in [3]. However, our Green's functions for the coupling between the electric currents of the microstrip line and the patch, magnetic currents of the apertures, and for the cross-coupling between the electric and magnetic currents are all calculated using the accurate and rapidly convergent complex image technique [4],[5]. This technique avoids the time-consuming numerical integration of Sommerfeld integrals and yields at least a tenfold reduction in computation time with less than 1% error as compared with the numerical integration. These complex images include the effect of the surface waves and leaky waves and, therefore, have no restriction on the substrate thickness. Other techniques have been used in the literature to enhance the speed of the Sommerfeld integrals such as the asymptotic subtraction method.

The next section explains our theoretical formulation. The third section provides comparisons between our results and several experimental and theoretical results. The final section provides conclusions.

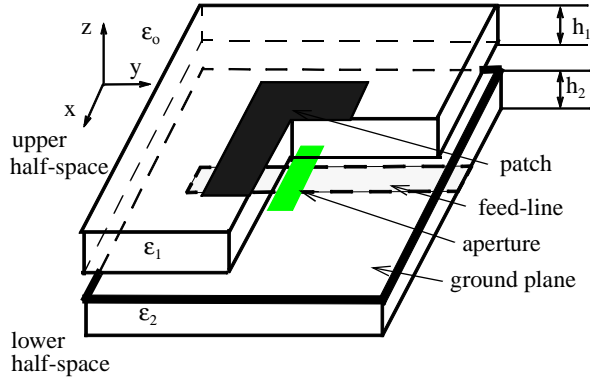


Fig. 1. Aperture-coupled patch antenna

## II. THEORY

To solve the aperture coupling problem, we split the structure of Fig. 1 into two subproblems, equivalent to the upper and lower half-spaces, as shown in same figure. Equivalent electric and magnetic currents flow on the microstrip line, microstrip patch and apertures, respectively, of both subproblems to satisfy the boundary conditions as follows:

*Boundary condition 1.* The continuity of the tangential electric field on the aperture is enforced by choosing the magnetic current on the aperture of the lower subproblem, which flows along the x-direction, to be equal and opposite to that on the aperture of the upper subproblem.

*Boundary condition 2.* The continuity of the tangential magnetic field on the aperture is satisfied by the following equation:

$$H_x^{(1)}(\mathbf{I}_e^{(1)}) + H_x^{(1)}(\mathbf{I}_{mx}^{(1)}) = H_x^{(2)}(\mathbf{I}_{ey}^{(2)}) + H_x^{(2)}(\mathbf{I}_{mx}^{(2)}) \quad (1)$$

where  $\mathbf{I}_e^{(1)}$ ,  $\mathbf{I}_{ey}^{(2)}$  are the electric currents flowing on the upper and lower microstrips, respectively, while  $\mathbf{I}_{mx}^{(1)}$ ,  $\mathbf{I}_{mx}^{(2)}$  are the x-directed magnetic currents flowing on the aperture in the upper and lower subproblems, respectively.

$H_x^{(1)}(\mathbf{I}_e^{(1)})$ ,  $H_x^{(2)}(\mathbf{I}_{ey}^{(2)})$  is the x-directed magnetic field on the aperture of the ith subproblem caused by an y-directed electric current on the microstrip line or a x-directed magnetic current on the aperture, respectively.

The fields in eq. (1) can be expressed in terms of the mixed potentials of electric and magnetic currents [6], as follows:

$$H_x^{(i)}(\mathbf{I}_{mx}^{(i)}) = -j\omega \int_{Aper} G_{Fxx}^{(i)}(r/r') J_{mx}^{(i)}(r') dS' + \frac{1}{j\omega} \int_{Aper} \frac{\partial}{\partial x} \left[ G_{qm}^{(i)}(r/r') \frac{\partial J_{mx}^{(i)}}{\partial x} \right] dS' \quad (2)$$

$$H_x^{(i)}(\mathbf{I}_e^{(i)}) = H_{x,yy}^{(i)}(\mathbf{I}_e^{(i)}) + H_{x,zy}^{(i)}(\mathbf{I}_e^{(i)}) \quad (3)$$

where:

$$H_{x,yy}^{(i)}(\mathbf{I}_e^{(i)}) = \left[ \vec{\nabla}_y \int_{M_i} G_{Axx}^{(i)}(r/r') \mathbf{J}_e^{(i)}(r') \hat{y} dS' \right] \cdot \hat{x} \quad (4)$$

$$H_{x,zy}^{(i)}(\mathbf{I}_e^{(i)}) = \left[ \vec{\nabla}_y \int_{M_i} G_{Azx}^{(i)}(r/r') \mathbf{J}_e^{(i)}(r') \hat{z} dS' \right] \cdot \hat{x} \quad (5)$$

In eq. 2, use has been made of the continuity equation for magnetic current and charge [6].

$G_{Fxx}^{(i)}$  in eq. (2) is the Green's function for the x-direction electric vector potential due to an x-directed magnetic current in the ith subproblem [7], whereas  $G_{qm}$  is the scalar potential due to magnetic charge [7].  $G_{Axx}^{(i)}$  in eq. (4) is the Green's function for the x-directed magnetic vector potential due to an x-directed electric current in the ith subproblem, whereas  $G_{Azx}^{(i)}$  in eq. 5 is the Green's function for the z-directed magnetic vector potential due to an x-directed electric current, with both source and field located inside a microstrip substrate. These Green's functions are given in [7].

$\hat{x}$ ,  $\hat{y}$  are unit vectors in the x- and y-directions, respectively, and  $M_i$  is the microstrip of the ith subproblem.

*Boundary condition 3.* The vanishing of the tangential electric field on the microstrip lines of the upper and lower subproblems is satisfied by:

$$E_{x,y}^{(i)}(\mathbf{I}_e^{(i)}) + E_{x,y}^{(i)}(\mathbf{I}_{mx}^{(i)}) = -E_y^{in} \quad (6)$$

where  $i=1, 2$  correspond to the upper and lower subproblems, respectively.  $E^{(i)}$  and  $E^{in}$  are the scattered and impressed electric fields, respectively. The electric and magnetic current densities are expanded as follows:

$$J_{e(x,y)}(x,y) = \sum_{n=1}^N \sum_{m=1}^{M-1} I_{x,y}^{nm} P_{e(x,y)}^{nm}(x,y) \quad (7)$$

and

$$J_{mx}(x) = \sum_{l=1}^L K_x^l P_{mx}^l(x) \quad (8)$$

where N, M and L are the number of segments on the microstrip and aperture, respectively.  $P_e$ ,  $P_m$  are roof top basis functions.

The Galerkin moment method [8] is then applied to eqs. (1) and (6), using the expansion functions of eqs. (7) and (8) also as weighting functions. This results in the following matrix equation:

$$\begin{bmatrix} \mathbf{0} \\ \mathbf{0} \\ V_{in} \end{bmatrix} = \begin{bmatrix} [Z_{ee}^{(1)}] & [Z_{em}^{(1)}] & [0] \\ [Z_{me}^{(1)}] & [Z_{mm}^{(1)}] + [Z_{mm}^{(2)}] - [Z_{me}^{(2)}] & \\ [0] & [Z_{me}^{(2)}] & [Z_{ee}^{(2)}] \end{bmatrix} \begin{bmatrix} I_e^{(1)} \\ I_{mx}^{(1)} \\ I_{ey}^{(2)} \end{bmatrix} \quad (9)$$

where  $Z_{ee}^{(1)}$ . and  $Z_{ee}^{(2)}$ . are the lower and upper microstrip impedance matrices, respectively [4].  $Z_{mm}^{(1)}$  and  $Z_{mm}^{(2)}$ . are the lower and upper magnetic-magnetic aperture impedance matrices, respectively. These represent the dual of the electric-electric impedance matrices in [4].  $Z_{me}^{(1)}$  and  $Z_{me}^{(2)}$  are the matrices for the magnetic voltages on the aperture due to unit electric currents on the microstrips o.  $Z_{em}^{(2)}$  and  $Z_{em}^{(2)}$  are the matrices for the electric voltages on the microstrips of the lower and upper subproblems, respectively, due to unit magnetic currents on the aperture. The details of the expressions and calculations of the self-terms of the matrices  $Z_{ee}$ ,  $Z_{mm}$  in eq. (9) may be found in [7].

It is important to mention that the Green's functions in this article are evaluated using the complex images method (DCIM) [4], [5]. Sommerfeld integrals are normally used to perform the inverse Fourier transform of the spectral functions. Instead, the spectral functions are approximated as finite sums of complex exponentials. The quasi-static images and the surface wave poles are extracted from the integrand of the Sommerfeld integral. Their contribution is handled through the residue theorem.

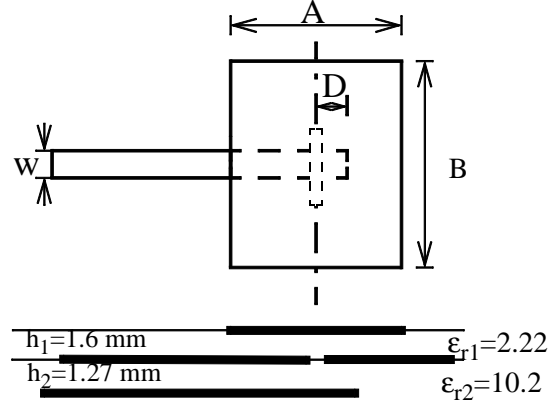


Fig. 2. Geometry for an aperture coupled microstrip patch. A=4cm, B=3cm, w=1.16mm, D=1.1cm, Slot width=1.1mm, length=1cm

Next the remaining integrand is approximated via a finite set of complex images with complex amplitudes and complex locations through the generalized pencil of functions (GPOF) method[7]. Finally the Sommerfeld integral is performed in a closed form using the Sommerfeld identity.

Our numerical tests have revealed that the complex images provide at least a tenfold reduction in computation time with less than 1% error as compared with the numerical integration of Sommerfeld integrals.

The current analysis uses the DCIM as applied to a single layer of dielectric, in either of the half spaces studied. The method itself was extended to handle several layers of dielectric materials for stacked patches [9]. Research is currently being made to handle vertical conductors in a multilayer environment, the results will be published soon.

### III. NUMERICAL RESULTS

To test the validity of the numerical model, the geometry in Fig.2 is analyzed using the technique described above. The configuration used for the substrate thickness and dielectric constants mimics the monolithic phased array applications. The feed substrate could be Gallium Arsenide for phase shifters and other active circuitry.

The results for the Smith chart for the calculated input impedance are shown in Fig. 3, in which the results are compared with the results published in

[10]. We notice that we have a good agreement with the measurements over the frequency band width simulated. The figures on the smith chart are the frequency in MHz.

several other examples are tested, with the results also are in good agreement with other commercial numerical software. Some of the results of these tests will be included in the presentation.

While, our testing for the efficiency of the methods was done as compared to the conventional method of analyzing printed antennas. New commercial CAD programs apply numerous acceleration schemes to enhance to speed of the execution of their code. Still, our code compares favorably in execution speed even with commercial software. The same example discussed above on the same machine was analyzed using both methods, our technique was almost twice as fast.

Care should be taken also, that as the geometry of the problem gets more complex, the time for the matrix solution becomes the dominant factor, and not the evaluation of the Green's function.

#### IV. CONCLUSION

In this study we have presented an accurate and computationally efficient method for solving the problem of aperture coupling from microstrip line to microstrip patch. This method uses a mixed potential integral equation, using both electric and magnetic currents with the method of moments. Comparison with the measured results demonstrates the accuracy of the proposed method.

Unlike other methods presented in the literature to solve this transition (like TLM and EFIE), our efficient application of the moment method (of discretizing only the strips and apertures) combined with the accurate and rapidly convergent complex images Green's functions, makes this method more suitable for use with CAD/CAE software to achieve optimum designs for aperture coupled microstrip patches.

#### ACKNOWLEDGEMENTS

This work is sponsored by NSERC and the University of Manitoba.

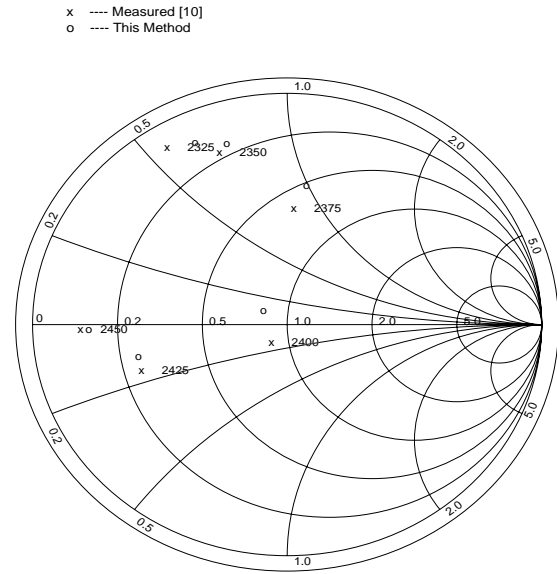


Fig. 2. The Smith chart plot for the input impedance of the antenna in Fig. 2. compared with the measurements in [10]

#### REFERENCES

- [1] N. Simons, A. Sebak and A. Ittipiboon, "Analysis of the aperture coupled microstrip antenna and circuit structures using the TLM method", IEEE Antennas and Prop. magazine, Vol. 37, pp. 27-37, 1995.
- [2] A. Badawi and A. Sebak, "Analysis of microstrip antennas integrated with feed networks", ANTEM96, pp. 391-394, Montreal, 1995.
- [3] R. C. Hall, and J. R. Mosig, "The analysis of arbitrarily shaped aperture-coupled patch antenna via a mixed potential integral equation" IEEE Trans. Ant. Propag., Vol. AP-44, 1996, pp. 608-614.
- [4] A. A. Omar and Y. L. Chow, "A Solution of Coplanar Waveguide and Air-Bridges Using Complex Images," IEEE Trans. Microwave Theory Tech., Vol. MTT-40, No. 11, Nov. 1992, pp. 2070-2077.
- [5] Y. L. Chow, J. J. Yang, D. G. Fang, and G. E. Howard, "A Closed Form Spatial Green's Functions for Thick Microstrip Substrates," IEEE Trans. Microwave Theory Tech., Vol. MTT-39, No. 3, March 1991, pp. 588-593.
- [6] R. S. Elliott, Antenna Theory and Design, Prentice Hall, Englewood Cliffs, NJ, 1981.
- [7] G. Dural and M. I. Aksun, "Closed form Greens function for general sources and stratified media" IEEE Trans. Microwave Theory Tech., Vol. MTT-43, No. 7, July 1995, pp. 1545-1552.
- [8] R. E. Collin, Field Theory of Guided Waves. Mc-Graw Hill, New York, 1991.
- [9] A. Badawi and A. Sebak, "Analysis of Stacked Microstrip Patch Antennas Using Closed Form Green's Function" URSI meeting Montreal, 1997, pp. 104.
- [10] D. M. Pozar, "A reciprocity method of Analysis of slot-coupled microstrip antenna". IEEE Trans. Ant. Propag., Vol. AP-34, Dec. 1986, pp. 1439-1446.

# TWO METHODS FOR EFFICIENCY INCREASE OF TRIPLATE ARRAY

*D.P. Gray*

Dept. of Electrical & Computer Engineering,

University of Manitoba, Winnipeg, Canada R3T 5V6 [dgray@ee.umanitoba.ca]

Advisor: L. Shafai

**Abstract**—Two methods to improve the aperture efficiency of a type of triplate array are presented.

## 1. INTRODUCTION

Triplate line fed arrays have been researched extensively over the last 10 years for DBS television subscriber antenna in Japan and Europe. The chief advantage of this type of planar array is the reduction of radiation from the array's feedlines. One class of triplate fed array employs a thin metal sheet with apertures punched for radiation from patches on the triplate layer [1], Figure 1. This type of triplate array is considered as a candidate for LMCS subscriber antenna. The focus of this research is to identify different methods for increasing the aperture efficiency of this type of triplate fed array, in order to counter the losses that are expected to occur at EHF.

With careful spacing of the radiating elements, the parallel plate mode can be suppressed, and an aperture efficiency of 73% can be achieved [2]. Addition of a small parasitic patch above each aperture has been shown to raise the aperture efficiency to 86%, rivalling the aperture efficiency of a parabolic reflector [2]. However, this requires an additional foam spacer and thin film layer, which are difficult to laminate to subsequent layers. Alignment is also a concern.

The computational results presented in this paper were obtained from the

commercially available MOM software, Zeland™ version 4.2.

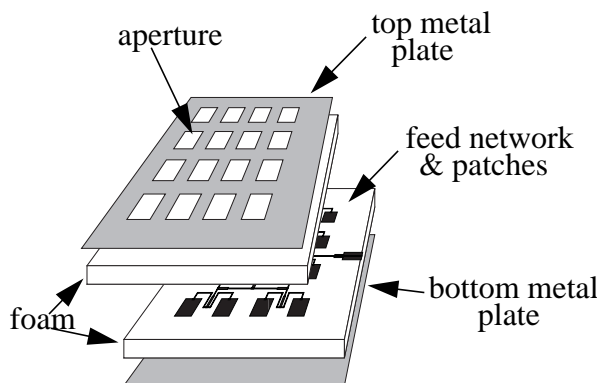


Figure 1: A Triplate Array Configuration

## 2. FEED NETWORK CONFIGURATIONS

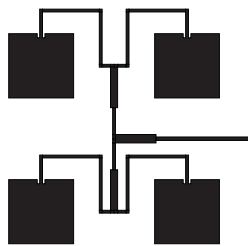


Figure 2

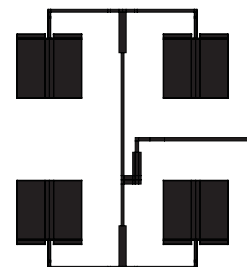


Figure 3

A standard configuration corporate feeding system has been used for triplate array in the past [1], Figure 2. It has been shown that replacing this standard configuration with one incorporating a 180° delay line for the 2 X 2 sub-arrays gives an improvement in aperture efficiency [3]. When applied to triplate array, Figure 3, the sidelobes in the E-plane are reduced and the radiation efficiency is increased over that of the normal configuration. This translates to an increase in

the aperture efficiency compared to the normal configuration, Figure 6. No additional manufacturing steps are required for this method, compared to that required for the existing array designs.

### 3. PARASITIC T ELEMENTS

The computational results presented show that the parasitic patches can be replaced by parasitic dipole elements punched out of the top ground plane, Figure 4. These parasitic elements give a similar improvement to aperture efficiency as gained by the parasitic patches, Figure 6. The main effect of the parasitic elements is an increase in the directivity of the 2 X 2 sub-array, Figure 5, which results from lower sidelobes in the E-plane and H-plane. The numerically controlled milling machines used to stamp out the apertures in the top ground plane are capable of punching the parasitic dipole elements. Thus a possible means of increasing aperture efficiency of triplate array has been found, that requires little additional manufacturing steps.

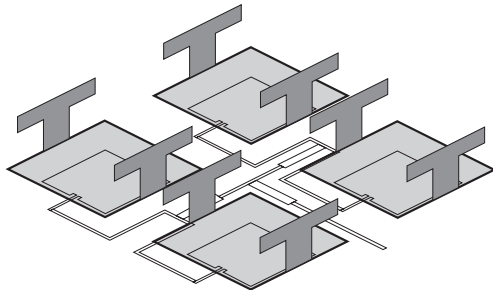


Figure 4

### 4. FUTURE WORK

Future work will entail experimental optimisation of the two methods for aperture efficiency improvement of this type of triplate array.

### 5. ACKNOWLEDGEMENTS

The authors wish to thank Prof. Misao Haneishi for his support and encouragement. This research is made possible by a TRILabs scholarship.

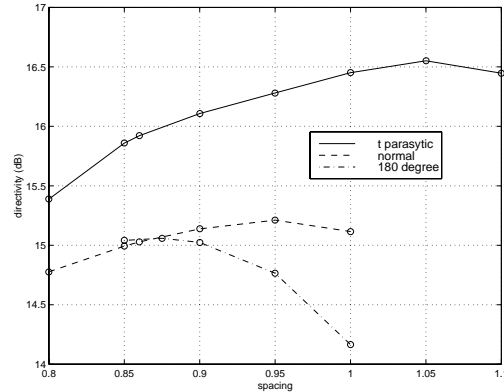


Figure 5

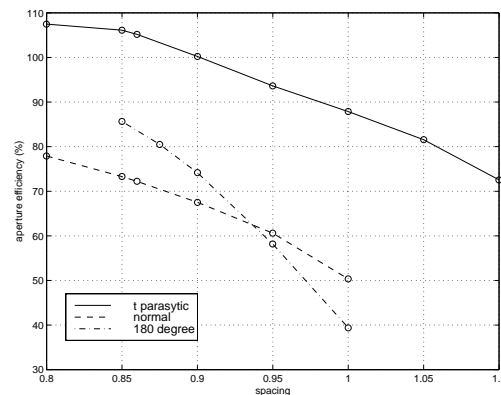


Figure 6

### 6. REFERENCES

- [1] H. Ishizaka, S. Wakushima, H. Mizugaki & M. Ohta, US patent 5510803
- [2] H. Ishizaka, M. Ohta, S. Wakushima & M. Haneishi, "Radiation properties of Triplate feed type Patch Antennas with Parasitic Elements", paper #B-61, Proceedings of the 1992 IEICE Conference {spring}, 1992
- [3] D. Gray, C.B. Ravipati & L. Shafai, "Corporate Fed Microstrip Array for LMCS", Poster Session P19, TRILabs Tech Forum, Oct. 1997

# EXTRACTION OF SCATTERING MATRIX COEFFICIENTS OF NRD AND WAVEGUIDE DISCONTINUITIES BY THE TLM METHOD

B. Ghosh\*, N. Simons\*\*, L. Shafai\* , A. Ittipiboon\*\* , A. Petosa\*\*, M. Cuhaci\*\*

\*Antenna Laboratory  
Department of Electrical and Computer Engineering  
University of Manitoba, Winnipeg, Manitoba, Canada R3 T 5V6.

\*\*Advanced Antenna Technology Group  
Communications Research Centre, 3701 Carling Avenue, Ottawa,  
Ontario, Canada K2H 8S2.

Email: ghosh@uda.dgcd.doc.ca, neil.simons@crc.ca, shafai@ee.umanitoba.ca,  
apisak.ittipiboon@crc.ca, aldo.petosa@crc.ca, michel.cuhaci@crc.ca

*Abstract* - The Transmission-Line Modelling Method is used to characterise a slot on the ground-plane of a non-radiating dielectric waveguide (NRD). An approach based on modal decomposition is developed to extract the generalised scattering parameters for a waveguide discontinuity.

## I. INTRODUCTION

NRD has received considerable attention due to its low loss nature and the ability to suppress radiation at bends and discontinuities. It is proposed to exploit the above properties to design a NRD based slot array. Previous work relied on measured data for the admittance of a single slot in the ground plane of the NRD. In this paper, a single slot in the NRD ground plane is characterised using the TLM method. The perfectly matched layer (PML) Absorbing Boundary Condition was used to ensure minimal reflection from the exterior boundaries of the computational domain. It is also shown that a  $s_{11}$  of -40 dB is achieved when the PML is used to terminate the NRD.

Modal decomposition was used to determine the scattering parameters for a discontinuity in a rectangular waveguide in the presence of evanescent modes. Results obtained were

found to be in close agreement to those in the literature. Currently, this method is being extended to evaluate the  $s_{11}$  of the slot on the ground plane of the NRD.

## II. PERFORMANCE OF THE 3-D TLMBASED PML

The PML was implemented in the same manner as in [Duba97]. For validation, the PML was first applied to a rectangular metallic waveguide and the results compared with previously published data [Bere97]. Based on this success, the PML was then applied to the termination of the NRD.

The rectangular metallic waveguide was excited by the  $TE_{10}$  mode with both ends terminated by PMLs, as shown in Fig.1. Two observation points were placed on one side of the excitation and the total field was observed in the frequency domain at these points. Using the approach in [Krup93], the reflection coefficient was then obtained. Fig.2 shows that for most of the operating range, a reflection coefficient of better than -40 dB was obtained. Using a similar approach, the reflection coefficient obtained for the case of the NRD with PML terminations on both ends was of the order of -40 dB, as shown in Fig. 3.

### III. SLOT IN NRD GROUND PLANE

Fig. 4 shows the configuration of the slot in the NRD ground plane. PMLs were used to terminate the computational domain in the air region above the slot. Fig. 5 shows the comparison between the simulated results and measurements performed using a HP 8510 Network Analyser.

### IV. EXTRACTION OF SCATTERING MATRIX COEFFICIENTS FOR A WAVEGUIDE DISCONTINUITY IN THE PRESENCE OF EVANESCENT MODES

In the computation of the scattering matrix coefficients for the case of a rectangular waveguide or the NRD, the observation points were placed a guided wavelength from the discontinuity to ensure that the evanescent modes from the discontinuity have decayed sufficiently. This necessitated the use of a large computational domain. In the method developed below, the scattering matrix coefficients for the case of a waveguide discontinuity were obtained close to the discontinuity. At this location, both higher order propagating as well as evanescent modes are present. A method similar to that outlined in [Haff92] for the FDTD method was used.

The transient EM fields computed by the TLM simulation were transformed to the frequency domain at two surfaces,  $S_1$  and  $S_2$ , on the incident side of the discontinuity. On the surface  $S_1$ , the EM fields can be determined from the potential function :

$$F_1(\omega) = A_1\psi_1(x, y)e^{-j\beta_1z} + B_1\psi_1(x, y)e^{j\beta_1z} + \sum_{n=2}^{\infty} B_n\psi_n(x, y)e^{j\beta_nz} \dots\dots\dots(1)$$

where  $A_1$  and  $B_1$  are the incident and reflected wave amplitudes respectively of the dominant

mode,  $B_n$  is the wave amplitude of the  $n^{\text{th}}$  mode reflected from the discontinuity,  $\beta_1$  and  $\beta_n$  are the propagation constants of the dominant mode and the  $n^{\text{th}}$  mode respectively,  $\psi_1(x, y)$  and  $\psi_n(x, y)$  are the potential functions of the dominant mode and the  $n^{\text{th}}$  mode respectively. Multiplying equation (1) by the eigenfunction of the incident dominant mode and applying orthogonality yields one of a pair of equations relating  $A_1$  and  $B_1$ . A similar operation on fields on the other surface  $S_2$ , yields another equation involving  $A_1$  and  $B_1$ , from which the  $s_{11}$  of the dominant mode can be obtained. Fig.6 shows the comparison between results obtained for the  $s_{11}$  of the waveguide discontinuity when the observation points were placed 5 cells from the discontinuity as compared to the case when the observation points were placed 94 cells from the discontinuity. The principle of conservation of power was used to further validate our approach as shown in Table 1.

### V. CONCLUSION

In this paper, the reflection coefficient from a single slot on the ground plane of the NRD has been studied. This enables us to design an NRD based slot array without the need for using the experimental design curves for a single slot in [Malh84]. Thereafter, the reflection coefficient of a waveguide discontinuity was obtained for the case when the observation points were located close to the discontinuity, thus significantly reducing the computational burden. We intend to apply the same approach to NRD discontinuities.

### ACKNOWLEDGEMENT

The authors would like to acknowledge J. Bradley of the Communications Research Centre for the measurements with the NRD and to the reviewers for their scrutiny and helpful suggestions.

REFERENCES

- [Duba97] J.L. Dubard and D. Pompei, "A Modified 3-D TLM Variable Node for the Berenger's Perfectly Matched Layer Implementation", *13th. Annual Review of Progress in Applied Computational Electromagnetics* Monterey, CA, pp. 661-665, Mar 1997.
- [Bere97] J.P. Berenger, "Numerical Reflection of Evanescent Waves from Perfectly Matched Layers", *IEEE Antennas and Propagation Symposium Digest*, pp. 1888-1891, July 1997.
- [Krup93] D.V. Krupezevic, V.J. Brankovic and F. Arndt, "The Wave-Equation FD-TD Method for the Efficient Eigenvalue Analysis and S-Matrix Computation of Waveguide Structures", *IEEE Trans. Microwave Theory Tech*, vol. MTT-41, no. 12, pp. 2109-2115, Dec. 1993.
- [Malh84] J.A.G. Malherbe, J.H. Cloete, I.E. Losch, M.W. Robson and D.W. Davidson, "The Design of a Slot Array in Nonradiating Dielectric Waveguide, Part II: Experiment", *IEEE Trans. Antennas Propagation* vol AP-32, no. 12, pp. 1341-1344, Dec. 1984.
- [Haff92] S. Haffa, D. Hollmann and W. Wiesbeck, "The Finite Difference Method for S-Parameter Calculation of Arbitrary Three-Dimensional Structures", *IEEE Trans. Microwave Theory Tech* vol. 40, no. 8, pp. 1602-1610, Aug. 1992

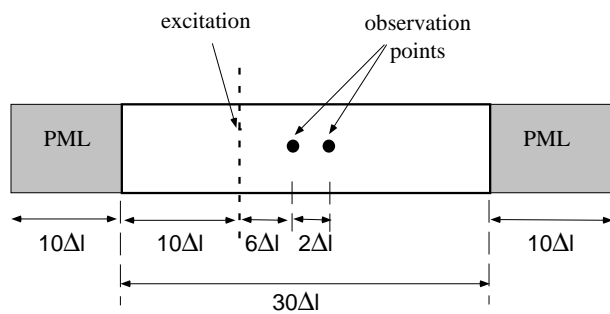


Fig. 1 Rectangular waveguide terminated by a PML on both sides.

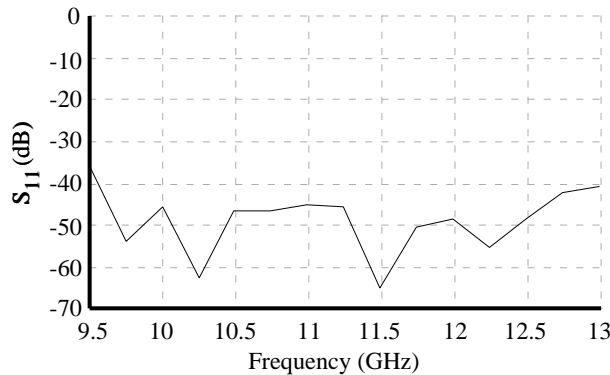


Fig. 3 Return loss for NRD with PML termination.

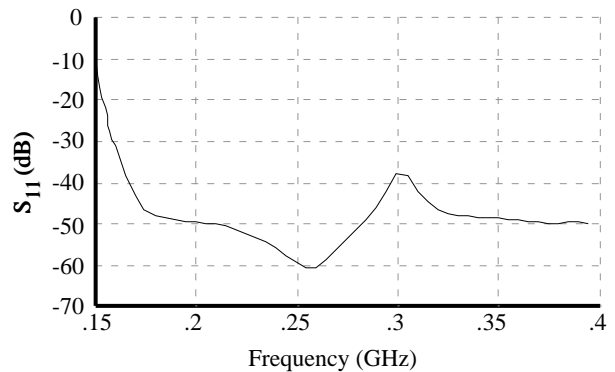


Fig. 2 Return loss for rectangular waveguide with PML termination.

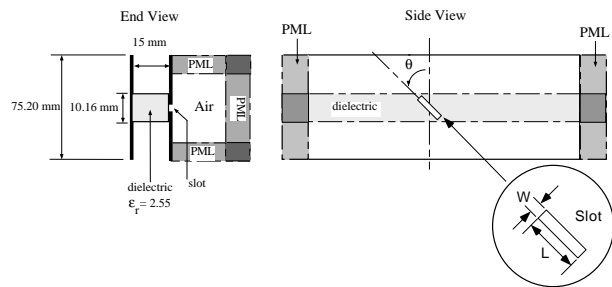


Fig. 4 Configuration of an NRD slot.

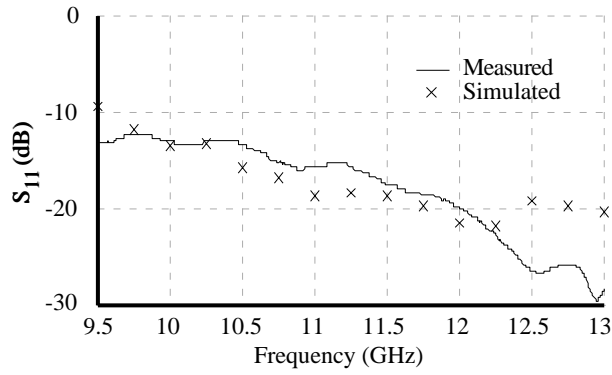


Fig. 5a Return loss for NRD with slot at  $\theta = 50^\circ$ .

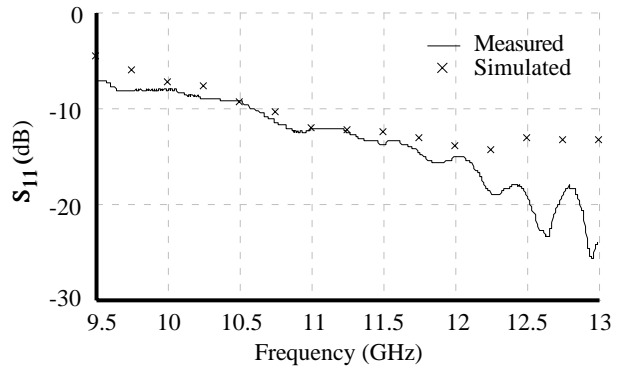


Fig. 5b Return loss for NRD with slot at  $q = 80.5^\circ$ .

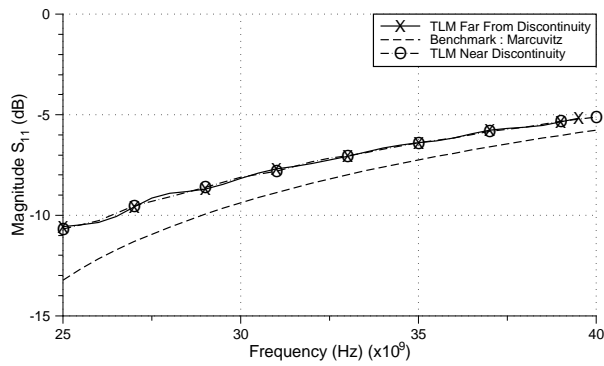


Fig. 6 Return loss for a waveguide discontinuity.

Freq. (GHz)	Reflected+Transmitted power as % of incident power
43.0	99.99
43.5	99.98
44.0	99.98
44.5	99.98
45.0	99.98
45.5	99.98
46.0	99.98

Table 1 Conservation of Power for a waveguide with multiple propagation modes.

# Review of TCP over Wireless Networks

*Sihong Lei*

shlei@ee.umanitoba.ca

Department of Electrical and Computer Engineering  
University of Manitoba, Winnipeg, Manitoba, Canada R3T 5V6  
Advisor: *David Blight* <blight@ee.umanitoba.ca>

*Abstract*-- A review of TCP performance over wireless networks is presented. This paper includes a literature review, an overview of proposed techniques designed to improve the performance of TCP in wireless networks, and a proposed research plan.

## 1. Introduction

With the rapid growth of the mobile computers in recent years, the study of reliable transport protocols such as TCP [1, 2] in wireless networks has become an important and active area of research. The Transmission Control Protocol (TCP) is a reliable transport protocol turned to perform very well in traditional wired networks by providing flow, congestion, and error control mechanisms. The increased interest in TCP over wireless links is motivated by the need of emerging network technology, the popular application of TCP in a wide variety of networks as well as economic considerations. A number of simulations and experiments have shown that TCP performance degrades in the wireless networks [5-7, 10]. The main reason is that errors (e.g. packet loss) in the wired networks are usually assumed to be as a result of congestion due to the relatively low transmission errors, however in the wireless networks errors are often caused by many other factors that are unrelated to congestion, such as the effects of fading, interference and mobility.

Because of the communication characteristics of wireless links such as limited bandwidth, high latencies, high bit error rates, and temporary disconnection caused by user mobility and handoffs [3-6], the modification of the TCP protocol to provide reliable connection for the transfer of data between applications in wireless networks is a challenging problem. Many papers address this topic. Proposed solutions include introducing a new session layer protocol on top of TCP at both base stations and mobile hosts without changing the protocol software on ordinary station hosts [7], modifying network-layer software at the base station and mobile host without violating end-to-end TCP semantics [8], splitting the TCP connection into two separate connections at the base station-- one between the fixed host and the base station, and other between the base station and the mobile host [11], combining forward error correction with link-layer retransmissions [6], the snoop protocol [8, 9], selective acknowledgments approach [14,15], the fast-retransmit approach [10] and link-level retransmissions [13] etc. These protocols are classified into three broad categories [12]: link-layer protocols, that provide local reliability; split connection protocols, that break the end-to-end connection into parts at the base station; and end-to-end proposals, where loss recovery is performed by sender. A comparison and analysis of the mechanism for improving TCP Performance over wireless link is also provided in [12]. From their experimental

results, a reliable link-layer protocol that is TCP-aware provides very good performance and selective acknowledgments and explicit loss notifications also result in significant performance improvements.

## 2. Future Research Plans

Future research plans include a more thorough literature review and reliable transport protocol design over wireless networks by using digital coding techniques and modifying the existing protocols. Following the selection of the most promising protocol design and modification, a model, implementation, simulation, performance evaluation and usage-based validation analysis will be undertaken.

## References

- [1] W.R.Stevens, *TCP/IP Illustrated*, Volume 1. Addison Wesley, Reading, MA, No v. 1994.
- [2] J.B. Postel, *Transmission Control Protocol. RFC*, Information Sciences institute, Marana del Re CA, September 1981. RFC 793.
- [3] D. Duchamp and N. F. Reynolds *Measured Performance of Wireless LAN* In Proc. of 17th IEEE Conf. on Local Computer Networks, pages 494-499, September 1992.
- [4] A. DeSimone, M.C. Chuah, and O.C. Yu *Throughput Performance of Transport Layer Protocols over Wireless LANs* In Proceeding of IEEE GLOBECOM '93, November 1993
- [5] R. Caceres and L. Iftode *The effect of mobility on reliable transport protocols*, Technical Report MITLTR-73-93, Matsushita Information Technology Laboratory, Princeton, New Jersey, November 1993.
- [6] E.Ayanoglu, S. Paul, T.F. LaPorta, K.K Sabnani, and R.D. Gitlin, *AIRMAIL: A Link-Layer Protocol for Wireless Networks*, ACM ACM/Baltzer Wireless Networks Journal, 1:47-60, February 1995.
- [7] R.Yavatkar and N. Bhagwat *Improving End-to-End Performance of TCP over Mobile Internetworks*, In Mobile 94 Workshop on Mobile Computing Systems and Applications, December 1994.
- [8] E.Amir, H.Balakrishnan, S. Seshan, and R.H. Katz, *Efficient TCP over Networks with Wireless Links* In Proc. Fifth IEEE Workshop of Hot Topics in Operating System, May 1995
- [9] H.Balakrishnan, S. Seshan, and R.H. Katz *Improving Reliable Transport and Handoff Performance in Cellular Wireless Networks*, ACM Wireless Networks, 1(4), December 1995.
- [10] R.Caceres and L. Iftode *Improving the Performance of Reliable Transport Protocols in Mobile Computing Environments*, IEEE Journal on Selected Areas in Communications, 13 (5), June 1995.
- [11] A.Bakre and B.R. Badrinath *I-ICP: Indirect TCP for Mobile Hosts*, Technical Report DCS-TR-314, Rutgers University, October 1994.
- [12] H.Balakrishnan, V. N. Padmanabhan, S. Seshan, and R.H. Katz *A Comparison of Mechanisms for Improving TCP Performance over Wireless Links*, IEEE/ACM Transactions on Networking, December 1997.
- [13] S.Paul, E. Ayanoglu, T.F. LaPorta, K.H. Chen, K.K. Sabnani, and R. D. Gitlin *An Asymmetric Link-Layer Protocol for Digital Cellular Communications*. In Proc. InfoComm '95, 1995.
- [14] M. Mathis, J. Mahdavi, S. Floyd, and A. Romanow, *TCP Selective Acknowledgment Option*, RFC-2018.
- [15] S. Keshav and S. Morgan *SMART Retransmission: Performance with Overload and Random Losses*, In Proc. Infocom'97, 1997.

# Turbo Processing Techniques for Digital Communications over Wireless Mobile Fading Channels

Ha Hoang Nguyen

Department of Electrical and Computer Engineering  
University of Manitoba; Winnipeg, Manitoba, Canada R3T 5V6  
nguyen@ee.umanitoba.ca  
Advisor: Prof. E. Shwedyk (shwedyk@ee.umanitoba.ca)

## I. INTRODUCTION

Wireless technology is creating a revolution in communications. While systems such as broadcast radio and television have been around for many years, many new types of wireless communication systems are emerging such as digital cellular, personal communications services (PCS), and packet radio. Two powerful techniques are usually employed to make communication over wireless mobile fading channel reliable, they are channel coding and interleaving. A typical communication system using these techniques is presented in Fig. 1.

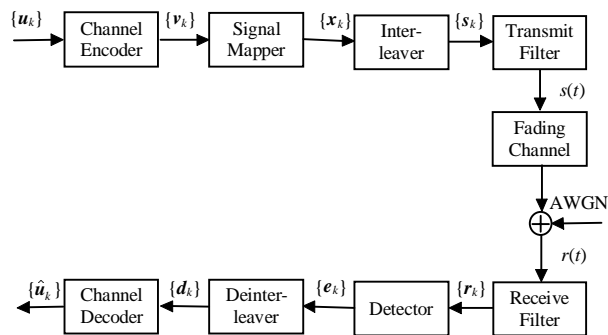


**Figure 1** Digital communication over wireless mobile channel

Turbo coding, introduced in [1] is a coding technique that uses an iterative decoding algorithm to give bit error rate (BER) performance near channel capacity; it is one of the most exciting and important development in coding research in recent years. Since most of the work on turbo codes has been related to

additive white Gaussian noise (AWGN) channel only, its application for digital communication over fading channels is necessary and worthwhile. Recently, the concept of turbo decoding has been applied to the design of a receiver for fading channels [8], [9], [10]. This interesting idea can also be further developed to build a new receiver for mobile fading channels of Fig. 1. Based on the above discussion the next section will outline the author's research proposal for the application of turbo coding technique, in particular and turbo processing technique, in general over mobile fading channels.

## II. RESEARCH PROPOSAL

### A. Turbo Codes for Mobile Fading Channels

For successful application of Turbo codes in mobile fading channel, two different types of fading channel need to be treated separately:

1) *Frequency-Flat fading Channels*: Early research on this topic is based on simplifying assumptions for the channel model, including perfect knowledge of the phase and amplitude of the fading process, and uncorrelated fading [3], [6]. The receiver structure developed in [7] for the frequency-flat fading channel is valid for correlated fast fading. However this receiver is not appropriate for iterative decoding of Turbo codes since it does not produce the necessary soft-output extrinsic information. Furthermore it is incompatible with the presence of the interleaving function in Fig. 1. Therefore modifications to that receiver structure have to

be done to make the application of Turbo codes in mobile fading channels possible.

2) *Frequency-Selective Fading Channels*: The application of Turbo trellis-coded modulation (T-TCM) has recently been investigated by the author in [5]. As far as the author known, it is the first successful application of Turbo codes with multi-level modulation over this type of channel. However in that paper it was assumed that the fading channel varies sufficiently slowly and hence it is possible to have the ideal channel estimator at the receiver. For frequency-selective fast fading channel, a new receiver structure need to be derived to make sure that both channel time-varying coefficients can be well estimated and Turbo decoding can still be done successfully. In this regards, the receiver structure developed in [2] seems to be an attractive candidate.

#### *B. Turbo Equalization for Frequency-Selective Mobile fading Channels*

The frequency-selective fading channel causes not only the signal attenuation but also the severe time dispersion of the adjacent pulses, a phenomenon is referred to as intersymbol interference (ISI). To eliminate ISI, an equalizer is required in the receiver of Fig. 1. In [4] various soft-output algorithms were investigated for the equalizer in an attempt to provide the channel decoder as much information as possible.

A new receiver structure for frequency-selective fading channel, called turbo-equalizer will be investigated. This receiver associates an equalizer and a soft-output channel decoder through an iterative process similar to turbo decoding. In the classical approach the equalizer is fed by the demodulator outputs and does not use the redundancy introduced by the channel coding to improve its performance. The performance of new receiver structure is believed to be superior since the equalizer is fed by both the demodulator outputs and the soft decisions provided by the channel decoder.

#### *C. Combined Turbo Equalization and Turbo Decoding*

Basically, the receiver structure proposed in the previous section is applicable for any channel coding techniques that can be decoded with soft-output decoder. However when the channel encoder employs Turbo codes, in order to take into account the effect of turbo coding, turbo equalization and turbo decoding should be carried out in a combined manner to optimize the system performance as indicated in [10].

### REFERENCES

- [1] Berrou, C., Glavieux, A., and Thitimajshima, P., (1993). "Near Shannon Limit Error-Correcting Coding and Decoding: Turbo-Codes", in *Proc. ICC'93*, pp. 1064-1070.
- [2] Dai, Q., and Shwedyk, E., (1994). "Detection of Bandlimited Signals over Frequency-selective Rayleigh Fading Channels", *IEEE Transactions on Communications*, pp. 941-950, Feb./Mar./Apr.
- [3] Goff, L., Berrou, C., and Glavieux, A., (1994). "Turbo Codes and High Spectral Efficiency Modulation", in *Proc. ICC'94*, pp. 645-649.
- [4] Ha, N. H., and Rajatheva, R.M.A.P., "Performance of Trellis-Coded Modulation on Frequency-Selective Rayleigh Fading Channels with Soft-output Algorithms", *Accepted for Publication in IEEE VTC'98 Conf. Rec., paper 03-02*, Ottawa, Canada, May 1998.
- [5] Ha, N. H., and Rajatheva, R.M.A.P., "Performance of Turbo Trellis-Coded Modulation on Frequency-Selective Rayleigh Fading Channels", *Submitted to IEEE GLOBECOM'98*
- [6] Hall, E. K., and Wilson, S. G., (1998). "Design and Analysis of Turbo Codes on Rayleigh Fading Channels", *IEEE Journal*

- on Selected Areas in Communications*, Vol. 16, No. 22, pp. 160-174, February.
- [7] Kong, H., (1997), Receiver Structures for Wireless Mobile Channels, PhD's Thesis, *The University of Manitoba, Winnipeg, Manitoba, Canada*.
- [8] Lodge, J., and Gertsman, M., (1997). "Joint Detection and Decoding by Turbo Processing for Fading Channel Communications", in *Proceedings of the International Symposium on Turbo Codes and Related Topics*, pp. 88-95, Sept.
- [9] Picart, A., Didier, P., and Glavieux, A., (1997). "Turbo-Detection: A New Approach to Combat Channel Frequency Selectivity", in *Proceedings of the ICC'97*, pp. 1498-1502.
- Raphaeli, D., and Zarai, Y., (1997). "Combined Turbo Equalization and Turbo Decoding", in *Proceedings of the International Symposium on Turbo Codes and Related Topics*, pp. 180-183, Sept.

# UPPER LIMB DYNAMIC ANALYSIS

*Reza Fazel-Rezai*

Department of Electrical and Computer Engineering,  
The University of Manitoba, Winnipeg, MB R3T 2N2, Canada  
fazel@ee.umanitoba.ca

Advisor: Ed Shwedyk (shwedyk@ee.umanitoba.ca)

**Abstract**—The upper limb is represented by a simplified link-segment model composed of three rigid segments with ten degrees of freedom. To define appropriate coordinate systems, the upper limb is instrumented by six markers. Using the motion data, the inverse dynamic problem is solved and force and moments generated in joints are found. Then using a new approach in this area, fuzzy logic, total force is distributed between individual muscles.

## I. INTRODUCTION

Understanding the kinematics and kinetics of upper limb movement requires motion data along with a link-segment model. Body segments can be studied from two points of view. Statically, where the body is at rest or moving with uniform motion. Dynamically, which is a study of segments moving with accelerated motion. Dynamics is further subdivided into: kinematics, a study without consideration of the forces that produces it and kinetics, which formulates the relationship between the forces and the resulting motion. In many human movement studies because of the lack of an appropriate model, motion analysis has been limited to two dimensions. Limited research has been conducted with respect to the upper limb motion analysis in three dimensional space. In general, the accuracy of the results of

dynamic analysis [1][2] depends on the number of degrees of freedom considered.

This paper presents a model of the upper limb in three dimensional space based on the motion data recorded by three cameras (Fig. 1) for dynamic analysis purpose. Ten degrees of freedom for the upper limb, seven rotational and three translational, are considered.

## II. METHODS

### A. Kinematic Model

Motion data for the upper limb movements were collected using the University of Manitoba Motion Analysis System (UM<sup>2</sup>AS) [3].

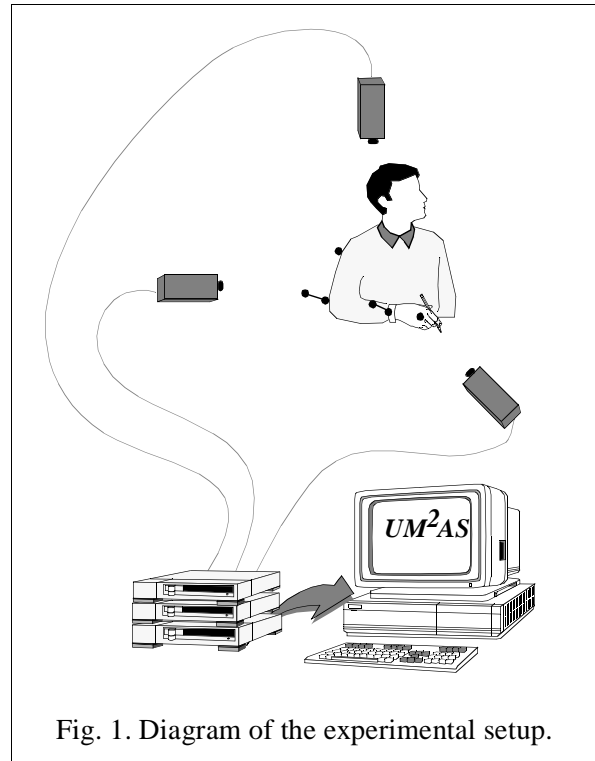
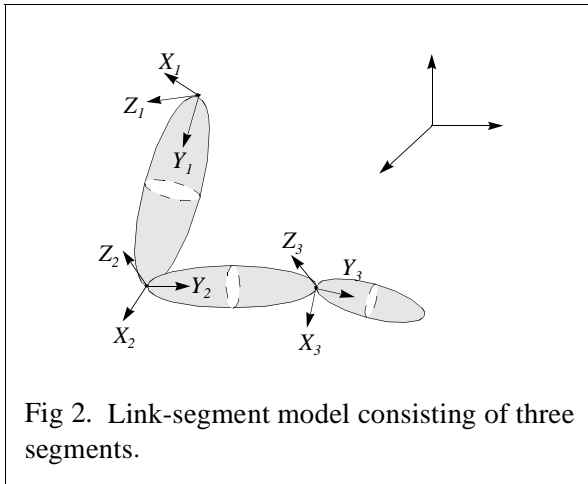


Fig. 1. Diagram of the experimental setup.

In UM<sup>2</sup>AS, markers are placed at defined locations on the upper limb to describe the link-segment model properly. A diagram of the experimental setup is shown in Fig.1. The direct linear transformation method is used to reconstruct three dimensional data from two dimensional images.

### B. Ten Degrees of Freedom

The physical system of the upper limb is represented by a simplified link-segment model composed of three rigid segments as shown in Fig. 2. The model has ten degrees of freedom: three translational and three rotational degrees of freedom for the arm, two rotational degrees of freedom for the forearm and two rotational degrees of freedom for the hand. To find the trajectory of the arm rotation axis and the Euler angles of the arm, forearm and hand, the upper limb is instrumented with six reflective markers. Markers are arranged in such a way that the upper limb can move without any constraint.



To perform dynamic analysis of the upper limb, the instantaneous position of the shoulder joint, i.e., the center of rotation of the arm

segment is necessary. The center of rotation is defined as the point of a moving segment whose velocity is zero at that time [4]. Because, in experimental measurements, it is nearly impossible to determine the velocity of different points on a body in motion, the center of rotation is usually approximated using two consecutive frames within a short period of time. There is a mathematical approach to calculate the center of rotation in two dimensional space [5].

This method does not work in three dimensional space, because the rank of  $[I - R]$  is two where  $I$  is identity matrix and  $R$  is rotation matrix. It means that there is no center of rotation in three dimensional space for a segment. In this research a new approach to calculate trajectory of rotation axis is introduced using the screw axis [3].

### C. Governing Equations

Kinematic equations are obtained using a homogeneous coordinate system which is easy to handle when the number of links increases and kinetic equations are derived using both Lagrangian and Newtonian methods.

### D. Force Distribution Problem

Intersegmental force and moment are the net kinetic effect that adjoining body segments have on each other. It is important to note that these forces and moments are conceptual kinetic quantities that are not physically present in any single anatomic joint. They are determined mathematically, because they cannot be easily be measured directly. Determining the intersegmental forces and moments

based on kinematic data requires solution of the inverse dynamic problem using either Newtonian or Lagrangian equations.

For specific purposes (in orthopaedics, rehabilitation, ergonomics, sports, etc.), it is necessary to know the forces in individual muscles. Partitioning of the intersegmental forces and moments is generally called the *force distribution problem*. The number of unknown variables usually exceeds the number of equations. Mathematically, this produced an indeterminate problem that has no unique solution. The difference between the number of unknown variables and the number of equations represents the degree of redundancy. There are two basic approaches for solving this problem; reduction method and optimization technique.

In the reduction method, to solve the indeterminate problem, the degree of redundancy must be reduced to zero by either introducing new equations or by decreasing the number of unknown variables. Muscles with similar functions or common anatomic insertions and orientation can be grouped together, whereas electromyogram signals can be used to eliminate inactive muscles.

The optimization approach is based on the assumptions that the load sharing between the muscles is more or less unique during motor activities, and that the neural control of the muscle action is governed by certain physiological criteria that guarantee efficient muscle actions. The objective function to be optimized corresponds to these physiological criteria. Since the physiological criteria are presently unknown, objective functions in the literature have been chosen for their simplicity and computational tractability.

Here a new technique using fuzzy logic has been developed. For each muscle specific rules based on the physiological facts are determined. Distribution of the force between muscles is done based on these rules.

### III. RESULTS

Some of the results from different parts of the research has been published [1][2][3][6][7][8][9]. For instance, three translational degrees of freedom calculated using a new method introduced in this research is shown in Fig. 3. The results for the force distribution problem using a fuzzy logic is in preparation to be published.

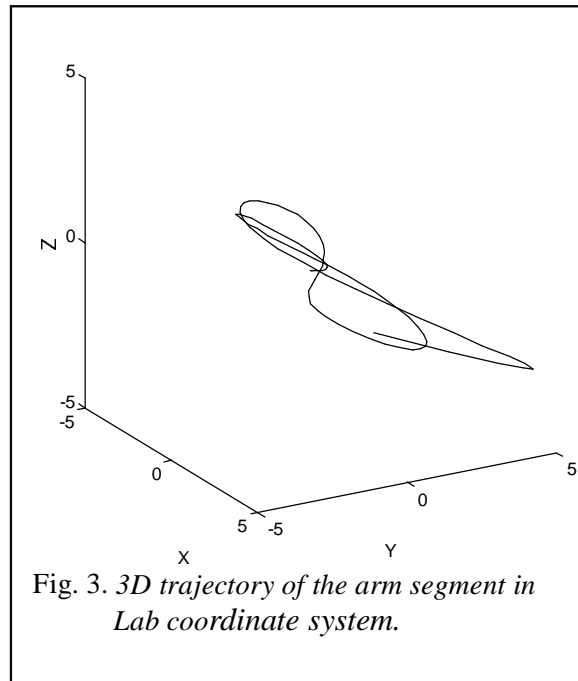


Fig. 3. 3D trajectory of the arm segment in Lab coordinate system.

**Acknowledgement**—Financial assistance of the University of Manitoba (the University of Manitoba Graduate Fellowship) is gratefully acknowledged.

#### IV. REFERENCES

- [1] R. Fazel-Rezai, J. E. Cooper, S. Onyshko and E. Shwedyk, "Generated moments at the upper limb during movement," *Proc. 9th Biennial Conf., Canadian Society for Biomechanics*, , pp. 328-329, Vancouver, 1996.
- [2] R. Fazel-Rezai, E. Shwedyk and S. Onyshko, "Power analysis of the upper limb," *Proc. 18th Annual Conf. of IEEE EMBS*, p. 66, 1996.
- [3] R. Fazel-Rezai, E. Shwedyk and S. Onyshko, "Three dimensional kinematic model of the upper limb with ten degrees of freedom," *Proc. 19th Annual Conf. of IEEE EMBS*, p. 137, 1997.
- [4] K. N. An, E. Y. Chao, "Kinematic analysis of human movement," *Annals of Biomedical Eng.*, vol. 12, pp. 585-597, 1984.
- [5] M. M. Panjabi, V. K. Goel, S. D. Walter and S. Schick, "Errors in the center and angle of rotation of a joint: An experimental study," *Trans. of the ASME*, vol. 104, pp. 232-237, 1982.
- [6] R. Fazel-Rezai and E. Shwedyk, "Biomechanic signal filtering for dynamic analysis purpose: A quantitative comparison between different methods," *Accepted for publication by European Society of Biomechanics*, Toulouse, France, July. 1998.
- [7] R. Fazel-Rezai, E. Shwedyk, J. E. Cooper, J. Ripat and S. Onyshko, "Changes in Upper Dynamics in Patients with rheumatoid arthritis," *Accepted for publication by European Society of Biomechanics*, Toulouse, France, July. 1998.
- [8] R. Fazel-Rezai, E. Shwedyk and S. Onyshko, "The equivalence of different methods to calculate power of a link segment model," *Submitted for publication in IEEE Trans. on Rehab. Eng.*, 1997.
- [9] R. Fazel-Rezai, E. Shwedyk and S. Onyshko, "Comparison of different biomechanical data smoothing methods," *Proceeding CMBEC 23*, pp. 32-33, Toronto, Canada, May 1997.

# CONTROL OF OPTIMAL PWM VOLTAGE SOURCE INVERTER USING SIGMOID AND PICEWISE LINEAR ARTIFICIAL NEURAL NETWORKS

M. Mohaddes

Department of Electrical Engineering, University of Manitoba

P.G. McLaren (Adviser)  
mclaren@ee.umanitoba.ca

A.M. Gole (Joint Adviser)  
gole@ee.umanitoba.ca

## ABSTRACT

A feed forward neural network is used to control a voltage source PWM inverter in a way that selected harmonics are removed from its output and the magnitude of fundamental is set at any desired level. Two cases are studied: neurons with the usual nonlinear (sigmoid) transfer function, and neurons with a piecewise linear characteristic. The latter shows good results and more easily lends itself to hardware implementation either by digital or analog networks.

## INTRODUCTION

Voltage source inverters are widely used in motor drives, uninterruptable power supplies and bidirectional AC-DC converters. Many different types of voltage source inverters with different configurations and control schemes have been suggested. Among them the pulse width modulation (PWM) inverter is most popular. Although several different circuits are proposed to realize the PWM inverter, the main operating principle is the same in most cases. The inverter consists of switches which allow each line of AC load to be one or the other end of the DC source. By suitable selection of switching instants for all switches, the desired output characteristics can be achieved. There are two major

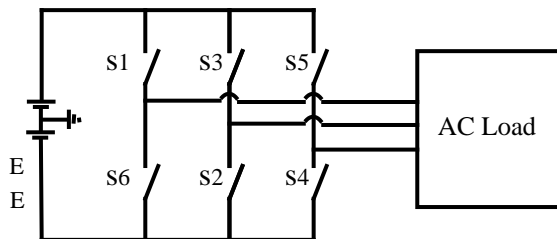


Fig. 1 Basic configuration of a three phase bridge two level VSI

approaches to find the best switching function: the time domain approach [1-3] and the frequency domain approach [4-5]. In the next sections we will concentrate on the frequency domain approach and will use a neural network for its implementation.

## HARMONIC ELIMINATION

Low harmonic content of the output voltage and current is always a major concern with voltage source inverters. For a two level inverter, where the output phase voltage is always either +E or -E (Fig. 2), the r.m.s. value of the voltage is always  $E\sqrt{2}$ . Since the mean squared of this voltage is equal to the sum of the mean squares of all harmonics, then for a given amplitude of fundamental harmonic, the total harmonic distortion is always the same, regardless of the selected switching method. But the switching instants can be adjusted such that the lower harmonics disappear (or decrease substantially) at the expense of increase in higher harmonics. Since loads are usually inductive, higher harmonics can be filtered more easily by the load without need of additional filters.

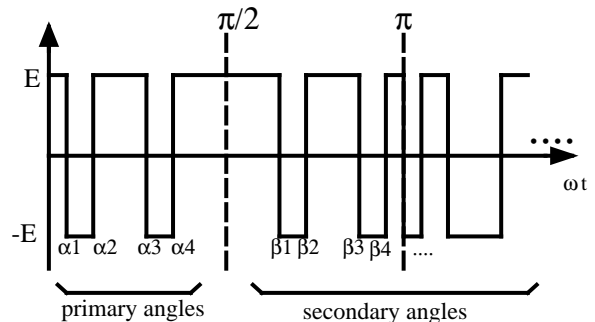


Fig.2 The output phase voltage waveform of a two level inverter

There are several methods to push the harmonics in a PWM waveform to the higher frequencies, but the harmonic elimination technique has the lowest number of switching actions.

The magnitude of harmonics for a PWM waveform with odd and half wave symmetries, and n switching actions per quarter cycle of fundamental, is obtained from the follow-

ing equations:

$$\begin{aligned}
 h_1 &= \left(8 \cdot \frac{E}{\pi}\right) \cdot [1 - 2 \cos \alpha_1 + 2 \cos \alpha_2 \\
 &\quad - 2 \cos \alpha_3 \dots 2 \cos \alpha_n] \\
 h_3 &= \left(8 \cdot \frac{E}{3\pi}\right) \cdot [1 - 2 \cos 3\alpha_1 + 2 \cos 3\alpha_2 \\
 &\quad - 2 \cos 3\alpha_3 \dots 2 \cos 3\alpha_n] \\
 &\vdots \\
 &\vdots \\
 h_k &= \left(8 \cdot \frac{E}{k\pi}\right) \cdot [1 - 2 \cos k\alpha_1 + 2 \cos k\alpha_2 \\
 &\quad - 2 \cos k\alpha_3 \dots 2 \cos k\alpha_n]
 \end{aligned} \quad (1)$$

where  $E$  is half of the DC source voltage,  $h_i$  is the magnitude of the  $i^{\text{th}}$  harmonic and  $\alpha_j$  is the  $j^{\text{th}}$  primary switching angle.

To find the  $\alpha$ 's needed for elimination of specific harmonics, it is sufficient to set the corresponding  $h$ 's in the above equations to zero and solve for the  $\alpha$ 's. The value of  $h_1$  could be any desired value between zero and some limit lower than  $1.25E$  (depending on the harmonics to be eliminated). For three phase inverters, usually the low order nontriplen harmonics are eliminated. Triplen harmonics do not appear in line voltages and currents in a three wire system.

As the number of eliminated harmonics increases, the waveform of output current improves, but since the number of chops also increases proportionately, the switching losses will be higher. There are also restrictions on the maximum frequency of switching devices. As a compromise, we decided to eliminate all harmonics up to the  $29^{\text{th}}$  in this study.

## NEURAL NETWORK

During the operation of the inverter, the desired value of  $h_1$  may change, so eq. (1) must be solved for new values of  $h_1$ . These equations are nonlinear and can be solved only by iterative methods. This process is time consuming, may diverge, and is therefore not suitable for on-line implementation. The conventional approach is to solve off-line for several values of modulation index  $M (=h_1/E)$ , and store solutions in a look-up table. Our new approach is to use a feed-forward neural network which accepts modulation index as input, and outputs the primary switching angles

(Fig. 3). The secondary switching angles (Fig.2) can easily be produced from the primary ones.

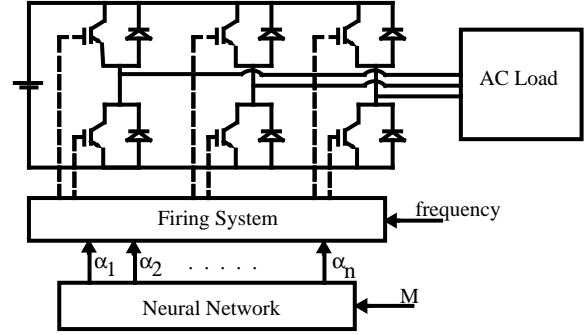


Fig. 3 The overall structure of the inverter

The neural network used has one input neuron and  $n$  output neurons (to produce  $n$  switching angles). Different numbers of hidden neurons were tested and it was found that about  $n/2$  hidden neurons are usually sufficient. The neurons have sigmoid characteristics and bias. The training set for the network was produced by off-line solving of equations for more than one hundred values of  $M$  with 0.01 steps. The Newton-Raphson method was used to solve the equations. To avoid jumping between different possible solutions and to make sure of convergence, the values of  $\alpha_i$  obtained for each  $M$  were used as the initial guess for the next value of  $M$ . Using this method, the off-line solution of eq.(1) is easy and there is no need to use complicated techniques like the Walsh function method, as suggested by some authors [6].

For values of  $M$  greater than 1.16 we could not find any solution for eq. (1), but this is not of practical importance, because, for these values of  $M$ , the inverter must produce such a narrow pulse that it is beyond the capabilities of most switching devices. The whole system including the neural network, the firing system, inverter and load was simulated using PSCAD-EMTDC electromagnetic transient simulation software. Figures 4 and 5 show the voltage and current waveforms and spectra for two arbitrary values of  $M$ . The load has a power factor of 0.8 lagging. As can be seen, the selected nontriplen harmonics are completely eliminated and the fundamental harmonic is at the ordered level.

## PIECEWISE-LINEAR NEURAL NETWORK

Hardware implementation of the neural network is not an easy task. The commercially available neural network chips and boards are expensive. Sequential processors can

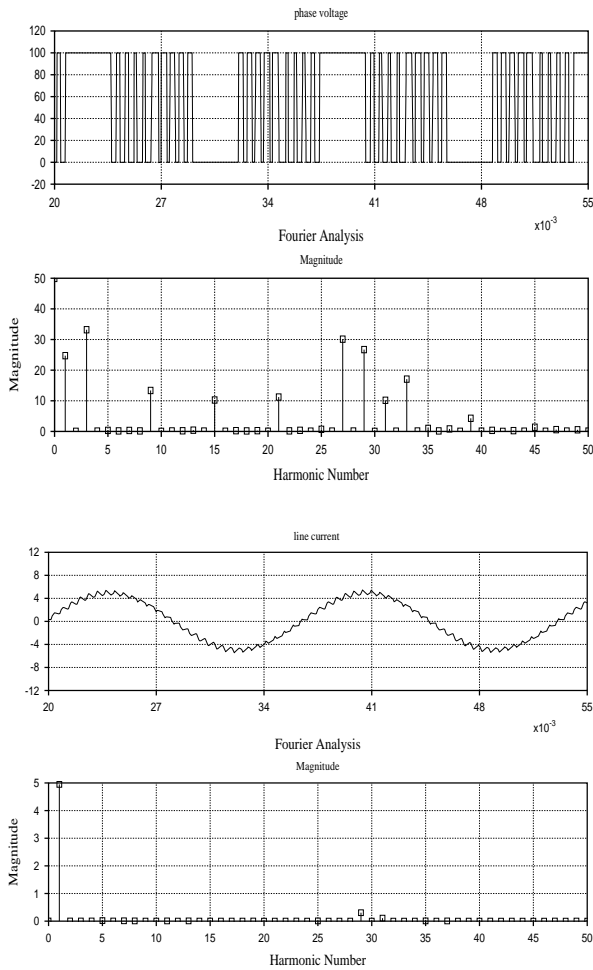


Fig.4 Voltage and current waveforms and spectra for  $M=0.5$

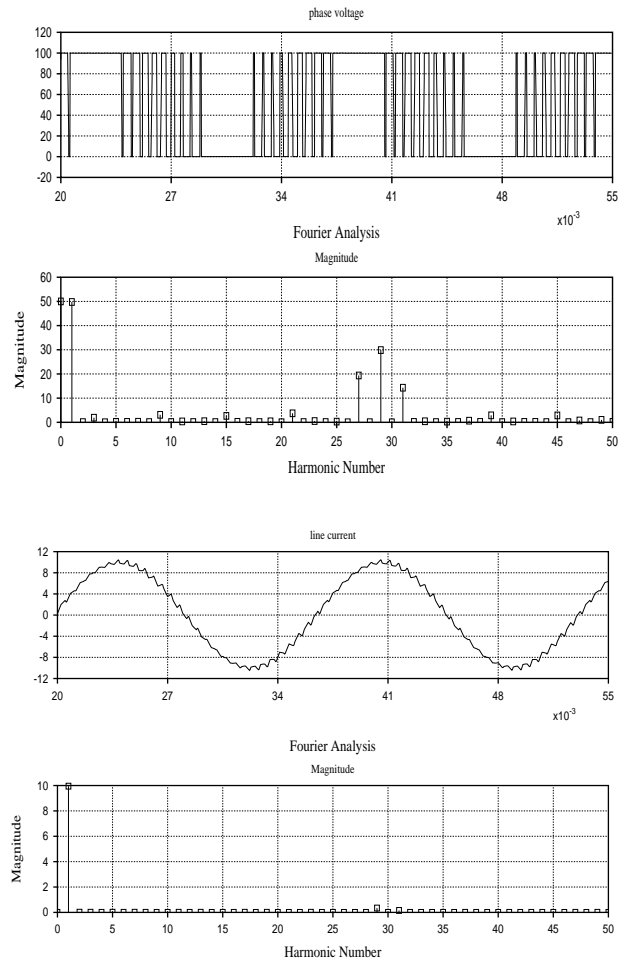


Fig.5 Voltage and current waveforms and spectra for  $M=1$

be used to emulate the neural network, but since calculation of exponential function and division takes a lot of time for each neuron, they are not fast enough. To solve this problem, we replaced the sigmoid transfer function of neurons with a piecewise-linear transfer function (Fig. 6). When we use this characteristic for the neurons with the same weights for the links as before, we obtain  $\alpha$ 's not far from the previous ones. But since the magnitude of harmonics in the output voltage is very sensitive to changes in  $\alpha$ 's, we have unacceptably large harmonics in the output. Fig. 7 shows a typical output voltage waveform and spectrum for this case. To solve this problem, we chose to train the network containing the piecewise-linear characteristic for neurons. Although in this case the objective function is not differentiable at all points, it is still continuous and therefore it is possible to find a global minimum. We used the weights of the previous network (with nonlinear neu-

rons) as the starting point and chose back propagation as the optimization technique. Since for modulation index  $M$  greater than 1 the variations of  $\alpha$ 's with  $M$  is highly non-linear, we limited  $M$  to 1. This way we could reduce the

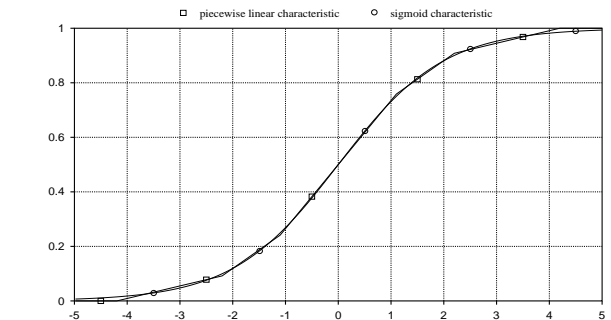


Fig.6 Piecewise linear characteristic

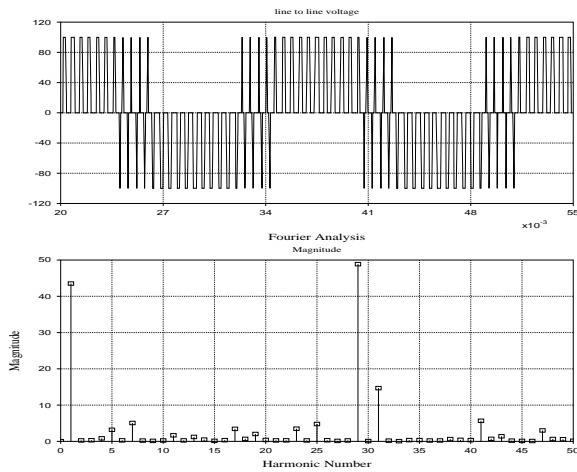


Fig.7 Results for piecewise-linear network with the weights of sigmoid-neuron network

number of hidden units to 3 and get quite satisfactory results. Fig. 8 illustrates the voltage and current waveforms and spectra for two different values of M. All harmonics up to the 29th are cancelled and the load current has very little ripple

### CONCLUSIONS

A neural network can be successfully used to control a voltage source inverter such that the fundamental component of output voltage has the desired magnitude and selected harmonics are eliminated. The fact that this control is independent of frequency control, makes this inverter a suitable tool for motor speed control and other variable speed-variable frequency applications. The inverter has low loss due to the low number of switching actions compared to other techniques. Using piecewise-linear characteristic for neurons makes it much easier to implement the network in hardware. We are now implementing the network using a digital signal processing board.

### REFERENCES

- [1] S.R. Bowes, "Novel Real Time Harmonic Minimized PWM Control for Drives and Static Power Converters", IEEE 8th Applied Power Electronics Conference, March 1993, San Diego, California.
- [2] O.Ogasawara, H.Akagi, A.Nbae, "A Novel PWM Scheme of Voltage Source Inverters Based on Space Vector Theory", proc. European conf. power electron. appl. EPE, Aachen, Germany, 1989.

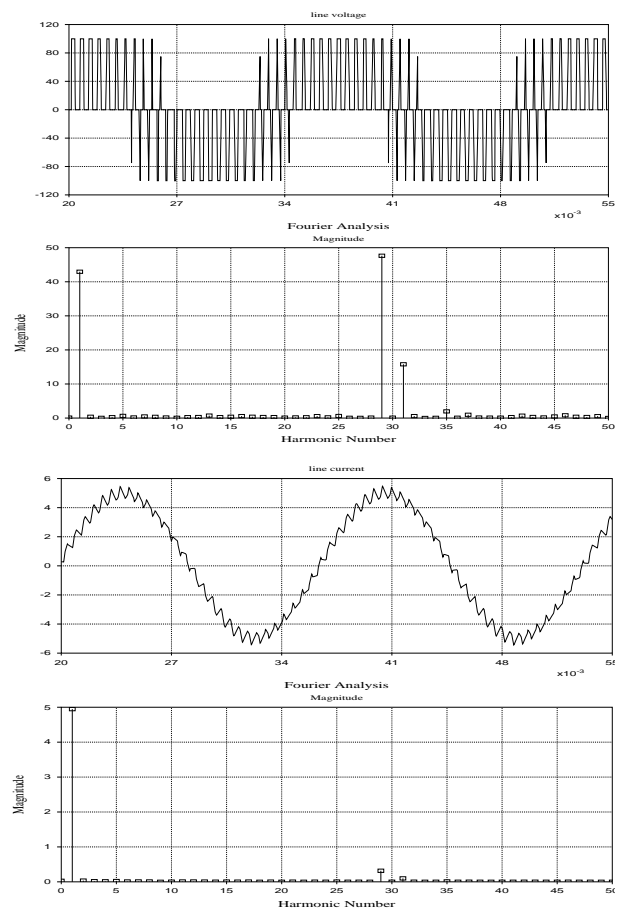


Fig.8 Voltage and current waveforms and spectra for piecewise-linear network

- [3] J.Holtz, B.Beyer, "The trajectory Tracking Approach- A New Method for Minimum Distortion PWM in Dynamic High Power Drives", IEEE Trans. Ind. App. Vol. 30, No. 4, July/Aug. 1994.
- [4] H.S.Patel, R.G.Hoft, "Generalized Techniques of Harmonic Elimination and Voltage Control in Thyristor Inverters", IEEE Trans. Ind. Appl. , pp. 310-317, 1973.
- [5] D.R.Alexander, S.M.Williams, "An Optimal PWM Algorithm Implementation in a High Performance 125KVA Inverter", IEEE 8th Applied Power Electronics Conference, March 1993, San Diego, California.
- [6] F.Swift, A.Kamberis, "A New Walsh Domain Technique of Harmonic Elimination and Voltage Control in Pulse-Width Modulated Inverters", IEEE Trans. Power Electron. Vol. 8, No. 2, April 1993.

# High Speed Transient Stability - A Multiprocessing Solution

**Author :** Wieslaw T. Kwasnicki, Manitoba HVDC Research Centre,  
Winnipeg, Canada, [wk@hvdc.ca](mailto:wk@hvdc.ca)

**Advisor :** Ani M. Gole, University of Manitoba,  
Winnipeg, Canada, [gole@EE.UManitoba.CA](mailto:gole@EE.UManitoba.CA)

**Abstract** - This paper presents a method for solving power system transient stability problem by multiprocessing computing. A new algorithm based on system splitting, partitioning and W-matrix techniques has been developed and implemented in the High Speed Transient Stability (HSTS) program. This program has embedded parallelism and can be executed on various platforms of parallel and distributed processing hardware.

**Keywords** - Transient stability, network solution, system splitting, current compensation, parallel processing, distributed processing, real-time simulation.

## I. Introduction

The emergence of parallel processing architectures has opened new opportunities and challenges for solving power system problems. For obtaining the transient stability solution using parallel processing hardware, suitable algorithms must be developed if high speed is to be achieved for large system size. Using these new algorithms implies significant modifications to existing programs [1,2]. In order to harness the new technology yet maintaining the strengths of existing solution methods, a multiprocessing network solution algorithm is proposed, which adapts the conventional library of dynamic models for execution on parallel or distributed processing hardware.

For transient stability problem the behavior of power system is typically described by two sets of equations :

$$\mathbf{X}' = f(\mathbf{X}, \mathbf{V}) \quad (1)$$

$$\mathbf{V} * \mathbf{Y} = \mathbf{I}(\mathbf{X}, \mathbf{V}) \quad (2)$$

where  $\mathbf{V}$  is a vector of bus voltages,  $\mathbf{I}$  is a vector of current injections,  $\mathbf{Y}$  is a matrix of system admittances, and  $\mathbf{X}$  is a vector of state variables. The first is a set of differential equations describing system dynamics and the

second is a set algebraic equation describing network connectivity. Usually the sets of differential equations (1) is solved first using an integration method and iterated with the solution of network equations (2) at every time-step.

There are no obvious parallelisms inherent in the mathematical structure of the conventional formulation of a transient stability problem. For this problem, a parallel (or near-parallel) formulation must be found that is amenable to multiprocessing implementations on parallel or distributed processing hardware. The computational efficiency of such an implementation is dependent on the suitability of the multiprocessing algorithm to the parallel architecture and the communication network.

There are available various single processor software packages which perform the traditional stability program solution at, or near, real-time speeds for mid-size power systems [6]. High computational efficiency is usually hard to achieve for large systems because admittance matrices are large and the repetitive solution of network equations (1 & 2) takes too much time. High performance computers are available now but the structure of a conventional stability programs can not be easily adapted to utilise the full power of this new technology. Even if such systems can deliver high performance computing, they usually require specialised software and hardware components, which increase system costs.

Recently, the prospect of building a supercomputer out of PCs is quickly emerging and is becoming a realistic alternative for high performance computing at low cost. The biggest challenge in synthesising clusters of commodity computers to work in parallel is to implement high performance communication and co-ordinated scheduling among distributed processors, each running independent operating system kernels.

## II. Multiprocessing Solution Method

The main objective of this project was to develop an algorithm for solving the power system transient stability problem on the existing hardware of a parallel processing computer such as the Real Time Digital Simulator (RTDS), with extensibility to other multiprocessing computers (multicomputers) and Distributed Processing Systems (DPS's). Various methods were considered and examined on several candidate platforms. Those methods included the Gauss-Seidel (GS) and Bergeron (BM) [7,8] iterative algorithms as well as various sparse matrix techniques for the direct solution of network equations.

Although iterative methods are potentially suited for parallel processing, they were abandoned in this project, due to their poor convergence characteristics for large power system sizes, in favour of direct methods. In this paper a suitable multiprocessing method for high-speed transient stability solution based on sparse matrix techniques [3,4,5] is presented. This new algorithm combines several techniques useful for parallel processing applications, which includes the following methods :

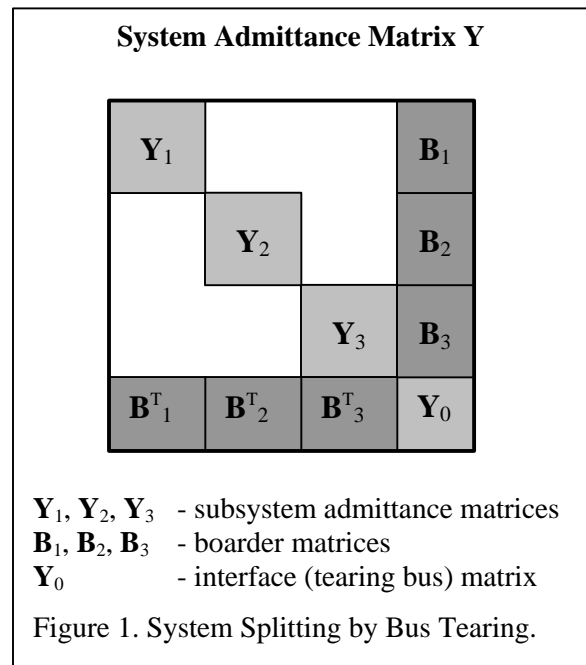
- LDU-decomposition and LDU-inverse for processing sparse matrices
- W-matrix method for solving network equations
- Node re-ordering scheme to minimise the number of fill-ins in the W-matrices
- Bus Tearing method for splitting large network into smaller subsystems
- Partitioning scheme for solving one subsystem on many parallel processors.
- Current Compensation method for handling the admittance changes

System splitting divides the whole power system into smaller subsystems so that the system admittance matrix  $\mathbf{Y}$  consists of diagonal subsystem matrices, an interface matrix, and a border matrices as shown in Figure 1.

Node ordering and the LDU factorisation are applied to each subsystem matrix  $\mathbf{Y}_i$  to maximise sparsity. Each subsystem is then assigned for solving on one single or multi-processor computer. If computers consist more than one

processor (such as the RTDS racks) the partitioning is also applied. Load balancing partitioning scheme is developed for this purpose which takes into account uneven distribution of matrix sparsity and assigns different number of row and columns of the factor matrices so that the work-load for each participating processors is approximately balanced.

In order to avoid matrix re-inversion when system admittance change take place a Current Compensation method is applied which computes equivalent current injections to system buses using only the initial LDU inverse factor matrices.



The system splitting by the Bus Tearing method is not only an effective method for partitioning the problem for multiprocessing but it can also produce significant savings even on single-processor computers. It was found that the system splitting by fragmenting the large admittance matrix into a few smaller matrices improves the overall sparsity of the inverse matrix and thus reducing the solution time as presented in Table 1 below.

The system splitting produces an approximately even-sized subsystem groups and one additional group consisting the tearing or

interface buses connecting the subsystems. The size of this subsystem depends on system topology and generally increases as the number of subsystem grows.

**Table 1:** 6-second simulation run on Sun workstation

Number of Subsystems	Execution Time [ sec]
1	76.3
2	50.8
3	55.0
4	54.3
5	52.1
6	68.9

However, beyond a certain number of subsystems the gains from improved sparsity can be overwhelmed because of the additional computation associated with solving a split subsystem which is proportional to the number of interface buses. In the case presented above this number happened to be 6.

### III. HSTS Program

The multiprocessing algorithm has been developed and incorporated in a stand-alone version of the High Speed Transient Stability (HSTS) program written in the 'C' computer language. The HSTS program is fully scalable and can be easily reconfigured for any number of computers (or RTDS racks) and any number of parallel processors on multicomputers. The Message Passing Interface (MPI) based communication is built in as an integral part of the program and is used not only for the distributed processing but also for the interface to other programs such the PSCAD/EMTDC electromagnetic transient simulation program.

The proposed multiprocessing algorithm for solving transient stability problem deals with computational and communication efficiency problems very effectively. In addition to the conventional LDU methods for processing large and very sparse admittance matrices other techniques are applied which allow solving the problem on many processors operating in parallel. System splitting, partitioning, and load balancing schemes are combined together to maximise the use of computational power of a

multiprocessor hardware. At the same time data exchange between processors is minimised to reduce the communication latency.

The network solution applied in the HSTS program has been tested on a selected 505-bus test system against the conventional, commercially available, stability programs such as BPA, PSS/E, and PSDS. Test results on workstations match very closely with the steady-state and post-faults curves obtained using other stability programs. The computational speed was comparable with the BPA program, and promises significant gains in the multi-processor environments.

### IV. Implementations

For the parallel processing implementations of the HSTS program, two multiprocessor environments are considered : the parallel-processing based RTDS and a Distributed Processing System (DPS) of a local area network (LAN). Those implementations require specific changes in the original HSTS program for the specific hardware architectures. The routines for compiling, downloading, initialization, communication and running the program in a multiprocessor environment are included for both applications.

In order to perform transient stability solution on the RTDS hardware for system size up to 10,000 buses, it is necessary to utilise many racks (each consisting of 36 NEC processors) operating in parallel. Due to limitations of the RTDS communication architecture, however, a subsystem not larger than 500 buses can be processed on one rack.

The network solution part of the HSTS program was implemented on one rack of the RTDS parallel processing hardware. Solving the 505-bus test system by a various number of processors was considered. Results have shown significant speed improvements when the number of processors increased from 1 to 15 as shown in Figure 2. Beyond that number, the granularity of the problem slowed down any further speed gains.

Further work is aimed at implementation of the High Speed Transient Stability program on Distributed Processing System (DPS) of a PC-

based computer network. This is a straightforward task because the HSTS program has been written in C language considering parallelism and the Message Passing Interface (MPI) routines for communications between computers are included in the program.

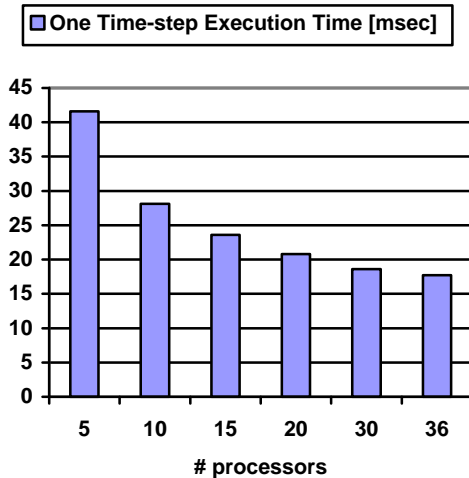


Figure 2. One Time-step Execution Time for Various Number of RTDS Processors

The DPS implementation of the HSTS program is based on the Single-Instruction-Multiple-Data (SIMD) paradigm. This means that the same program with embedded parallelism is executed on several processors which are using parts of a partitioned data.

The execution and communication times are evaluated for different distributed network configurations. Gains are observed even when no high performance communication is applied.

### III. Conclusions

For solving the power system transient stability problem a method suitable for parallel and distributed processing has been proposed. The computational efficiency of the proposed multiprocessing algorithm is dependent on the parallel architecture and the communication network of a given implementation.

It has been shown that, even with high communication latency, significant speed improvements can be achieved when the multiprocessing solution is applied for solving the transient stability problem. With the use of high performance computers or special

communication hardware, computation speeds approaching real-time.

### IV. Acknowledgements

This research project has been sponsored by the Manitoba HVDC Research Centre where the HSTS program has been developed and implemented. The author would like to thank all the members of the Centre staff who participated in this project for their contribution and bringing new ideas that led to the formulation of a final solution method and its implementation in the HSTS program.

### IV. References

- [1] J.S. Chai, A. Bose, "Bottlenecks in Parallel Algorithms for Power System Stability Analysis", IEEE Transactions on Power Systems, Vol. 8, No. 1, February 1993.
- [2] D. J. Tylavsky A. Bose, "Parallel Processing in Power System Computation", An IEEE Committee Report by Task Force of the Computer and Analytical Methods Subcommittee of the Power System Engineering Committee, Transactions on Power Systems, Vol. 7, No. 2, May 1992
- [3] A. Padilha, A. Morelato, "A W-Matrix Methodology for Solving Sparse Network Equations on Multiprocessor Computers", IEEE/PES Summer Meeting, San Diego, 1991
- [4] F. F. Wu, "Solution of Large Scale Networks by Tearing", IEEE Trans. on Circuits and Systems, Vol. CAS-23, 1976
- [5] O. Alsac, B. Stott, W. F. Tinney, "Sparsity Oriented Compensation Methods for Modified Network Solutions", IEEE PES 1982 Summer Meeting, San Francisco, California, 1982
- [6] J. Q. Wu, A. Bose, J. A. Huang, A. Valette, F. Lafrance, "Parallel Implementation of Power System Transient Stability Analysis", IEEE/PES 1994 Summer Meeting, San Francisco, CA.
- [7] K. Werlen, H. Glavitsch, R. Bacher, "From Bergeron's Method to Node-oriented Loadflow Solution", 11-th Power System Computation Conference, Avignon, France, 1993
- [8] W. T. Kwasnicki, D. A. Woodford, X. Wang, A. M. Gole, "Bergeron Based Network Solution Algorithm for High Speed Dynamic Stability", 12-th Power System Computation Conference, Dresden, Germany, 1996.

# ADAPTIVE ALGORITHMS FOR PERSONAL AGENTS

Imran Khan, imran@ee.umanitoba.ca

Microelectronics and Software Systems Lab

Advisor: Howard C. Card, hcard@ee.umanitoba.ca

**Abstract--**This paper presents three projects which represent work in progress. First, a Computerized Adaptive Tutor (CAT) using a novel domain knowledge representation model is discussed. Second, the abstraction to Web documents is proposed using a self-supervised backpropagation network which is trained on alphanumeric characters. Finally, a data visualization scheme using a spirally weighted grid layout for Web documents.

## I. CAT PROJECT

The Computerized Adaptive Tutor (CAT) also called an Intelligent Tutoring System (ITS) includes the following computer-resident knowledge attributes: (i) knowledge of the domain (expert model), (ii) knowledge of the student (student model), (iii) knowledge of teaching strategies, and (iv) ability to diagnose errors and to tailor remediation based on diagnosis. For more information on ITS and its precursors, refer to [1], [2], and [3].

The term CAT is preferred to ITS because ITS implies that the system is intelligent. In contrast, CAT replaces the word *intelligence* with *adaptive* which implies that the system can adapt to the client. The term CAT also replaces the word *system* with *tutor* since the CAT resembles a human tutor rather than a conventional Computer Assisted Instruction system.

### A. Model

The high level block diagram of the CAT is shown in Fig. 1. The student is given some textual material to read and may choose to consult other sources of information through the Web. The CAT is composed of five main components.

First, the *Student Evaluator* module conducts an interactive questionnaire which determines the profile of the student. Some of the main preferences which it evaluates are the goal, time commitment, level of dedication, level of knowledge desired, thinking style, learning aptitude, relevant background, and comprehension skills of the student. Based on the student profile, the CAT suggests a study plan to achieve the desired student goals and knowledge level within the specified time frame.

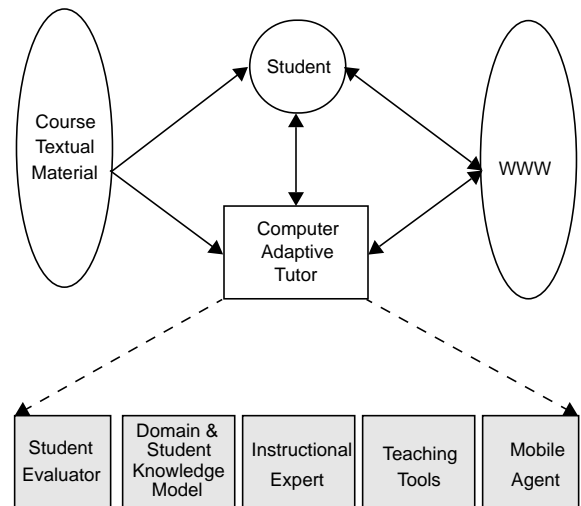


Fig. 1. Block diagram for the interaction between the student and the CAT.

Second, the *Knowledge Representation* module has two components: (i) it represents the domain knowledge which the CAT relies on to teach and (ii) it represents the student's comprehension of the material. This module is discussed further in the next subsection.

Third, the *Instructional Expert* module contains the different teaching strategies which can be used to convey concepts and ideas. It also determines what material to include, when to cover it and in which sequence it is presented. This module also tracks the student's progress and misconceptions through the use of questions and by referring to the student knowledge representation module. It is also responsible for the appropriate type of remedial action to perform.

Fourth, the *Teaching Tools* module has access to self-enhancement techniques to help improve the student's learning capabilities. These include effective time management, speed reading, enhanced memory, and effective habit building techniques. These techniques are accessed by the Instructional Expert module when it is considered appropriate since not all students will want to spend time improving or developing good

learning techniques.

Finally, the *Mobile Agen* module gives the CAT the ability to become a dynamic system. A stand-alone CAT operates as a personal agent for an individual student. Thus, it does not teach other students nor does it acquire additional domain knowledge teaching experience from other students and other similar tutors. A Mobile CAT (MCAT) operates as a roaming agent. It teaches more than one student, and gains relevant teaching feedback from the entire group. It also has the capability to increase its domain knowledge and even to collaborate with other MCATs, thus gaining even more diversified experience and knowledge.

A typical session between the CAT and student is shown in Fig. 2. The first time the student and CAT interact, they define their goals and roles. The interaction takes place via a conversational style questionnaire. At the end of the first meeting, they agree upon the goals of the student, in what time frame these will be accomplished, and a meeting schedule. The student is also requested to read the assigned material. On the second meeting, the CAT reviews what was in the textual material. The CAT then tests the student's level of comprehension using various styles of questions (fill in the blank, true/false, and multiple choice). After each question, the student's answer is compared with the correct answer. If it is correct, then a slightly harder question is asked based upon the same idea. If the answer is wrong then the correct answer is identified and explained. The CAT may perform further actions to undo previous misconceptions or lack of knowledge. The student's knowledge model is updated and the next concept is addressed. The amount of time spent and the amount of detail covered on each topic adapts to the developing profile of the student. The student is then assigned the next material to read. This process continues until all the topics necessary to accomplish the goal of the student are completed.

### B. Knowledge Representation Model

The purpose of the knowledge representation model is to (i) store the domain information and (ii) assist in tracking the gradual comprehension of the domain knowledge by a novice learner through iterative cycles. This model has two main components: (i) the domain expert component which represents the knowledge that the CAT employs and (ii) the student comprehension component which represents the information that the student has obtained thus far. Before discussing these components, we digress for a moment to briefly explain the concept of a knowledge molecule.

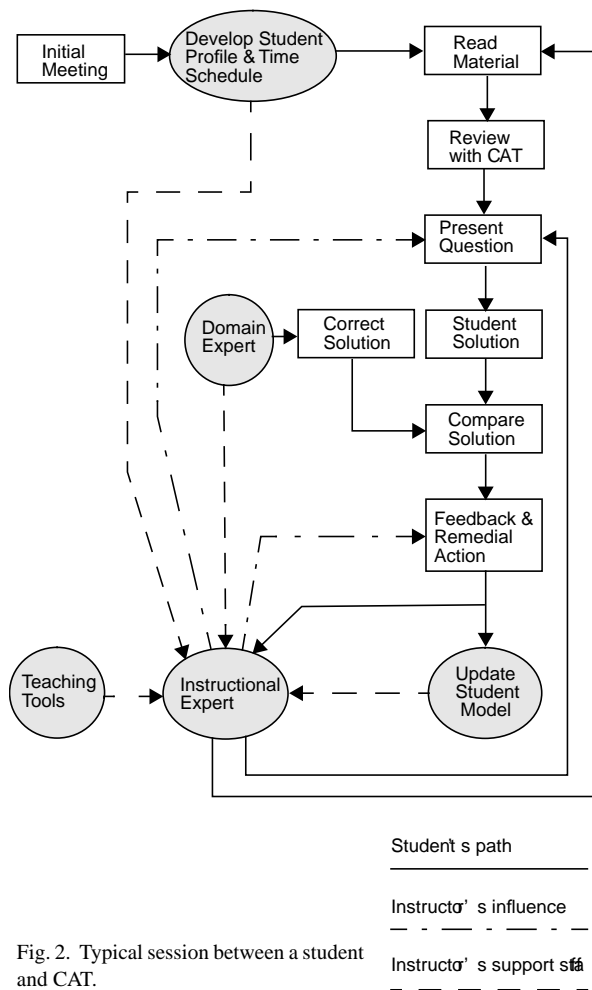


Fig. 2. Typical session between a student and CAT.

### 1) Knowledge Molecule

The brief discussion in this section introduces a method for systematic knowledge representation based on organic chemistry. Structural formulas in organic chemistry are routinely used to represent organic matter. This structural theory is based upon millions of facts about individual compounds which have been brought together and arranged in a systematic way. Similarly, it is conceivable that one can create structural formulas to represent domain knowledge content. These formulas are to be determined after the domain knowledge is analyzed in order to identify the interrelationship between the individual concepts.

The concept of a *knowledge molecule* is a structural arrangement of knowledge elements or atoms which are primitive ideas that can not be broken down into simpler ideas. Furthermore, a topic is a collection of molecules with more or less uniform themes. Thus, a knowledge molecule is a very small unit of a topic. In order to

represent specific domain knowledge content, a compound topic or domain tissue is identified which is made up of two or more topics.

## 2) Domain Expert Component

There are three steps to model the domain knowledge. First, identify the knowledge elements (i.e. the simplest set of ideas) using automatic textual analysis techniques [4]. Second, combine the elements to form knowledge molecules (i.e. building blocks for a topic). Finally, we use the knowledge molecules to create compound topics (i.e. the domain knowledge of the particular subject area).

## 3) Student Comprehension Component

The Instructional Expert component uses the above molecular structure as a blueprint to determine what action to take in order to best duplicate the knowledge for the student comprehension model. Questions are used to determine which elements have been understood. The instructional expert can then compare its original blueprint with the dynamic student knowledge tissue to see which molecules are missing, which are lacking details or proper atomic structure, and which should not be present.

The CAT continues to enhance the comprehension of the student until the knowledge molecule structure of the student is comparable to the original structure.

## C. Implementation

The proposed model of the CAT is being developed to tutor novice financial investors using JAVA. The domain knowledge for the CAT is based on the Canadian Securities Course (CSC) textbooks [5] which are produced by the Canadian Securities Institute (the National Educational Organization of the Canadian Securities Industry).

## II. DATA ABSTRACTION PROJECT

The Personal Adaptive Web (PAW) agent [6] is a software program which monitors its user and learns the category of web documents that the user is interested in. The learning is accomplished by training the agent using competitive learning. One difficulty which arises in training the PAW agent is that it is time consuming to collect a sufficient number of web documents to train the network on.

A possible solution is to pre-train a neural network to cluster data into several categories using a well defined data set. If the chosen data set has statistics which are similar to that of the desired web space of documents then the trained neural network will be able to categorize the web documents properly.

### A. Model

A self-supervised backpropagation network is shown in Fig. 3. The input pattern and the output pattern are exactly the same. The network architecture develops a compact representation in a self-organized manner for the input data. Basically, the network architecture computes the principal components of the input data. For more information on neural networks, the reader is referred to [7].

### B. Implementation

The proposed data set is the alpha-numeric characters. The data set will include characters from different fonts with the addition of gaussian noise (i.e. flip each pixel in the character with N% probability) or non-gaussian noise (i.e. flip each pixel and each adjacent pixel in the character by N1% and N2% probability respectively).

The self-supervised backpropagation network is simulated using NeuroSolution and the image processing is done in MATLAB's image processing toolbox.

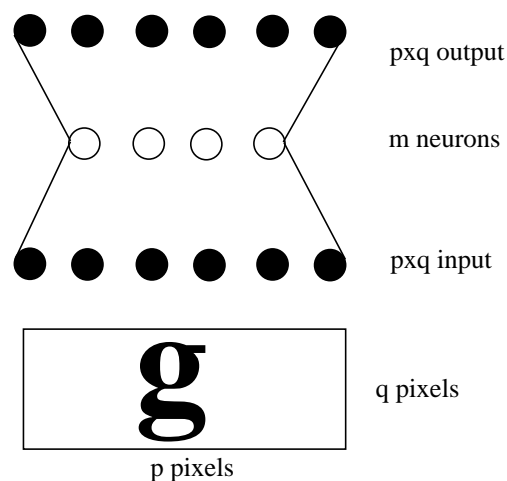


Fig. 3. Self-supervised backpropagation neural network.

### III. DATA VISUALIZATION PROJECT

The PAW agent [6] uses automatic text analysis techniques to generate binary vectors to represent Web documents. Each component in the vector is given the same weight. Using this approach, vector components that are more significant are treated the same as lesser significant components. This approach was used because of the requirements of the competitive learning algorithm that was implemented.

#### A. Model

It is proposed that terms with greater importance are given larger weights than terms with lesser importance. One possible solution is to place the components of the vector on a  $n \times n$  grid starting from the center and spiral them outwards. The component in the center of the grid has the largest weight and subsequent spiralling components have weights which are increasingly smaller.

Each document is now represented by a  $n \times n$  grid which can be visualized. As well, a new distance metric which uses the grid layout is in development which will categorize the Web documents using the self-supervised back-propagation architecture discussed in section 2.1. A further advantage of placing the document vectors in a spiral format on a grid is that different fields of computation can be performed depending on the time constraint.

If a quick comparison of documents is required then only the center pixel and its immediate neighbors are compared. On the other hand, if a thorough comparison is required then the complete grid is used.

#### B. Implementation

The proposed new algorithm is currently being developed in MATLAB's neural network toolbox.

### IV. CONCLUSION

The paper presents three projects which represent work in progress. First, the CAT is being developed in JAVA to tutor novice financial investors using a novel knowledge representation model. Second, a technique for Web document abstraction from a trained self-supervised backpropagation ANN using alpha-numeric characters is presented. Finally, a data visualization technique using a spirally weighted grid layout is presented for Web documents.

### ACKNOWLEDGEMENTS

The guidance of Professor Howard C. Card is gratefully appreciated. The financial support of the Canadian Microelectronics Corporation, National Sciences and Engineering Research Council, and the Internet Innovation Center is also gratefully acknowledged.

### REFERENCES

- [1] C. R. Dills & A. J. Romiszowski, *Instructional Development Paradigms*. Educational Technology Publications, 1997.
- [2] V. J. Shute and J. Psocka, *Intelligent Tutoring Systems: Past, Present, and Future. Handbook of research for Educational Communications and Technology*. New York: Simon & Schuster Macmillan, 1996.
- [3] I. Khan, *The Intelligent Tutoring System: A Myth or the 21st Century Reality?* UM/ECE Tech. Report 97-81529-1 ([www.ee.umanitoba.ca/~imran/tr.html](http://www.ee.umanitoba.ca/~imran/tr.html)). University of Manitoba, 1997.
- [4] G. Salton, *Introduction to Modern Information Retrieval*. McGraw-Hill, 1982.
- [5] Canadian Securities Institute, *Canadian Securities Course Textbook*. Prepared and published by Canadian Securities Institute, 1997.
- [6] I. Khan, D. Blight, R. D. McLeod, and H. C. Card, *Categorizing Web Documents using Competitive Learning: An Ingredient of a Personal Adaptive Agent*. In *Proceedings of International Conference on Neural Networks*, 1997.
- [7] S. Haykin, *Neural Networks: A Comprehensive Foundation*, MacMillan, 1994.

# COMPUTATIONAL INTELLIGENCE IN ATM CALL ADMISSION CONTROL

Peter Czezowski

Telecommunications Research Laboratories  
10 - 75 Scurfield Boulevard  
Winnipeg, MB, Canada, R3Y 1P6  
pczezow@win.trlabs.ca

Department of Electrical and Computer Engineering  
University of Manitoba  
Winnipeg, MB, Canada, R3T 5V6  
czezow@ee.umanitoba.ca

Advisor: Witold Pedrycz, pedrycz@ee.umanitoba.ca

**Abstract - We summarize our current research on the applications of computational intelligence in asynchronous transfer mode networks. Our goal is to improve network performance (call blocking, utilization) through “intelligent” call admission control. We discuss the need for a methodology of applying computational intelligence in this environment.**

## I. INTRODUCTION

Asynchronous transfer mode (ATM) is a key paradigm in the delivery of broadband integrated services digital networks (B-ISDN) [1,11]. Aside from high-performance switching, ATM's most important feature is its ability to guarantee quality of service (QoS) for all connections. Maintaining QoS guarantees is critical if a network is to successfully carry the demanding traffic of future multimedia applications.

Since ATM is a cell-switching protocol, a path through the network is determined at call set-up. A *traffic contract*, including the QoS and other parameters, is established between the source and the network. The elements of the traffic contract are used by routing and call admission control (CAC) algorithms in an attempt to prevent or manage congestion in the network. During transmission, a source is expected to adhere to its traffic contract commitments. The network has the authority to invoke *policing mechanisms* which may drop non-compliant cells.

In general, our research concerns the roles that computational intelligence (CI) techniques can play in improving ATM performance (call blocking, network utilization) over conventional versions of the algorithms mentioned above. The main goal is to develop a methodology for applying CI in ATM environments that produces near-optimal results.

The remainder of this paper is organized as follows: Section II presents the traffic models describing the var-

iable bit rate (VBR) sources used throughout the simulations. Section III introduces the relationships of the three main categories of CI techniques. ATM CAC is discussed in Section IV. Finally, the simulation environment is presented in Section V.

## II. VBR TRAFFIC MODELS

ON/OFF models are popular choices for modelling VBR sources in ATM networks. We follow this convention and implement three categories as summarized in Table I below. ON/OFF sources have two states; corresponding to their idle and active periods (see Fig. 1. below).



Fig. 1. ON/OFF model.

The state duration probability and cell generation rate during active periods define the source type.

TABLE I  
CHARACTERIZATION OF VBR SOURCES

Source Type	State Duration	ON Rate
<i>MMFP</i>	Exponential distribution: $f(x) = \lambda_i e^{-\lambda_i x}$	PCR
<i>MMPP</i>	Exponential distribution: $f(x) = \lambda_i e^{-\lambda_i x}$	Poisson distribution: $f(x) = \frac{e^{-\mu} \mu^x}{x!}$
<i>Heavy tailed</i>	Pareto distribution: $f(x) = \beta a^\beta x^{-\beta-1}$ where $a, \beta \geq 0, x \geq a$	PCR

The functions listed in second column of the table are the probability density functions for exponential and Pareto random distributions. The function listed in the table's third column is the probability mass function for the Poisson random distribution.

Markov modulated fluid processes (MMFP) have exponentially distributed state durations and generate traffic at a constant rate (PCR) when active. Markov modulated Poisson processes (MMPP) also follow exponential distributions for their state durations. However, when active, the MMPP's cell generation rate is specified by a Poisson distribution.

Recent work [10,16] has shown ethernet traffic to have the self-similar property of burstiness over many time scales. Such self-similar traffic is typically modelled by the superposition of multiple heavy tailed ON/OFF sources. When active, these sources generate cells at a constant rate. The phrase "heavy tailed" refers to the shape of the probability distribution function specifying the source's state durations. Here, we use a Pareto distribution with infinite variance.

### III. COMPUTATIONAL INTELLIGENCE

The phrase "computational intelligence", refers to adaptive numerical algorithms for solving traditionally "hard" problems, such as pattern recognition and optimization of complex systems. There are three complementary classes of CI algorithms [12]: artificial neural networks (ANN), fuzzy systems, and evolutionary (genetic) algorithms. The relationships between these algorithms are summarized in Fig. 2 below.

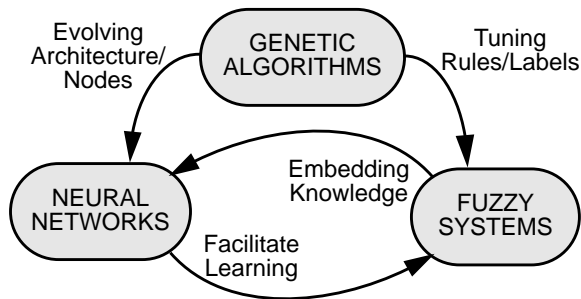


Fig. 2. Relationships of the CI techniques.

This figure illustrates that neural networks and fuzzy systems may closely interact. Neural network data processing and learning capabilities can be used to facilitate learning in fuzzy systems. Conversely, fuzzy systems may be used to embed structured knowledge within neural networks at initialization.

Though genetic algorithms are somewhat separated from the other two, they can effectively perform the role of a trainer for both neural networks and fuzzy systems to help them be optimized. Since we are interested in

robust solutions, it is anticipated that evolutionary systems combining these techniques will be appropriate for application in an ATM environment [13-15].

There is much research [2,3,4,8,9,14,15] being devoted to using CI for improving ATM performance (throughput, utilization and call blocking) via advancing policing mechanisms, CAC, and routing algorithms. Typical research papers quote that by using some relatively simple ANN or fuzzy controller for adaptive decision making inside the ATM switch, they realize approximately a ten percent improvement in throughput over conventional techniques.

Since it is not yet a matured research field, the studies of CI applications in data networks still do not include detailed in-depth reports on methodologies. Though much of this research is insightful and has merit, none of it lays down a clear and well documented methodology, with well set up experiments and sensitivity analysis, to indicate how much of the performance improvement promise may be realized.

### IV. ATM CALL ADMISSION CONTROL

A good CAC function is critical for avoiding congestion in the network. The CAC function should be fair; accepting all calls deemed to be serviceable. However, there still exists the potential for increased call blocking because admitting one very large call may prevent the admission of many small transmissions. Unfortunately, such a scenario would require dividing users into classes based on bandwidth usage and allocating virtual paths in the network.

Fig. 3 below illustrates the modelling of statistical multiplexing of traffic from multiple sources onto a single output port in an ATM switch. This is the environment that we simulate for analyzing our CAC algorithms. The source traffic is simulated using the models described in Section II.

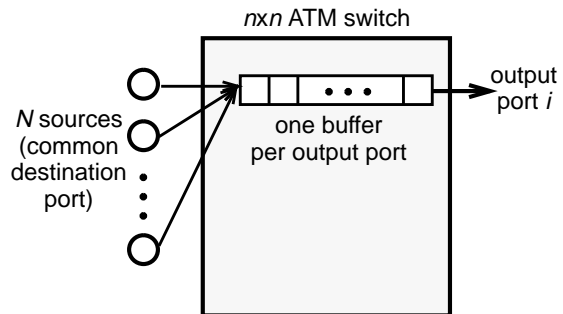


Fig. 3. Modelling traffic from multiple sources onto a common output port.

Conventional ATM CAC algorithms range from simplistic PCR pre-booking (guarantees performance,

but wastes bandwidth), to those based on the concept of effective bandwidth (EB) [5,6,7].

EB is appealing because it is intuitive to think that a VBR source should have some effective required bandwidth (less than its peak rate) at which its QoS requirements are still met. If so, an EB based CAC algorithm would simply compare the sum of EBs to the channel capacity. However, it is only computationally practical to approximate the EB. Furthermore, the equations are available for only specific (Markovian) families of VBR source models. Our simulations show that these conventional EB algorithms can still leave the links under-utilized.

In considering the conventional CAC algorithms, we note that they are quite dependent on accurate assumptions of source models and the ability of sources to declare their characteristics. CI based techniques offer the potential to overcome these dependencies by using expert knowledge and automated extraction of source characteristics.

Furthermore, the conventional techniques do not necessarily include simultaneous consideration of multiple QoS parameters or provide soft control decisions. Here, CI based techniques include such possibilities. Finally, the conventional techniques exhibit little adaptability. CI based techniques may easily be constructed to be adaptive. Accordingly, several measurement based CAC algorithms using CI techniques have been proposed [2,3,4,9,14].

Chang and Cheng [3,4] describe a system using fuzzy logic controllers in ATM for CAC and transmission rate management. The impetus for this approach is the difficulty for a network to obtain complete statistics of its input traffic, together with the somewhat unclear choices of parameters (under dynamic conditions) in conventional techniques. These factors lead to decision processes full of uncertainty. The proposed system accepts or rejects new calls based upon fuzzy rules involving the current buffer state, change in buffer state, a description of how well the existing QoS guarantees are being, together with estimates of the capacities required by the call and available in the network.

## V. SIMULATION ENVIRONMENT

As stated previously, the main goal of this thesis is the development of a methodology for applying CI based algorithms in ATM environments. The techniques developed using this methodology should outperform existing approaches; both conventional and CI based. Ideally, the use of this methodology should lead to solutions that provide tight upper bounds on the exact bandwidth requirements over the whole range of traffic scenarios. The research experimentation and the simula-

tion environment must support the development of a methodology for either directly or indirectly establishing tight upper bounds for these curves. The performance improvements of the resulting algorithms can then be directly measured, in terms of increased link utilization and/or decreased call blocking probability, versus the existing algorithms as well as the exact empirical values.

To date, the model in Fig. 3 has been coded and is being tested. A functional model of this simulation environment is shown in Fig. 4 below. The results of ongoing simulations, implementing MMFP and MMPP sources, and conventional EB based CAC algorithms, will be used as baseline performance measures. Heavy-tailed ON/OFF models, used to generate self-similar traffic such as ethernet and VBR video sources, are also available for simulation.

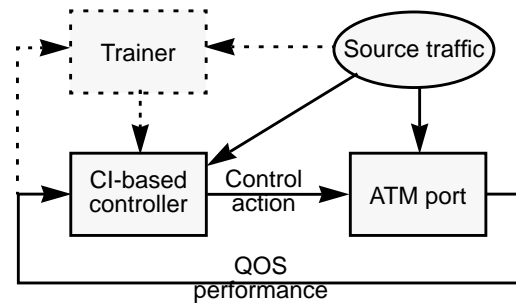


Fig. 4. CAC simulation environment.

Comparative performance analyses versus other algorithms shall be provided throughout the experiments. To develop a methodology for the application of the CI based algorithms, the model will be expanded again to include a monitoring/training process depicted in figure using dashed lines. This hybrid system will be rigorously examined, have its performance evaluated and sensitivity analyzed.

In their implementation, the simulation models must consider the following:

- choice of models for the sources
- traffic contract parameters
- buffer capacities
- output link capacity
- choice of CAC algorithm and its associated parametric requirements

Meanwhile, the simulations must keep track of the following:

- QoS performance metrics
- cell throughput
- link utilization
- number of ongoing calls
- number of calls serviced
- number (ratio) of blocked calls

Our baseline simulations of conventional EB based CAC algorithms (on Markovian traffic sources) indicate many instances where the output link utilization ranges from 30% to 70%. Clearly, under these circumstances there is room for improvement in the utilization, and it suggests that adaptive measurement based techniques may potentially achieve better performance.

## VI. CONCLUDING REMARKS

Literature reviews have been undertaken to examine: (i) conventional ATM CAC techniques (concentrating on effective bandwidths), and (ii) the applications of CI techniques in ATM networks (concentrating on applications in CAC algorithms and routing). These reviews, together with our baseline simulations of conventional EB based CAC algorithms, indicate that the CI techniques do have the potential to improve ATM performance with respect to link utilization and call blocking.

However, the lack of a proper methodology for applying CI to ATM networks is also evident. We propose to establish such a methodology, supported by well documented, well set-up experiments and thorough comparative performance analyses, to fully realize any potential improvements in ATM network performance.

The algorithms being developed are adaptive and measurement based. They will provide robust performance in the face of non-stationary traffic and will not be dependant on source model assumptions.

Though not mentioned in this report, we are also interested in the use of CI based strategies to calculate link metrics in ATM network. This approach shows promise for producing improved routing algorithms.

## ACKNOWLEDGEMENT

This research was supported by Telecommunications Research Laboratories (TRLabs).

## REFERENCES

- [1] ATM specifications available from the ATM Forum: <http://www.atmforum.com/>
- [2] Bensaou, B., S.T.C. Lam, H.-W. Chu, and D.H.K. Tsang, "Estimation of the cell loss ratio in ATM networks with a fuzzy system and application to measurement-based call admission control", *IEEE/ACM Transactions on Networking*, v.5, no. 4, pp. 572-584, August 1997.
- [3] Cheng, R-G., and C-J. Chang, "Design of a fuzzy traffic controller for ATM networks", *IEEE/ACM Transactions on Networking*, v.4, no.3, pp. 460-469, June 1996.
- [4] Cheng, R-G., and C-J. Chang, "A neural-net based fuzzy admission controller for an ATM network", *INFOCOM '96*, v.2, pp. 777-784, 1996.
- [5] Choudhury, G.L, D.M. Lucantoni, and W. Whitt, "Squeezing the most out of ATM", *IEEE Transactions on Communications*, v.44, no.2, pp. 203-217, Feb. 1996.
- [6] Elwalid, A.I., and D. Mitra, "Effective bandwidth of general Markovian traffic sources and admission control of high speed networks", *IEEE/ACM Transactions on Networking*, v.1, no.3, pp. 329-343, June 1993.
- [7] Guérin, R., H. Ahmadi, and M. Naghshineh, "Equivalent capacity and its application to bandwidth allocation in high-speed networks", *IEEE JSAC*, v.9, no.7, pp. 968-981, Sept. 1991.
- [8] Hellendoorn, H., "Fuzzy control in telecommunications", *NAFIPS '96*, Berkeley, CA, pp. 444-448, 1996.
- [9] Hiramatsu, A., "ATM network control by neural network", *Handbook of Neural Computation*, IOP Publishing and Oxford University Press, 1997.
- [10] Leland, W.E., et al., "On the self-similar nature of ethernet traffic (extended version)", *IEEE/ACM Transactions on Networking*, v.2, no.1, pp. 1-15, February 1994.
- [11] McDysan, D.E., and D.L. Spohn, *ATM: Theory and Application*, McGraw-Hill, Inc., 1995.
- [12] Pedrycz, W., *Computational Intelligence: An Introduction*, CRC Press, 1997.
- [13] Pedrycz, W., R.R. Gudwin, and F.A.C. Gomide, "Nonlinear context adaptation in the calibration of fuzzy sets", *Fuzzy Sets and Systems* 88, pp. 91-97, 1997.
- [14] Uehara, K., and K. Hirota, "Fuzzy connection admission control for ATM Networks based on possibility distribution of cell loss ratio", *IEEE JSAC*, v.15, no.2, pp. 170-190, Feb. 1997.
- [15] Vasilakos, A.V., K.G. Anagnostakis, and A. Pitsilides, "An evolutionary fuzzy algorithm for QOS and policy-based inter-domain routing in heterogeneous ATM and SDH/SONET networks", *EUFIT'97*, Aachen, Germany, Sept. 1997.
- [16] Willinger, W., et al., "Self-similarity through high-variability: statistical analysis of ethernet LAN traffic at the source level", *SIGCOMM '95*, pp. 100-113, 1995.

# Modelling Emergent Behaviours for Construction Tasks

*Douglas Holmes* University of Manitoba, dholmes@insicorp.com

## Abstract

Emergent behaviours have been used in biology to model construction tasks, and in robotics to produce control behaviours. Simulations have been used to show that constructive behaviours based on existing robot control behaviours is possible.

## Introduction

Emergent behaviour provides a new paradigm for modelling. The interaction of multiple simple actions give rise to aggregate results which are not only more complex than the sum of the interacting parts, but exhibit a coherency which is not obvious from the description of the interactions.

This emergence has been used to model behaviours of biological systems ranging from biochemical to societal [Beck92, Cale92, Seid92, Colo92, Drog92, Bona96]. These models have been useful in understanding how complex behaviours could have arisen from simple reflexive actions.

The model of emergent behaviours has been successfully applied in robotics [Colo94, Mata95, Stee94, Ram94, Dona93]. Rather than being used to explain complex behaviours, it has been used to define them. Starting from the mechanical controls available in robots, emergent behaviours have been developed by searching for the appropriate responses to environmental stimuli that give the correct degree of interaction. A variety of techniques have been used both for expressing and searching for these behaviours.

The behaviours developed to this stage have, for the most part, been control behaviours, that is behaviours which relate to how a robot operates its own mechanisms.

Current behaviours have been tedious and difficult to develop. Adding an extra layer of complexity to the tasks would make such behaviours too time-consuming and difficult to

develop. It would be advantageous to build on such behaviours as already exist, and develop new behaviours which take advantage of what has gone before. Early behaviours have been defined on mechanical controls, new behaviours will be built on virtual controls, the already existing robotic behaviours.

To determine the possibility of developing such higher level behaviours, this research has focussed on one particular type of behaviour, that of construction. There has already been some success in applying emergent behaviour to construction tasks in biological research. Extending this to the field of robotics seems a natural extension.

Preliminary experiments have shown that such higher level behaviour is possible. These experiments used several basic control behaviours such as moving and homing and a three dimensional cellular automata approach to construct a cube out of cubic blocks in a cubic lattice. These experiments were based on hypothetical agents operating in a simplistic and perfect world.

## Objective

The objective of this research is to determine if a class of behaviours for useful robotic construction tasks can be modelled as a higher layer of behaviour on lower level control tasks. The two basic questions are whether higher level behaviours can be defined in terms of control behaviours, and whether constructive behaviours can be defined, modelled and implemented. This hierarchy is illustrated in Figure 1.

This paper describes one set of experiments into producing emergent constructive behaviour. The target was to have multiple agents produce a regular structure unlike any normally produced by agents in nature. A cube was chosen for its simplicity.

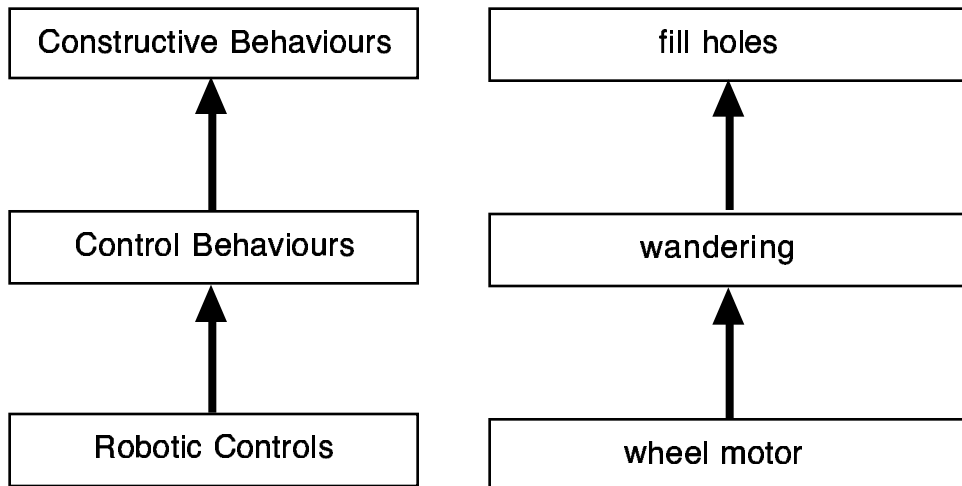


Figure 1. The hierarchy of behaviours, in general, and with an example.

The environment was a three dimensional cubic lattice. A seed block was placed in center of the space. Each agent maintained an internal state and all agents operated from the same set of rules. The rules were set up as a sequence of masks on the 26 cells neighbouring the agents current location in the lattice as well as the agents current location.

In each time increment, each agent examined its environment and compared it to each of the rule masks in turn. When a match was found, the associated action was performed.

### Initial Experiment

The set problem was to build a cube. The construction behaviours expected were getting the agents to build straight lines and fill in to make a solid structure. A simple set of hand crafted rules were used initially.

The actions which were implemented for the agents were: forward-movement, turning, placing a block in the current location, searching for material and homing.

Perception was based solely on whether there were blocks in the immediate environment. Agents were not able to see each other, but the software ensured that no two agents occupied the same location at the same time.

Each rule consisted of an 27 position mask and

an action pair. The mask represented the location the agent was in, and the neighbouring 26 locations. This mask was compared to all of the different views of the agent's local environment when its turn in the time interval arrived. The mask allowed three states, a block was present, no block was present, and don't care. Probabilities were attached to the rules. This slowed down the rate of construction, but provided more flexibility in controlling growth rates.

The three behaviours implemented by the rules were to extend corners outward, to add along edges and to fill in surfaces. The cube emerged as layers were added to the seed cube. The rules which lead to extension were given a lower probability than the rules which lead to filling in.

The flaw in the construction process was that the expansion would occur before the surface had been filled in. Also, expansion was not always even, so the cube would become brick like, differing in size between the dimensions. The probabilities which lead to a reasonable balance between growth and filling in were different depending on the size of the structure completed. Finally, there was no way to limit the size of the cube, except by the length of the simulation.

### Extended Experiment

For the second set of experiments, it was

decided to add some complexity to the agents in an attempt to address some of the shortcomings from the initial experiment.

In terms of their interaction with the environment, rather than simply occupying a space, their orientation in that space was made to accommodate the surface. This meant that in addition to occupying a space, the agents were standing with their feet on a surface and facing in a direction. This made their travel on the surface of the structure more sensitive to its irregularities.

The agents were given two sets of rules, one for expansion and one for cleaning up the surface. Which rule set to use was based on the agent's state. Based on information about honey bees, which progress through different roles as their wings wear, the concept of energy level was introduced to the agents, which was depleted through time and activity. At lower energy levels, the robots followed a second set of rules. Only at high energy levels would more material be gathered and placed. At lower levels, material was shifted on the structure. When energy levels were completely expended, the agents disappeared. This allowed for restricting the size of the structure as well. A sample rule set is provided in figure 3.

```

1***** 9 25
-*****Bx*x*****B**** 2 1
-*****xB**x*****B**** 2 1
-*****xBx*****B**** 2 1
-*****BBB*****xBx*** 2 1
-*****x*****BB*BB 2 5
-*****x*****BB*BB* 2 5
-*****XXXBX*** 2 1
-*****XXX*B*X*X 2 1
-*****B**** 1 0

```

Figure 2. Sample rule set, showing 10 rules with mask, action and delay.

To permit the agents to clean up the surface, a new action, picking up a block, was added to the model.

Probabilities were taken out of the model, but a delay was added to replace them. Each agent was aware of how long it had been in a particular state, and some rules were not valid until the

agent had been in the correct state long enough. In some sense, they had to run out of patience.

### Observations

The goal is to understand how basic robot behaviours can be used as actions to evolve higher level construction behaviours. Several decisions were made in constructing the model without any reference to a physical model. Many of the parameters to the environment and agents behaviours would not be parameters in a real solution, but rather would be restrictions.

Instead of trying to solve for one particular problem without recognizing its relevance or significance, it was decided that a more structured approach to the problem of evolving construction behaviours was desirable.

### Conclusions

A literature review has shown that emergent behaviour can be successfully applied to modelling observed behaviour in animals, and to the application of robots in both simulated and physical environments. In both cases, the behaviour is based on the interaction of several basic actions or reflexes.

The difficulties of developing behaviours in the physical world argues that not only must simulations be used to develop complex new behaviours, but that these behaviours must take advantage of existing behaviours. It must also be pointed out that there has been limited attempts in transferring simulated behaviours to physical robots.

Some experimentation has also shown that basic constructive behaviour, such as building a cubic structure, can be developed in a simulated environment. This behaviour made use of lower level behaviours rather than direct interaction with the agents primary effectors.

While the experiments indicated possibility, they did not show how such behaviours could be implemented using physical agents, such as robots.

Research has also shown that while a number of robotic behaviours have been developed, there is no standard definition of what the behaviours are, or how to model them for simulations which

would be based on the behaviours.

### References

- [Beck92] R. Beckers, J. Deneubourg, S. Goss, Trails and U-turns in the Selection of a Path by the Ant *Lasius niger*. *Journal of Theoretical Biology* 159, 1992, pp397-415.
- [Bona94] E. Bonabeau, *et al.*, The Building Behavior of Lattice Swarms. *Proceedings of the 4th International Workshop on the Synthesis and Simulation of Living Systems (Artificial Life IV) (ALIFE94)*. Cambridge, MA, USA, 1994, pp. 307-312.
- [Bona96] E. Bonabeau, G. Theraulaz, J. Deneubourg, Mathematical Model of Self-Organizing Hierarchies in Animal Societies. *Bulletin of Mathematical Biology*, 1996, Jul, V58 N4:661-717.
- [Cale92] V. Calenbuhr, J. Deneubourg, A Model for Osmotropotactic Orientation. *Journal of Theoretical Biology* 158, 1992, pp359-393.
- [Colo94] M. Colombetti, M. Dorigo, Training Agents to Perform Sequential Behavior, *Adaptive Behavior* 2(3), 1994, pp247-276.
- [Colo92] A. Colorni, M. Dorigo, V. Maniezzo, Distributed Optimization by Ant Colonies. *Toward A Practice of Autonomous Systems: Proceedings of the First European Conference on Artificial Life*, IT Press, 1992, pp. 134-142.
- [Dona93] R. Donald, J. Jennings, D. Rus, Information Invariants for Cooperating Autonomous Mobile Robots. *Proc. International Symposium on Robotics Research*, Hidden Valley, PA, 1993.
- [Down90] H. Downing, R. Jeanne, The regulation of complex building behaviour in the paper wasp, *Polistes Fuscatus* (Insecta, Hymenoptera, Vespidae). *Animal Behav* 39, 1990, pp105-124.
- [Drog92] A. Drogous, *et al.* A Behavioral Simulation Model for the Study of Emergent Social Structures. *Toward A Practice of Autonomous Systems: Proceedings of the First European Conference on Artificial Life*, MIT Press, 1992, pp. 161-170.
- [Kars93] I. Karsai, A. Penzes, Comb Building in Social Wasps: Self-organization and Stigmergic Script. *Journal of Theoretical Biology* 161, 1993, pp.505-525.
- [Mata95] M. Mataric, Issues and Approaches in the Design of Collective Autonomous Agents. *Robotics and Autonomous Systems*, 16, Nos. 2-4, December 1995, 321-331.
- [Ram94] A. Ram, *et al.* Using Genetic Algorithms to Learn Reactive Control Parameters for Autonomous Robotic Navigation. *Adaptive Behavior* v2, issue 3, 1994, pp. 277-304.
- [Seid92] P. Seiden, F. Celada, A Model for Simulating Cognate Recognition and Response in the Immune System. *Journal of Theoretical Biology* 158, 1992, pp.329-357.
- [Stee94] L. Steels, A case study in the behavior-oriented design of autonomous agents. *From Animals to Animats, Simulation of Adaptive Behavior (SAB '94)*, Brighton, UK, MIT Press, 1994.

# PERSONAL PROXY CACHE

Sajid Hussain, sajid@ee.umanitoba.ca

Microelectronics and Software Systems Lab

Advisor: Robert D. McLeod, mcleod@ee.umanitoba.ca

**Abstract--**This paper presents a personal proxy cache at the proxy server where objects are pre-fetched from the Internet to provide faster downloading for bandwidth limited users. The personal caching agent determines the objects to be pre-fetched. It increases the probability of getting the desired object at the personal proxy cache thus fewer objects are downloaded directly from the Internet.

## I. INTRODUCTION

The Internet is becoming increasingly popular at home, work, school and all other institutions. At home, users have bandwidth constraints which delay the retrieval of information. The goal is to bring the source objects closer to the user so that less time is needed to download the data at the bandwidth bottleneck.

Caching on local browsers helps to reduce the delays for reloading recently accessed objects. The retrieval time could be further reduced by pre-fetching (push-caching) [1] the objects that are not requested by the user but are likely to be requested in the future. Since the user at home have bandwidth constraint channel, pre-fetching the objects at home computer will not be effective. Pre-fetching could be effective by providing a personal cache for the user at the proxy server. The objects are pre-fetched to the personal proxy cache using large bandwidth channel between proxy server and the source website.

Personal proxy cache agent could be used to determine the objects to be pre-fetched for the user. The agent monitors the history of the user and determines the desired objects. The personal proxy caching increases the chances of getting the object from the pre-fetched objects.

The following section discusses the personal proxy cache, section III discusses the prototype implementation and finally the conclusion.

## II. PERSONAL PROXY CACHE

Most home users suffer from communication delays. The cost of disk space and computation time is significantly less than the cost of communication. Personal proxy cache provides extra user cache on the proxy server. The

local web browser cache is quite beneficial for users but they still suffer from communication delays. The Internet download time through a modem is very long when compared to the download time of the same object from a proxy server.

Figure 1 shows that there is a greater bandwidth channel between the proxy server and the Internet than between the home user client and the proxy server. Thus, while an object is downloaded for a user from the proxy server during the same time several other objects can be pre-fetched from the Internet to the proxy server. These pre-fetched objects will accelerate the downloading process.

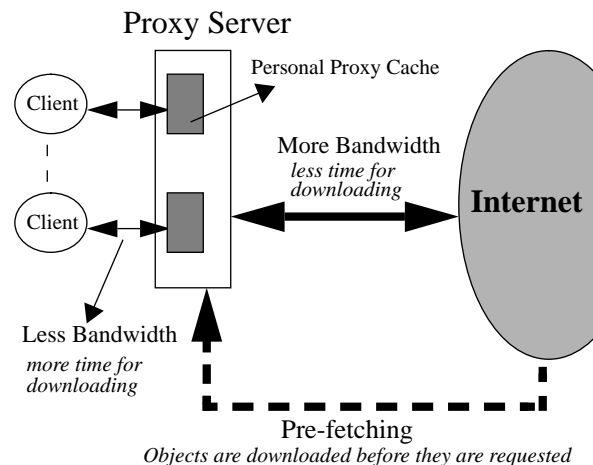


Fig. 1. Pre-fetching to Personal Proxy Cache

### A. Hierarchy

A hierarchy of caches improves the system's performance [2]. The personal proxy cache adds an additional layer in the hierarchy. Figure 2 shows the hierarchy of caches in the prototype implementation of personal proxy cache. The first layer is the local browser cache, second is the personal proxy cache and third is the proxy server cache. The inefficient addition of more layers in the hierarchy of caches may increase the document retrieval time [3]. When the proxy server

cache is full and an object is replaced then usual least recently used (LRU) algorithms give poor performance [4]. Since the likelihood of finding the objects in the personal proxy cache is greater than finding the objects in the proxy server cache, the addition of an extra layer in the hierarchy reduces the objects downloading time.

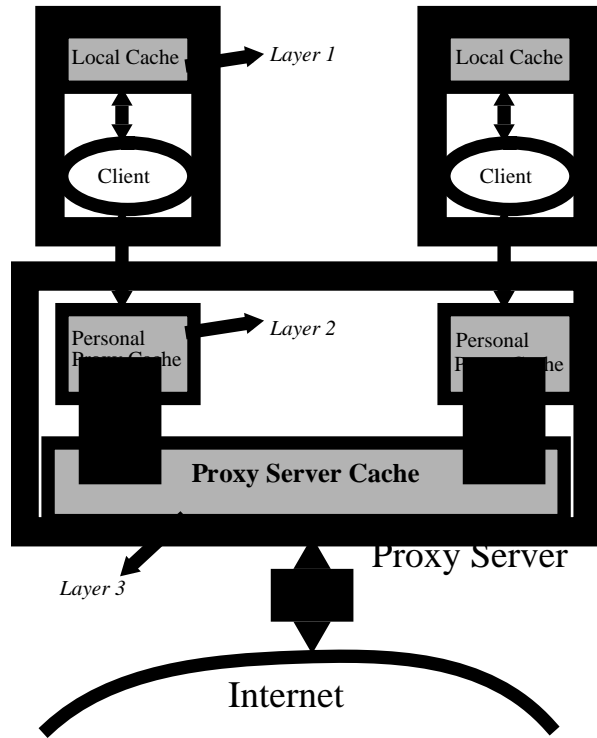


Fig. 2. Hierarchy for Personal Proxy Cache

### B. Personal Caching Agent

A Personal caching agent determines the objects to be pre-fetched. The user browsing history helps to determine possible candidates. Furthermore, simple heuristic rules may also help in determining the possible candidates. For instance, if the user visits a particular newspaper or entertainment site everyday, then it may be required to pre-fetch the objects to the personal proxy cache. As well, if the user visits a list of links then it is better to pre-fetch the other objects in the list while the first object is being downloaded [5].

### III. IMPLEMENTATION

The prototype for the *personal proxy cache* is implemented for the Microelectronics and Software System's Lab. The personal proxy cache is implemented

in the */usr/local/tmp* directory for users on the Sun Solaris 2.5 operating system. The users can utilize the free disk space (*/usr/local/tmp*) for their pre-fetching and thus download the documents at a faster rate. Squid ver. 1.1.21 is used as the proxy server and wget ver. 1.5.0 is used to pre-fetch the objects from the Internet. The objects referenced by the links in the current document are downloaded to the personal proxy cache.

### A. Algorithm

A simple algorithm is proposed to pre-fetch the objects. The algorithm is easy to implement and does not require large over-head.

1. Retrieve the visited link from the log file of the user
2. Pre-fetch the other objects referenced by the links in the current object
3. IF the user visits some other link THEN terminate the pre-fetching process

The pre-fetching is proportional to the time spent at the website by the user.

### B. User Request Path

When a user makes a request, the object is first searched in the local browser cache. If the document is not found then the request is given to the proxy server. The Proxy Server checks the documents in the personal proxy cache for the user. If the document is available in the personal proxy cache then it is given to the user. If the document is not located in the personal proxy cache, it is searched in the proxy server cache and if it is not available there then the object is retrieved from the Internet.

When the object is retrieved from the Internet, then a copy of the object is stored in the proxy server cache and another copy is stored in the personal proxy cache.

### IV. CONCLUSION

Objects are pre-fetched to the personal proxy cache to get faster downloading. Since the personal caching agent is used, the probability of finding the objects at the proxy server is greater and fewer objects are downloaded from the Internet.

### ACKNOWLEDGEMENTS

The guidance of Professor Robert D. Mcleod is gratefully appreciated. The financial support of the

Internet Innovation Center and the Engineering Research Council is gratefully acknowledged.

#### REFERENCES

- [1] J. Gwertzman, "Autonomous Replication in Wide-Area Networks," *Masters Thesis, Harvard University* April 95.
- [2] A. Chankhunthod, P. Danzig, C. Neerdaels, M.F. Schwartz and K. Worrell, "A Hierarchical Internet Object Cache," in *Proc. USENIX 96*, <http://excalibur.usc.edu/cache.html>, 1996.
- [3] R. Tewari, M. Dahlin, H. Vin, and J. Kay, "Beyond Hierarchies: Design Considerations for Distributed Caching on the Internet" *Technical Report, Dept. of Computer Science, University of Texas at Austin* February 1998.
- [4] M. Abrams, C. R. Standridge, G. Abdulla, S. Williams, and E. A. Fox, "Caching proxies: Limitations and Potentials," in *Proceedings of the Fourth International Conference on the WWW* (Boston, MA), December 1995.
- [5] R. D. Mcleod, D. C. Blight and S. Hussain, "A Personal Caching Agent", in TR-98-04, <http://www.wee.umanitoba.ca/~sajid/TR-98/cache.html>, 1998.

# PROGRESSIVE IMAGE TRANSMISSION USING WAVELET AND OTHER FRACTAL TECHNIQUES

*Richard Dansereau*

eMail: richard.dansereau@pobox.com

Department of Electrical and Computer Engineering, Signal and Data Compression Laboratory,  
University of Manitoba, Winnipeg, Manitoba, Canada R3T 5V6.

and

TRLabs (Telecommunications Research Laboratories)  
10-75 Scurfield Boulevard, Winnipeg, Manitoba, Canada R3Y 1P6

Advisor: W. Kinsner <kinsner@ee.umanitoba.ca>

**Abstract** - This is a digest of the work and research completed thus far in developing a progressive image transmission scheme. Efficient and quick communication of perceptually important image information is desired resulting in this research with wavelet and fractal techniques for the identification and extraction of perceptually important features. This is done with the final goal of interactive control over the panning, zooming, and termination of the image reconstruction with minimal recomputation at progressive steps.

## I. INTRODUCTION

TRANSMISSION and manipulation of large images, such as satellite or aerial images of natural resources and city streets, proves to be a time and resource consuming task. Images, such as that in Fig. 1, are often used by city planners, telephone companies,



Fig. 1 Aerial ortho image of urban area  $2648 \times 2759$   
(courtesy of Linnet Geomatics, Inc.).

hydro companies, and natural resource institutions and usually require high accuracy and resolution for project planning. Uses for these high resolution images include tasks such as deciding where to place new sewer pipelines and telecommunication lines, or analyzing images of farm land to determine the best application pattern for pesticides, herbicides, and nutrient supplements. Other applications for high resolution images include astronomy image warehousing, medical image database distribution, and photographic cartography.

Unfortunately, images of the required resolution often exceed 25 megabytes. The sheer size and high resolution required makes storage, transmission, and manipulation of the images prohibitive. To compound these problems there may be hundreds or thousands of these images in a remote database. This makes searching through a remote database and zooming on regions of interest in an image even more difficult.

We therefore investigate and develop new progressive image transmission techniques for distributing such images efficiently and effectively. Through the proper *extraction, ordering, and control* of the flow of transmitted data, image compression and transmission can be improved upon to suit a larger class of image distribution problems than current progressive image transmission techniques can efficiently handle. First of all, image compression by itself can reduce the amount of data that must be transmitted from source to destination. If image compression is done such that increasing levels of perceptually important details are transmitted then this improves the early recognition of important features in the image before all of the image is transmitted. If the user notices that the image is not desired then transmission is terminated prematurely and the user can move on to another image. This extra control over the transmission is useful in helping reduce total transmission time. Another important feature is the ability to zoom interactively in and out of different regions of an image or pan around in a zoomed image. If zooming and panning is done in a smart way, the data stream can be changed

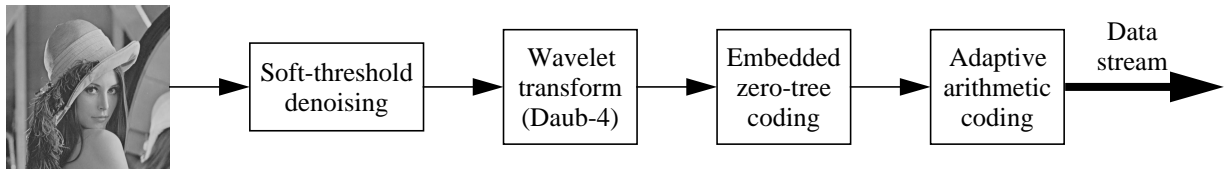


Fig. 2 Data flow of a basic progressive wavelet image coder.

dynamically to send only the image information required for the area of the image being viewed. This does require a smarter transmitter/receiver configuration but the extra flexibility is indispensable for some of the listed applications. This whole scheme can be classified as an *adaptive* progressive image transmission model.

The remainder of this paper presents the important aspects of research and work done so far for achieving this adaptive progressive image transmission scheme. Section II outlines some of the work done with wavelets in developing progressive image transmission. Section III outlines a new technique developed for the representation of image textures through fractal surface interpolation. Section IV outlines the begins of a quantitative measure of image quality based on the fractal complexity. Section V outlines some of the initial work done with image denoising to improve the compressibility of images which will reduce transmission time. And finally, Section VI briefly describes the client/server testbed under development to field test the developed progressive image transmission schemes.

## II. PROGRESSIVE IMAGE TRANSMISSION USING WAVELETS

A number of approaches are being investigated and are under development to efficiently and effectively perform the progressive transmission of images. The primary approach looked at consists of decomposing images using the wavelet transform and then selectively choosing and ordering which wavelet coefficients best perceptually represent the image. A data flow diagram of one of the implemented progressive image transmission schemes using wavelet decomposition is illustrated in Fig. 2 [DaKi98a]. Here, we have an image that is feed through a soft-threshold denoiser [Dono95] to remove noise that hinders the compressibility of the image. This resulting denoised image is passed through a wavelet transform filter and then embedded zero-tree coding [Shap93] is used to order and compress the wavelet coefficients according to energy magnitude. Finally, adaptive arithmetic coding [WiNC87], which is a lossless entropy coder, is used to remove further data

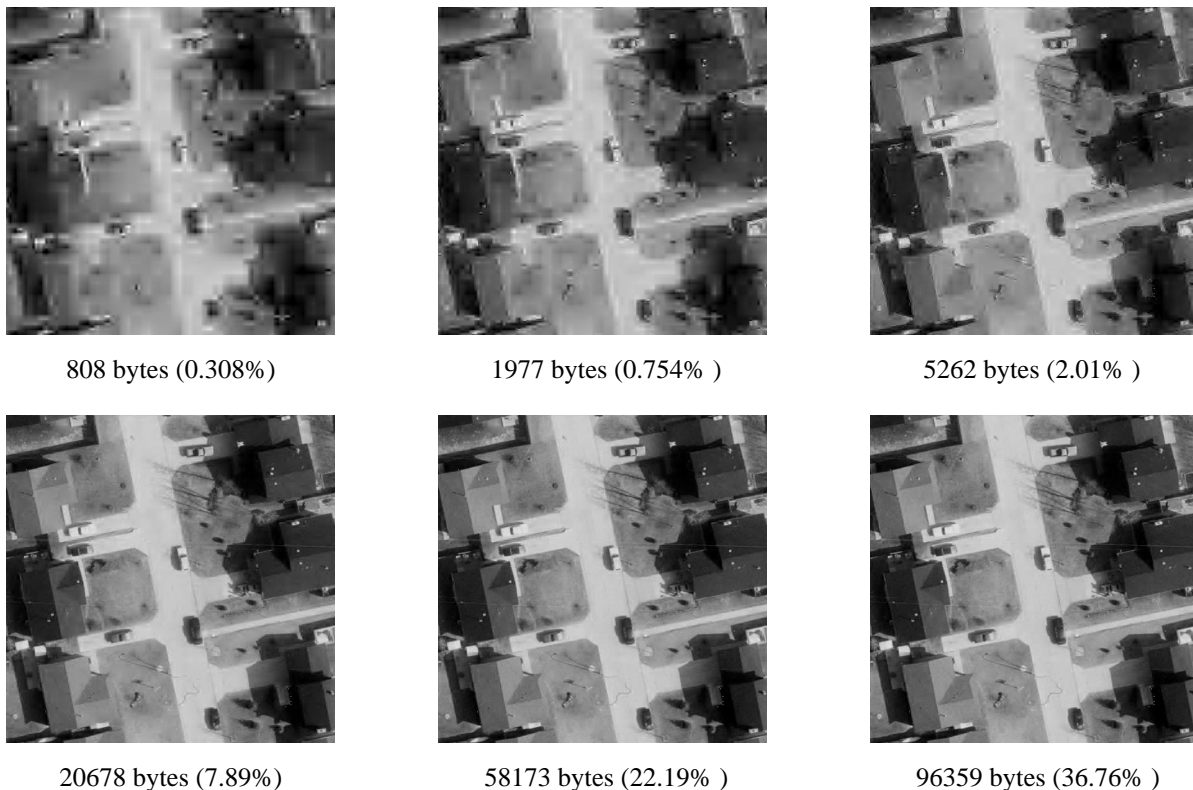


Fig. 3 Progressive transmission of the aerial ortho image denoised to 35 dB with size in bytes and % of original.

redundancy left in the data stream before transmission. A set of sample steps from a progressive image transmission using this scheme is shown in Fig. 3.

### III. PROGRESSIVE IMAGE TRANSMISSION THROUGH FRACTAL SURFACE INTERPOLATION

Another approach to progressive image transmission being investigated is to use fractal surfaces to synthesize textures within an image. Work began with developing techniques to *measure, represent, and synthesize* image textures using fractal techniques. A new technique for image compression was developed where fractal surfaces, such as the one illustrated in Fig. 4, are used to recreate image surfaces through *fractal surface interpolation* (FSI) [DaKi96]. This is done by measuring the fractal dimension of the surfaces throughout an image and then recreating these surfaces using 2D fractional Brownian motion (fBm) through the midpoint displacement algorithm (MPD) [Saup88]. This technique was found to work best with random looking textures due to the nature of the randomness in the MPD. Further work was done with FSI where fractal surfaces were overlaid on coarse wavelet compressed representations of images [DaKi97]. This improved the compression ratio of the images since wavelets do a better job at the overall surface tendencies in images while the fractal surfaces can represent the random noise texture features perceptually present on top of these surfaces.

The ideas of FSI for image compression were then extended to a progressive image transmission scheme [DaKi98b]. The natural progressive nature of the image reconstruction steps, as illustrated by the three successive steps in Fig. 4, lends itself well to the progressive transmission of the surface information so that increasing levels of detail in the surfaces are reconstructed.

### IV. MEASURE OF IMAGE COMPLEXITY AT PROGRESSIVE STEPS

Along with the actual progressive image transmission schemes being developed, we are also interested in the quality of the image at successive steps during the progressive image transmission. This is a primary interest since understanding how specific progressive image transmission schemes break down and order the image information is vital in evaluating the performance of the progressive image transmission. Also, understanding how the progression occurs helps in tuning the selection of parameters to improve the early steps of the progressive image transmission.

Traditionally, only the *peak signal-to-noise ratio* (PSNR) of an image is used to evaluate its quality. Unfortunately, this only relates the reconstructed image

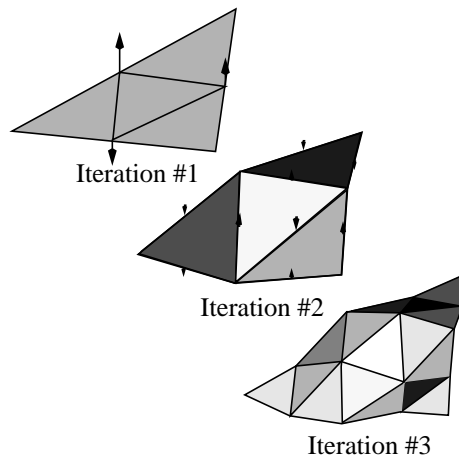


Fig. 4 Example of 2D fBm illustrating FSI.

with the original image in terms of energy. This is limiting and since more appropriate measures can be developed for evaluating the successive steps in a progressive image transmission. To this end, development is underway on a quantitative image quality measure based on the Rényi generalized entropy [DaKi98a][Kins94]. Using the Rényi dimension measure, a range of fractal dimensions is calculated which gives a measure of the fractal complexity within the image. Combining both the PSNR and the fractal complexity measures of the Rényi dimension, optimal selection of wavelet coefficients of an image is possible to improve its quality at successive steps in the progressive transmission. Using this, successive steps in the transmission should be perceptually superior to a selection scheme based on energy alone since the fractal complexity within the successive images is better represented.

### V. SOFT-THRESHOLD DENOISING

Another important aspect of the progressive image transmission scheme, or any image compression scheme in general, is the removal of unwanted, incompressible noise from the image as a preprocessing step. This is in line with the goals of the progressive image transmission since identification of perceptually important image features is required which rarely includes noise components.

The general notion of denoising is the removal of noise that is present in a signal, leaving only the clean signal. Normally, though, the noise component is unknown so denoising seems an impossible task. Using the a priori knowledge that noise usually has different statistical properties and characteristics from those of the clean image, we can differentiate between the noise and image components in the signal. Removal of this noise generally improves the compression rate of the

image and therefore reduces the time required for the progressive transmission of the image.

Research done to date in this area includes using soft-threshold denoising [Dono95]. Here, we apply a nonlinear thresholding scheme to the empirical wavelet coefficients of a transformed image. This process smooths out noise in the image but tries not to degrade sharp, prevalent structures such as edges which are normally removed when using classical smoothing operators. Also, soft-threshold denoising does not introduce spurious artifacts into the denoised image that later may be interpreted as significant. The denoised image will be as smooth as the original.

## VI. CLIENT/SERVER TESTBED FOR PROGRESSIVE IMAGE TRANSMISSION

The first phase of the implementation of the client/server software is completed. A testbed for image display, transmission, and progressive reconstruction has been developed with work now shifting on the interactive control of the progressive image transmission.

The idea behind the client/server testbed is to make the system smart enough so that the client can reconstruct the image as image information is received. Also, the system is designed so that the server can dynamically react to interactive requests made by the client during the transmission of a particular image. This interactive control includes panning, zooming, and termination of transmission for the image.

Dynamic control over the progressive transmission makes it possible to reduce bandwidth requirements since the server only needs to transmit requested portions of an image instead of blindly transmitting the entire image even if it is not desired. Also, the server can transmit only those portions and details of the image that the client does not already have. This is especially important for panning and zooming since much of the image is already available on the client side and only the additional image information required because of the panning or zooming action needs to be transmitted.

## VII. SUMMARY

A number of techniques have been explored to achieve the desired progressive transmission of images. Wavelet techniques have shown to produce favourable results for decomposing images and allowing selection of important image features for transmission. Fractal surface interpolation presents another technique for progressive image transmission since surface textures can be represented by increasingly detailed random fractal surfaces. The Rényi dimension has been found to be useful for measuring the complexity within an image

and hence is useful as a quantitative quality measure of complexity for images. This is useful in the selection of image features to more faithfully represent the successive images in the progressive transmission. Soft-threshold denoising proves effective at removing noise and improving the compressibility of images though some level of the signal is also removed. Further work of reintegrating the removed signal is planned. Finally, a client/server testbed for field testing the progressive image transmission schemes has been developed.

## ACKNOWLEDGMENT

This research has been supported by the Natural Sciences and Engineering Research Council (NSERC) of Canada and by Telecommunications Research Laboratories (TRLabs).

## REFERENCES

- [DaKi96] R. Dansereau and W. Kinsner, "Perceptual image compression through fractal surface interpolation," *Proc. Canadian Conf. on Elec. and Comp. Eng. (CCECE'96)*, pp. 899-902, 1996.
- [DaKi97] R. Dansereau and W. Kinsner, "Image compression through fractal surface interpolation and wavelet compression," *Proc. of WESCANEX'97*, pp. 94-99, 1997.
- [DaKi98a] R. Dansereau and W. Kinsner, "Progressive transmission of images using wavelets: Evaluation using the Rényi generalized entropy," to appear in *Canadian Conf. on Elec. and Comp. Eng. (CCECE'98)*, May 1998.
- [DaKi98b] R. Dansereau and W. Kinsner, "Progressive transmission of images through fractal surface interpolation," to appear in *Canadian Conf. on Elec. and Comp. Eng. (CCECE'98)*, May 1998.
- [Dono95] D. L. Donoho, "De-noising by soft-thresholding," *IEEE Trans. on Inf. Theory*, vol. 41, pp. 613-627, May 1995.
- [Kins94] W. Kinsner, "Fractal dimensions: morphological, entropy, spectral and variance classes," *Technical Report, DEL94-4*, Univ. of Manitoba, 146 pp., 1994.
- [Shap93] J. Shapiro, "Embedded image coding using zerotrees of wavelet coefficients," *IEEE Trans. Signal Processing*, vol. 41, pp. 3445-3462, Dec. 1993.
- [Saupe88] D. Saupe, "Algorithms for random fractals," *The Science of Fractal Images*, ed. H.-O. Peitgen and D. Saupe, Springer-Verlag, pp. 71-136, 1988.
- [WiNC87] I. H. Witten, R. Neal, and J. G. Clear, "Arithmetic coding for data compression," *Comm. ACM*, vol. 30, pp. 520-540, June 1987.

# Segmentation and Compact Representation of Moving Objects in Facial Image Sequences

P. Yahampath

Advisor: Prof. W. Kinsner

Department of Electrical & Computer Engineering, University of Manitoba

Winnipeg, Manitoba, Canada, R3T 5V6

*email:* pradeepa@ee.umanitoba.ca

*Abstract*— This research addresses the problem of moving object detection in image sequences, with application to very low bit rate video coding. An approach to segmentation of moving objects in facial image sequences is presented. In this approach a split-and-merge procedure is used to resolve the difficulties arising out of the mutual dependence between motion estimation and segmentation. The basis of the approach is the segmentation of a given frame based on edge detection and subsequent merging of regions based on motion analysis. The edge detection has been achieved using the wavelet transform. The motion estimation is based on a geometric model for the objects to be detected. Preliminary results obtained with typical head and shoulder images are presented.

## I. INTRODUCTION

THE very low bit rate coding of video (*i.e.*, as low as 10 Kb/s) has been necessitated by the ever growing demand for visual communication services over the public networks. It has been shown that *object-based coding* can be used to achieve much better perceptual image quality at low bit rates, compared to the classical block-based coders [MuHO89]. The fundamental idea behind object-based coding is to extract and encode messages describing the moving objects in a video sequence. At the decoder, the sequence is reconstructed by synthesizing images using the transmitted messages. This requires modeling of moving objects, and different types of models including 2D and 3D models have been proposed in the past [LiLF94]. In this paper we use a 2D model to represent the projections of actual 3D objects on the image plane, and avoid the problem of dealing with 3D objects. Thus, the object detection problem reduces to the segmenta-

tion of an image sequence into regions that conform to the given model. In comparison to a block-based coder, the object based coder uses arbitrarily shaped regions for motion compensation. This approach entails certain complexities with respect to a block-based coder. Firstly, it is necessary to establish the temporal correspondence of moving regions between frames, and possibly throughout the entire image sequence. Secondly, it requires, in addition to motion information, the shape of objects or segmentation information to be transmitted to the decoder, leading to an additional coding overhead compared to a block-based coder. Therefore, the segmentation of moving objects must be carried out such that the inter-frame variations of detected objects are minimal.

This paper presents an approach to object detection in head and shoulder image sequences. Our work has been motivated by the application of object-based video coding to such sequences and achieving bit rates in the vicinity of 10 Kb/s. Hence, we attempt to segment the image sequence into regions that closely corresponds to the actual objects, *i.e.*, head and shoulders of a person. This ensures the consistency of objects through the sequence, and allows the coding of only the small inter-frame variations of object-shapes. The process can be divided into two steps: (i) short term analysis that identifies moving objects in two consecutive frames, and (ii) long term analysis that ensures a temporally coherent “image scene”. This paper deals with the first step. The second step involves segmentation projection and object tracking. The main feature of the segmentation method presented in this paper is the use of an object model. We use a split-and-merge procedure in finding ac-

curately the boundaries of moving objects that confirm to the model. In the *split* phase, a given frame is segmented into set of regions using wavelet-based edge detection [MaZh92]. This allows the accurate location of intensity boundaries in the image. Next, the motion estimation is carried out to identify the regions that belong to moving objects. In the *merge* phase, the adjacent regions that undergo similar motion are merged to form complete moving objects.

## II. OBJECT MODEL AND MOTION ESTIMATION

In the context of this paper, an “object” is a region covered by the projection of a 3D moving object onto the image plane. It is desired that images in a sequence be segmented along the boundaries of such projections. In order to detect the boundaries we have to use some *a priori* knowledge about the underlying objects, expressed in the form of an object model. Since the purpose of our work is to detect objects in head-and-shoulders images, it is necessary to use a model that can best represent such objects. In this paper, the quadratic surface model with 3D rigid motion presented in [Diehl91] has been used. This model is a good approximation to the general surface shape of human face. Also, the commonly used affine model is included in this model as a special case. Let  $\mathcal{R}$  denote set of pixels defining a moving region, and let  $(u, v)$  be the optical flow field at a point  $(x, y) \in \mathcal{R}$ . Also denote image intensity function by  $I(x, y, t)$  at time  $t$ . Assuming that 3D-2D mapping is the parallel projection, the above object model leads to the parametric optical flow field given by

$$u = a_1x^2 + a_2y^2 + a_3xy + a_4x + a_5y + a_6 \quad (1)$$

$$v = b_1x^2 + b_2y^2 + b_3xy + b_4x + b_5y + b_6 \quad (2)$$

where  $a_i$  and  $b_i$  are the motion parameters that characterize the region. Let  $(\hat{u}, \hat{v})$  be an estimate for the optical flow field based on some estimates for motion parameters  $a_i$  and  $b_i$ . It is assumed that the intensity of a point remains constant along its motion trajectory. Then, if  $\mathcal{R}$  is known, the optimum values for motion parameters can be estimated by minimizing the quadratic error measure

$$\mathcal{E}_{\mathcal{R}} = \sum_{\mathcal{R}} [I(x, y, t) - I(x + \hat{u}, y + \hat{v}, t - 1)]^2. \quad (3)$$

In our experiments, we used the gradient-based minimization. For this purpose we assume that the local spatio-temporal variations are linear, which holds true only if the motion of a region  $\mathcal{R}$  is small. We address this problem by using a hierarchical estimation, based on a multi-resolution image pyramid [AnBH93].

The main objective of the image sequence segmentation problem addressed here is the partition of each frame into regions which are uniform with respect to the motion parameters in (1) and (2). This requires the knowledge of motion parameters. However, we need to know the region boundaries to estimate the motion parameters. As a solution to this problem, we propose a split-and-merge procedure, as depicted in Fig. 1. In the split-phase, an initial partition of the image is obtained by segmentation using spatial-features (texture boundaries in our case) in a given frame. The regions so obtained are then used for motion estimation using two consecutive frames. Subsequently, the observed motion is used as a similarity criterion in identifying fragmented objects. The complete moving objects are constructed by merging adjacent regions with similar motion.

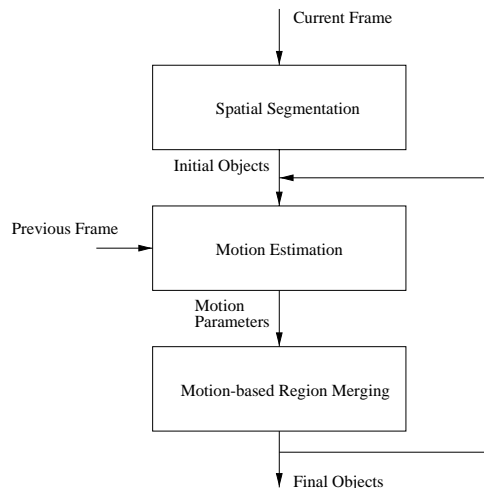


Fig. 1. Proposed split-and-merge algorithm of moving object segmentation.

## III. SEGMENTATION AND OBJECT DETECTION

### A. Wavelet-based Boundary Detection

The objective of this step is to find an initial set of regions to be used for motion estimation. Therefore

it is desirable to identify significant texture boundaries, a subset of which is likely to be the motion boundaries. Therefore we adopt segmentation by boundary detection or “edge” detection. One of the basic methods of edge detection is the use of derivatives. An image generally contains details at different scales. For example, an image may contain several large objects and each of the objects may contain details at smaller scales. A commonly used approach to eliminate unwanted details is the processing of the image using a smoothing operator, prior to computing the derivatives. This leads to the idea of multi-scale edge detection. In this paper, we adopt the wavelet-based multi-scale edge detection proposed in [MaZh92]. It has been shown that the edges in an image can be found by detecting the locations of the modulus maxima of wavelet transform, when the underlying wavelet is a derivative of a smoothing function. We used a cubic-spline smoothing function and therefore a quadratic-spline wavelet [MaZh92].

### B. Motion-based Region Merging

In the texture segmentation, the projections of the same 3D object may be fragmented into several regions according to texture variations. The boundaries corresponding to 3D objects can be found if all adjacent regions that move coherently are merged together. Since a similar 3D motion does not always result in a unique set of motion parameters on a 2D plane [Adiv89], they cannot be compared to determine the similarity of regions. In this paper we use an implicit measure based on the image quality obtained by motion compensated image reconstruction. Specifically, a set of motion parameters is estimated for each pair of adjacent regions. If the motion compensated prediction error is below a certain threshold, the two regions are merged together. The procedure is repeated for each pair of adjacent moving regions. In deciding upon a suitable threshold, we used peak signal-to-noise ratio (PSNR) within a region as a measure of image quality. It was assumed that a PSNR greater than 30 dB corresponds to insignificant perceptual distortion.

## IV. EXPERIMENTAL RESULTS

Figures 2 & 3 show the preliminary results obtained by applying the segmentation algorithm de-

scribed in the previous section to the image sequence *Claire*, using three consecutive frames (Fig. 2, a-c) from this sequence (frame rate 12 Hz). The results obtained after wavelet-based segmentation of last two frames are shown in Fig. 2 (d-e). These results have been obtained after post-processing of the initial segmentation. This involved closing of gaps in detected boundaries, followed by elimination of small regions. It was found that all images in this sequence, as well as other similar sequences, were segmented into about 30 regions. These regions were then used to estimate motion according to the object model described in the Section II. The Figs. 2 (f-g) shows the model-failures detected after motion-compensated image reconstruction. These regions correspond to areas affected by facial expressions and uncovered background. The Fig. 2 (h-i) shows the objects formed by motion-based region merging. We note that the person's head has been detected in both frames as the moving object. Finally, Fig. 3 shows the images reconstructed by motion compensation of objects shown in Fig. 2 (h-i). These images require coding of only the 12 motion parameters of the main object, *i.e.*, the face, except in the model failure regions shown in Fig. 2 (f-g). However, since model-failure regions tend to have random shapes, both the shape and the texture of these regions cannot be easily predicted. At present texture in model-failure regions is assumed to be coded in a lossless manner.

## V. CONCLUSIONS

The experimental results have shown that a typical head-and-shoulders image sequence can often be reproduced with acceptable perceptual quality, by coding only the motion parameters associated with few large objects (two in most cases). A bottleneck, however, is the coding of a few model-failure regions, and background regions exposed by the motion of objects. It was observed that the object detection based on the analysis of two frames alone does not always yield consistent results in the context of an image sequence. Also, it does not allow us to establish the correspondence between objects detected over an image sequence. Future work in this direction includes the extension of the method presented here to incorporate long term object tracking.



(a) Frame #92. (b) Frame #94. (c) Frame #96.



(d) (e)



(f) (g)



(h) (i)

Fig. 2. Simulation results: Claire sequences.

#### ACKNOWLEDGMENTS

This work has been supported by Telecommunications Research Laboratories (TRLabs) of Winnipeg.

#### REFERENCES

[Adiv89] G. Adiv, "Inherent ambiguities in recovering 3D motion and structure from a noisy flow field," *IEEE Tr. Pattern Analysis and Machine Intelligence*, vol. PAMI-II, no. 5, pp. 477-489, May 1989.



(a) (b) (c)



(d) (e) (f)

Fig. 3. The original frames # 94, #96, and #98 (top) and their reconstructions (bottom), based on the motion compensation of objects shown in Fig. 2.

[AnBH93] P. Anandan, J. R. Bergen, and K. J. Hanm, "Hierarchical model-based motion estimation," in *Motion Analysis and Image Sequence Processing* (M. Sezan and R. Lagendijk eds.), Ch 1, Kluwer Academic Publishers, 1993.

[Diehl91] N. Deil, "Object-oriented motion estimation and segmentation in image sequences," *Signal Processing: Image Communications*, vol. 3, pp. 23-56, 1989.

[LiLF94] H. Li, A. Lundmark, and R. Forchheimer, "Image sequence coding at very low bit rates," *IEEE Tr. Image Processing* vol. 3., no. 6, pp. 589-608, September 1994.

[MaZh92] S. Mallat and S. Zhong, "Characterization of signals form multiscale edges," *IEEE Tr. Pattern Analysis and Machine Intelligence*, vol. 14, no. 7, pp. 710-732, July 1992.

[MuHO89] H. G. Musman, M. Hotter and J. Ostermann, "Object-oriented analysis-synthesis coding of moving images," *Signal Processing: Image Communications*, vol. 1, no. 2, pp. 117-138, 1989.

# POWER SYSTEM TRANSIENTS CHARACTERIZATION AND CLASSIFICATION USING WAVELETS AND NEURAL NETWORKS

Fan Mo

<email: yingfan@ee.umanitoba.ca>

Electrical and Computer Engineering, University of Manitoba, Winnipeg, Manitoba, R3T 3M2

Advisor: Witold Kinsner <email: kinsner@ee.umanitoba.ca>

## Abstracts

**This paper presents a framework for transients classification using wavelet transform and two specific artificial neural networks, probabilistic neural networks (PNN) and resource allocating neural networks (RAN). One significant feature of wavelet for transients characterization is its time-scale two dimensional but compact representation. One distinguishing feature of PNN and RAN is the ability to adjust their architecture automatically to adapt to new environment quickly and accurately, which makes them the promising candidates for transients classification in power system. Some experimental results have indicated the suitability of this framework for transients classification.**

## I. INTRODUCTION

Electromagnetic transients in power systems result from a variety of disturbances on transmission lines, such as switching, lightning strikes, faults, as well as from other intended or unintended events. Such transients are extremely important, for it is at such times that the power system components are subjected to the greatest stresses from excessive currents or overvoltages[KiSh83][MoKi96].

In recent years, an increasing demand has been observed for power system monitoring and transient recording (including faults) combined with analysis, classification, and reporting. One important component of such system is the digital transient recorder, which has been available in some well-equipped substations to record various transients and provide assistant information about the transients for system operators to analyze them and take actions whenever a fault occurs. However, present transient recorders lack classification capability to distinguish “interesting” events from “trivial” events.

The desired intelligent transient recorder should have the ability to distinguish and classify different kinds of transients, provide a means to filter out meaningful information needed to assess system performance, classify faults and other disturbances to help identify stability, fault or other power quality issues, and even more importantly to provide a means to look automatically for early anomalies that could cause catastrophic failure.

Transients are signals with a finite life, that is, a transient dies to zero in a finite time. Frequency based analysis has been common since Fourier’s time; however, frequency anal-

ysis is not ideally suited for transient analysis, because Fourier based analysis is based on the sine and cosine functions, which are not transients. This results in a very wide frequency spectrum in the analysis of transients. A solution to the problem is to appeal to the use of transients to analyze transients. Wavelet transform is the right tool for transients analysis using a small transient - wavelet.

The capability of artificial neural networks (ANN) to learn complex mappings, linear or nonlinear, from the input space to output space, while remaining robust in a noisy environment, has resulted in their application to power systems, ranging from fault classification and localization to power load prediction. The fundamental feature of neural networks is the ability of learning, however, in many applications of neural networks in power systems, the learning ability has not been fully realized. Such limitations and corresponding improvements are introduced in part III.

## II. WAVELET CHARACTERIZATION OF TRANSIENTS

Wavelet theory is the mathematics which deals with building a model for non-stationary signals, using a set of components that look like small waves, called wavelets. It has become well known as a useful tool in several fields, including signal processing, image compression, biomedical applications, speech processing, acoustics, numerical analysis[Kins97] [KiLa93].

Given a time-varying signal  $x(t)$ , a wavelet transform consists of computing coefficients that are inner products of the signal and a family of “wavelets”. In a continuous wavelet transform (CWT), the wavelet corresponding to scale  $a$  and location  $b$  is

$$\Psi(a, b) = \frac{1}{\sqrt{|a|}} \Psi\left(\frac{t-b}{a}\right) \quad (1)$$

where  $\Psi(t)$  is the wavelet “prototype”, usually called a “mother wavelet”. Each wavelet,  $\Psi(a, b)$ , is a scaled (compressed or dilated) and translated version of the same original function  $\Psi(t)$ .

The DWT of a simulated single-phase fault waveform using Daub4 is shown in Fig. 1. The diagrams show that at scales 1, the instance of important events (fault occurring, circuit breaker opening and reclosing) are clearly localized, while at scales 5, the local variations of the fundamental frequency are clearly shown. The tiling of time-scale plane by wavelet transform for these two types of transients are shown in Fig. 3 [MoKi97].

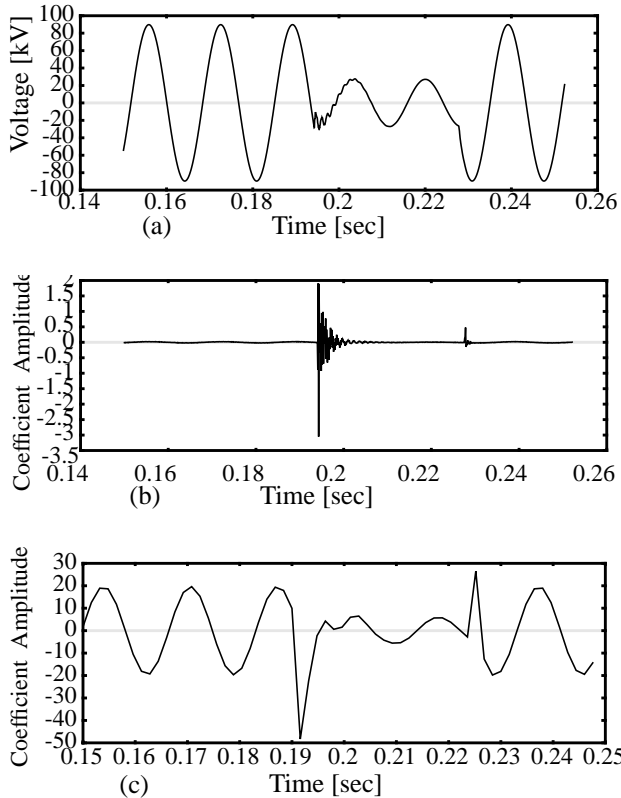


**Fig. 1.** (a) The original waveform of a single-phase fault and wavelet transform coefficients at (b) scale 1, (c) scale 5.

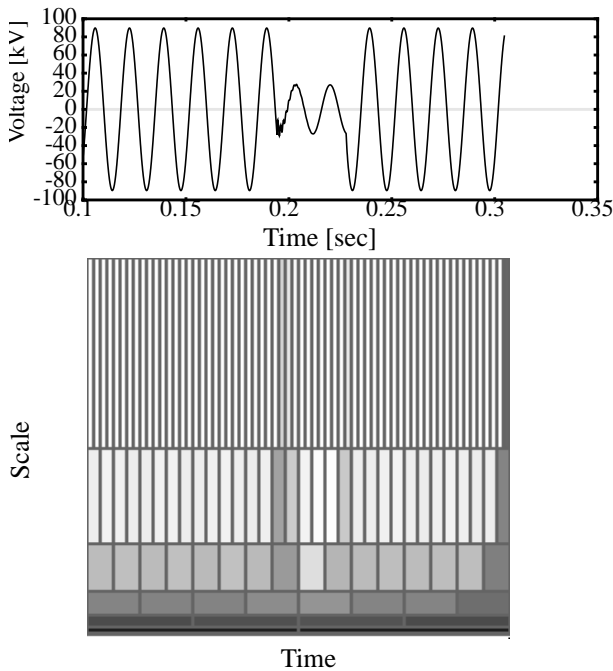


**Fig. 2.** The tiling of time-scale plane by wavelets for single-phase fault.

### III. NEURAL NETWORK APPROACH TO TRANSIENTS CLASSIFICATION

The use of pattern recognition for power system security analysis was first investigated in 1968. Since neural network can be fully applied for pattern recognition, it has been widely investigated for transient classification (including faults). It was evident even in 1968 that the generation of training set by off-line simulation would be prohibitively tedious. All automatic learning approaches to system security analysis or transients analysis are confronted by the obstacle of training-set generation arising from the tremendously large number of combinations of variables and topologies and the computation required for each simulation. Besides the combinatorial problem, there is the problem of generating a sufficiently large population of “insecure” states for a highly meshed network. How to deal with this problem is still an open problem. One approach is to develop some on-line instead of off-line training-set generation technique, at the same time make neural network more flexible and more suitable for on-line incremental learning.

Among many types of neural networks, the multilayer feed-forward neural network, also known as backpropagation (BP) network, and Radial basis function network (RBFN) have become the main architecture of choice, but both have some problems like limited flexibility, long time training, and unsuitability for on-line automatic learning.

One major problem with BP network is its architecture parameters have to be tried experimentally, which is very time consuming. Also if the architecture of neural network is decided after these tries and then fixed, the network will have difficulties to adapt itself to a new environment. Since many power systems are expanding and new facilities are added, new transient types with different appearance must be added to the neural network. The BP network cannot incorporate such information easily. One possible way is to retrain the network with all the past and new training samples, which would be very time consuming. Another way is to only use the new samples to train the neural network, but it may lead to the overall performance degradation caused by the new training samples. The basic reason for the degradation is that the BP network is a globally connected network, thus new samples affect all the weights globally.

RBFN is based on a set of radial basis functions which provide the property of localized influence, therefore, the system can develop and refine its parameters quickly in one region of the measurement space without affecting its learning in distant regions, which occurs in BP network. But traditional implementation of RBFN still has some drawbacks. The main problem is the number of centroids of RBFN has to be determined in advance. If the number of centroids is not decided properly, the accuracy of RBFN is seriously affected.

An ideal neural network should be capable of adjusting not only its weights but also its architecture, to match its

architecture complexity to the complexity of a specific problem in a on-line fashion. At the beginning of work, a neural network may just have been trained by a limited training set obtained off-line with quite simple architecture, but with the continues exposure to new classes of events, which is unavoidable in power systems, the neural net may incorporate into itself new classes of transients by adjusting its architecture. For transients belonging to same class but with different appearance, the network could either adjust its weights with only local influence or add new neurons to represent the same class transients which have big difference.

Two candidates of this ideal neural network are probabilistic neural networks (PNN) and resource allocating networks (RAN).

### 3.1 PROBABILISTIC NEURAL NETWORKS (PNN)

PNN, first proposed by Specht in 1988 [Spec88], was implemented in [MoKi98] for power line faults classification. With its solid mathematical foundation, the PNN implements the Bayes classification rule, which minimizes the expected error of classification, thus improving its accuracy. Furthermore, due to its modular architecture and fast learning speed, PNN is very suited for learning system which is always evolving, and the on-line and incremental learning can also be easily achieved.

The architecture of the PNN is shown in Fig. 3. The pattern layer contains one neuron for each training case. Specifically, it represents a certain number of training samples ( $j, k, l, \dots$ ) from each of  $C$  different classes for a total of  $R$  training samples. Each neuron in the pattern layer computes a distance measure between the unknown input and the training case represented by the neuron. An activation function, known as

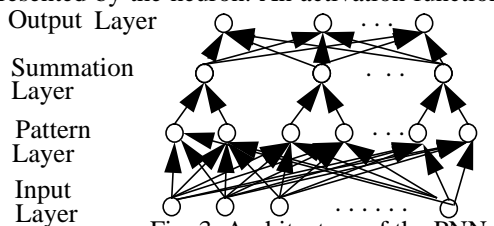


Fig. 3. Architecture of the PNN.

the Parzen window, is applied to the distance measure. In the summation layer, there is one neuron for each of  $C$  classes. These neurons sum the values of the pattern layer neurons corresponding to that class to obtain an estimated density function of the class. The number of neurons in the output layer is also equal to the number of classes,  $C$ . The output layer is often a simple threshold discriminator which activates a single neuron to represent the projected class of the unknown sample.

To demonstrated the suitability of PNN for fault classification, a PNN is employed to identify the different patterns generated from a simple transmission system which is shown in Fig. 4.

The training patterns are created to cover a variety of fault inception angles, fault resistance, source capacities and loads.



Fig. 4. Transmission system used for the PNN studies.

The transients caused by capacitor switching operation are also included to test if the PNN could distinguish faults from switching operation. Different kinds of noise are added to simulate real-world effects.

The training time of PNN for the small scale problem is a couple of seconds. With the optimal window size, the PNN can classify samples in testing set with 100% correct rate. In contrast, the BP network took 5 minutes to train, but achieved only 90% correct classification rate. So, compared to the BP network, the PNN has a very fast training speed and at the same time achieves high accuracy. Furthermore, the PNN can easily add new pattern neurons to incorporate new typical transients or even new classes of transients.

### 3.2 RESOURCE ALLOCATING NETWORKS (RAN)

The RAN was developed as a means to overcome the problem of NP-completeness in learning with fixed-size network [Plat91]. Its motivation was coming from the fact that by allocating new resources, learning could be achieved in polynomial time. Platt views the task of RAN as combining memorization with adaptation, in which memorization is achieved by storing the input-output observation similar to Parzen window estimation method. He improves on this method by storing fewer observations which makes the size of the RAN grow sublinearly and eventually saturate. The architecture of the RAN is shown in Fig. 5.

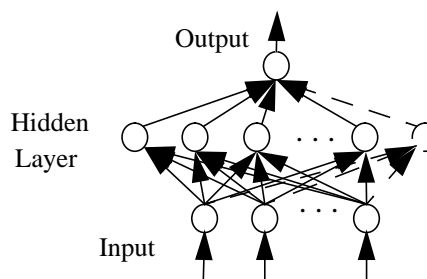


Fig. 5. Network architecture of the RAN. The dashed line show the addition or deletion of hidden units.

At first, the system creates a coarse representation of the function, then refines the representation by allocating units with smaller and smaller widths. Finally, when the system has learned the entire function to the desired accuracy and length scale, it stops allocating new units.

The RAN is first tested on a particular chaotic time series created by the Mackey-Glass delay-difference equation. The prediction result are shown in Fig. 6.

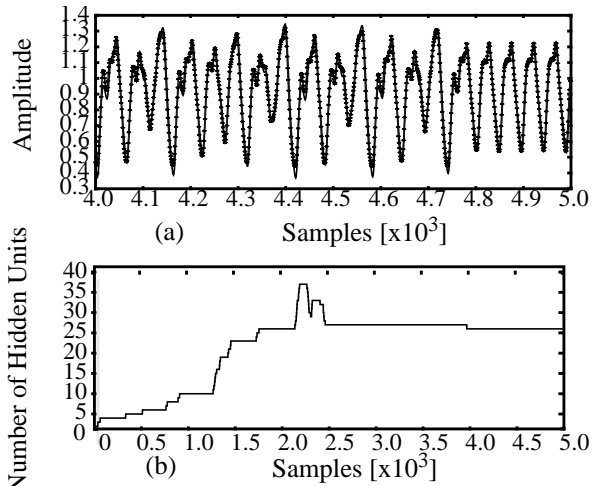


Fig. 6. 17-sample ahead prediction and waveform.

We then used load data from Manitoba Hydro to test the predict ability of the RAN technique [MoKi98]. The prediction experiments were performed with three different lead time, 1 hour, 24 hours, and 168 hours (1 week) respectively. Figure 7 shows the results of 24-hour ahead prediction over 250 hours period. The results shows that RAN can grow up or shrink to match its architecture complexity to the underlying dynamic changes. The application of RAN for transients classification is still undergoing and the results will be presented in the future.

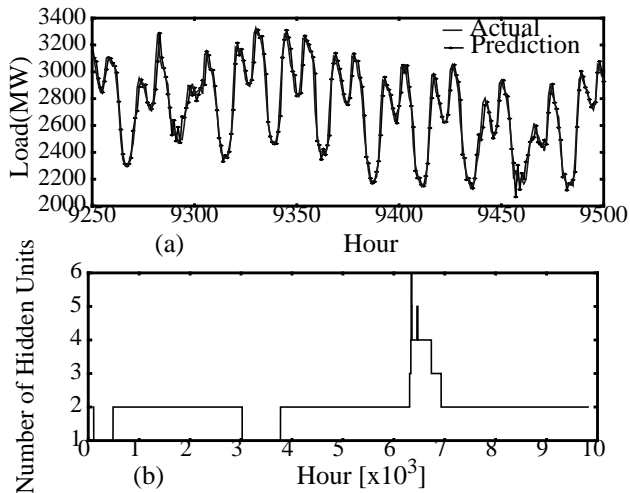


Fig. 7. 24-hour ahead prediction, MAPE = 2.0%.

#### IV. SUMMARY

This report described a framework to characterize and classify power system transients. Wavelet transform has shown its advantage to characterize transients in a more compact and representative way. Due to the difficulty to generate training-set from the tremendously large number of combinations of variables, topologies and the computation

required for each simulation, a more flexible neural network which is suitable for on-line training is desired. The PNN and RAN, with their capability to fast adapt their architecture to dynamic environment, have been found to be promising candidates for on-line transients classification.

#### ACKNOWLEDGEMENTS

This work was supported in part by Manitoba Hydro and the Natural Sciences and Engineering Research Council (NSERC) of Canada.

#### REFERENCES

- [KiSh83] W. Kinsner, I. Shpancer, M. Jullian, and M. Kauldher, "Design, implementation, and testing of HVDC and AC power line fault locators," *Internal Reports*, Winnipeg, MB: Industrial Applications of Microelectronics Centre, 1983.
- [KiLa93] W. Kinsner and A. Langi, "Speech and image signal compression with wavelets," *Proc. IEEE Communications, Computer & Power Conf., WESCANEX'93* (Saskatoon: SK: May 17-18, 1993), IEEE Cat. No. 93CH3317-5;pp. 368-375.
- [Kins97] W. Kinsner, "Wavelet analysis in power systems," *Proposal*, University of Manitoba, January 14, 1997.
- [MoKi96] F. Mo, and W. Kinsner, "Review of diagnostic techniques of power system transients," *Proc. IEEE 1996 Can. Conf. Electrical and Computer Eng., ICE&CE'96* (Calgary, AB; May 26-29, 1996), ISBN 0-7803-3143-5, pp.
- [MoKi97] F. Mo, and W. Kinsner, "Wavelet modelling of transients in power systems," *Proc. IEEE Communications, Computer & Power Conf., WESCANEX'97* (Winnipeg: MB: May 22-23, 1997), IEEE Cat. No. 97CH36117-5;pp. 132-137.
- [MoKi98] F. Mo, and W. Kinsner, "Predicting and modeling of nonstationary temporal signals with fractal characteristics," submitted to CCECE'98.
- [MoKi98] F. Mo, and W. Kinsner, "Probabilistic neural networks for power line fault classification," submitted to CCECE'98.
- [Plat91] John Platt, "A resource-allocating network for function interpolation", *Neural Computation*, vol. 3, pp. 213-225, 1991.
- [Spec88] D. F. Specht, "Probabilistic neural networks for classification, mapping, or associative memory", *Proc. IEEE Int. Conf. Neural Networks*, San Diego, CA, vol. 1, pp. 525-532, July 1988.

**GRADUATE STUDENT CONFERENCE**

**GRADCON'98**

<http://www.ee.umanitoba.ca/~gradcon/>

**AUTHOR INDEX**

	<b>PAGE</b>
A9 Inas El-Babli . . . . .	12
A10 Ashraf Badawi . . . . .	16
C3 Peter Czezowski . . . . .	47
C7 Richard Dansereau . . . . .	58
B4 Reza Fazel-Rezai . . . . .	31
A12 B. Ghosh, N. Simons, L. Shafai, A. Ittipiboon, A. Petosa, and M. Cuhaci . . . . .	22
A11 D.P. Gray . . . . .	20
C4 Douglas Holmes . . . . .	51
C6 Sajid Hussain . . . . .	55
C5 Sinisa Iliskovic	
B9 David A.N. Jacobson	
C2 Imran Khan . . . . .	43
B10 Wieslaw T. Kwasnicki . . . . .	39
A4 Ling Yun Lee	

B2	Sihong Lei	26
B6	Hongwei Li	
C1	Dean McNeill	
B1	Saleh Mneina	
C9	Fan Mo	66
B7	Mojtaba Mohaddes	35
B5	Rajen M. Murugan	
B8	Dharshana Muthumuni	
B3	Ha Hoang Nguyen	28
A1	Sima Noghalian	1
A5	Wujun Quan	
A6	David R. Swatek	
A2	Kin Yip Sze	4
A7	Alex Tugulea	
C8	Pradeepa Yahampath	62
A3	Qiubo Ye	8
A8	Ming Zhang	